Analysis of Non-conforming Contacts



Beth Eames

A thesis submitted for the degree of
Doctor of Philosophy

Supervised by
Prof. David Hills

Balliol College

Department of Engineering Science
University of Oxford
Hilary Term 2026

Preface

This thesis is submitted for the degree of Doctor of Philosophy in Engineering Science at the University of Oxford, United Kingdom. The research presented in this thesis was carried out by the author between October 2021 and March 2026, under the supervision of Professor David Hills.

To the best of my knowledge, the work described in this thesis is original, except where due reference acknowledges the work of others.

The work presented herein has been partially published in the following journal papers:

B. Eames, D.A. Hills, A review of partial slip solutions for elastic contacts, *European Journal of Mechanics - A/Solids,* Volume 113, 2025, 105698, ISSN 0997-7538, https://doi.org/10.1016/j.euromechsol.2025.105698.

B. Eames, D.A. Hills, M.R. Moore, Near edge tractions for a rounded quarter-plane pressed into an elastically similar half-plane, *Tribology International,* Volume 186, 2023, 108582, ISSN 0301-679X, https://doi.org/10.1016/j.triboint.2023.108582.

B. Eames, D.A. Hills, M.R. Moore, Elastic, flat and rounded finite contacts: When should we use half-plane theory?, *European Journal of Mechanics - A/Solids,* Volume 106, 2024, 105306, ISSN 0997-7538, https://doi.org/10.1016/j.euromechsol.2024.105306.

B. Eames, D.A. Hills, J.R. Barber, Elastic, flat and rounded finite contacts in partial slip: A novel solution based on wedge and half-plane formulations, *International Journal of Solids and Structures*, Volume 321, 2025, 113543, ISSN 0020-7683, https://doi.org/10.1016/j.ijsolstr.2025.113543.

B. Eames, L. Blades, S.A. MacLeod, D.A. Hills, Matching the slip condition at two types of contact, *Tribology International.* In press, 2026.

Abstract

Fretting fatigue cracks initiate local to contact edges, where the stress field is steep, mixed-mode, and governed by local contact mechanics rather than by just a remote bulk stress (as in plane fatigue). The standard analytical tool for modelling these edges assumes that both contacting bodies can be treated as elastic half-planes. For many incomplete contacts this provides an accurate local approximation, but when the contacting body has a flat face with rounded edges and the flat segment is long compared to the edge radius, the nearby traction-free surfaces influence the stress state, and the half-plane idealisation becomes inadequate.

This thesis develops a closed-form framework for describing near-edge tractions in geometrically coupled contacts. The approach matches the local rounded contact edge behaviour, controlled by half-plane theory, to an outer field governed by Williams' eigensolutions for the appropriate wedge geometry, thereby capturing the geometric coupling that arises when normal loading excites shear tractions and vice versa. Comparisons with finite element analyses establish when half-plane theory remains adequate for flat-and-rounded contacts and when it does not, providing quantitative guidance in terms of the flat length to edge radius ratio when half-plane theory for the contact as a whole is acceptable.

The framework is then extended to partial slip under multi-stage and cyclic loading by expressing the near-edge behaviour in terms of stress intensity factors quantifying changes in contact edge position and shear traction change. This makes it possible to import well-established partial slip solution strategies into geometries where half-plane theory is not globally valid, and it reveals that the two edges of a geometrically coupled contact can exhibit different slip states under the same external loading because of sensitivity to load path. A practical consequence is developed in the final contribution, where the asymptotic edge parameters are used to match the near-edge conditions of a plane receded contact to an equivalent Hertzian contact, providing a method for characterising complicated contact configurations using standard laboratory experiments.

Throughout, the analysis is restricted to two-dimensional, linearly elastic, elastically similar contacts with Coulomb friction. The work is directed primarily towards specifying threshold behaviour, i.e. where the contact-edge stress field controls whether a crack will initiate, and it provides a foundation for more practical grounded approaches to assess the fretting fatigue life.

Acknowledgments

First, I would like to thank my supervisor and former tutor, Professor David Hills. Throughout my time at Oxford, David has taught me many things: from calculating bending moments along a cantilever beam to recognising when it is time to go for a dog walk and think about not thinking about work in order to make progress. His confidence in me during my undergraduate degree opened the door to academia and to many opportunities alongside it, including the discovery of amazing American diners a mere three bus journeys away... For all of this, I am truly grateful.

I would also like to thank the Department of Engineering Science at the University of Oxford for its financial support throughout my research. I am also grateful to James Truelove, Luke Blades, Madeline Moore, and Jim Barber for their time, technical support, and guidance throughout my DPhil, all of which helped me grow as a researcher.

I would especially like to thank my family. My mum has been on the other end of my countless video calls, and deserves a medal if not my PhD. I am more grateful to her than she will ever know. My dad has helped keep me going, whether that was a lift to the gym when my brain was fried or proudly informing all members of his aqua class that I am studying engineering. I am so grateful for their unwavering love, humour and support. I would also like to thank my brother, Jack, for his 3am paper recommendations and for always being by my side. I also want to make a special mention of my wonderful grandies, Val and Ken, who are both true icons and deserve every bit of Oxford I can share with them.

Finally, I would like to thank my incredible friends who encouraged me to take on a DPhil in the first place, and who have made my time at Oxford so much fun. To my friends and coaches from hockey, powerlifting, Spanish and my endeavour into tennis, to my friends from Hilda's, Balliol and home, and to those who have supported me behind the scenes — thank you. So, in honour of my six-year-old self, it for once seems fitting to close with her rehearsed Oscar acceptance speech: "Thank you to my friends and family for supporting me through thick and thin," and "For anyone out there who thinks they can't — this is your sign that you can".

For the girls

Contents

List of Figures **vi**

List of Symbols **vii**

1 Introduction **1**

1.1 Motivation 2

1.2 Thesis Structure 4

2 Literature Review **7**

2.1 Introduction 8

2.2 Elastic coupling and conditions for Slip and Stick 10

2.3 Half-plane problems - constant normal load 13

2.4 Half-plane problems - varying normal load 16

2.5 Partial slip half-plane solutions using edge dislocations 21

2.6 Complete contacts 25

2.7 Complete, common-edge contact 28

2.8 Receding contacts 31

2.9 Shakedown 33

2.10 Conclusion 35

3 Near Edge Tractions for a Rounded Quarter-plane Pressed into an Elastically Similar Half-plane **44**

3.1 Introduction 46

3.2 Asymptotic representation of the state of Stress 48

3.2.1 Finite (b/d finite) 50

3.2.2 Validity of the asymptotic series expansion 50

3.3 Semi-infinite flat punches with rounded edges 52

3.3.1 Half-plane formulation 52

3.3.2 Three-quarter plane formulation 55

3.3.3 Pure Mode I Loading 55

3.3.4 Pure Mode II Loading . . . 58
3.4 Conclusion . . . 61

4 Elastic, Flat and Rounded Finite Contacts: When Should We Use Half-Plane Theory? 65
4.1 Introduction . . . 67
4.2 Half-plane formulation of a flat and rounded contact . . . 69
4.3 Rounded, three-quarter plane formulation of a flat and rounded contact 70
4.4 Application of the rounded, three-quarter plane solution to the finite contact . . . 72
4.5 Comparison of solutions . . . 74
4.5.1 Contact tractions . . . 74
4.5.2 Contact Laws . . . 77
4.6 Conclusion . . . 81

5 Elastic, Flat and Rounded Finite Contacts in Partial Slip: a novel solution based on wedge and half-plane formulations 84
5.1 Introduction . . . 86
5.2 Summary of half-plane formulation for contact edge - *Phase (3)* . . . 91
5.3 Three-quarter plane formulation: Calibrations - *Phase (2)* . . . 93
5.4 Geometry specific calibration: External loads to Williams' Solution - *Phase (1)* . . . 94
5.5 Combining the phases: Contact law . . . 95
5.6 Combining the phases: Tractions under full stick . . . 98
5.7 Comparison of methods under full stick . . . 99
5.7.1 Finite-element reference solution . . . 99
5.7.2 Validation . . . 101
5.8 Condition for partial slip . . . 105
5.9 Shear tractions with partial slip . . . 107
5.10 Conclusion . . . 114

6 Matching the Slip Condition at Two Types of Contact 118
6.1 Introduction . . . 121
6.2 Effects of small perturbations of loads . . . 124
6.3 Calibrations for receded contact . . . 125
6.3.1 Bounded pressure asymptote (L_I) . . . 126
6.3.2 Singular traction changes (K_I, K_{II}) . . . 127
6.3.3 Effect of remote tension . . . 129

6.3.4 Summary of calibrations for the receded contact 129
6.4 Validation 132
6.5 Calibrations for Hertzian contact 134
6.6 Results of matching 135
6.6.1 Mean pressure term 136
6.6.2 Singular normal-traction term 136
6.6.3 Singular shear-traction term 136
6.6.4 Design form of the matching equations 137
6.6.5 Worked example 137
6.7 Limitations 138
6.8 Conclusion 141

7 Conclusions and Future Work **144**
7.1 Summary of Contributions 146
7.1.1 Key Findings from Chapter 3 147
7.1.2 Key Findings from Chapter 4 148
7.1.3 Key Findings from Chapter 5 149
7.1.4 Key Findings from Chapter 6 150
7.2 Overall Significance 150
7.3 Limitations 151
7.4 Future Work 152
7.5 Closing Remarks 162

Appendix: Statements of Authorship **164**

List of Figures

2.1 Five contact classes considered in this review. 9
2.2 An adhered complete contact, between two symmetrical bodies. . . . 11
2.3 Shear tractions for an adhered complete contact. 13
2.4 A Hertzian contact. 16
2.5 Stick, slip and sliding in P, Q-space. 17
2.6 Loading trajectory with partial slip. 20
2.7 Dislocations in partial slip. 22
2.8 Critical coefficients of friction to maintain adhesion. 27
2.9 Contact between identical strips, loaded axially and in shear. 29
2.10 Contact between identical cylinders, loaded axially and under torsion. 30
2.11 Depiction of the bilateral solution for a receding contact. 32
2.12 A semi-infinite receded contact 32

3.1 Schematic of a semi-infinite flat and rounded contact 48
3.2 Asymptotic representations of contact pressure for three contact types. 51
3.3 Comparison of methods, mode I loading: tractions at contact edge . . 57
3.4 Comparison of methods, mode I loading: tractions along interface . . 58
3.5 Comparison of methods, mode II loading: tractions at contact edge . 59
3.6 Comparison of methods, mode II loading: tractions along interface . . 60

4.1 Finite flat-and-rounded contact: geometry, loading and coordinate system. 69
4.2 Transformation between P, Q, K_I, K_{II} and L_I, L_{II} spaces 73
4.3 Comparison of methods for different geometries at contact edge. . . . 75
4.4 Comparison of methods along interface. 77
4.5 Detailed diagram of finite flat and rounded contact 78
4.6 Contact-law comparison between methods for different geometries (part I). 79
4.7 Comparison of methods for different geometries: contact law part II. . 80

5.1 Flat and rounded contact under 4 types of loading. 87
5.2 Illustration of the refined, three-quarter plane formulation. 88
5.3 Schematic of contact pressure with its near-edge and decaying asymptotes. 90
5.4 Local axis set for the left and right corners. 94
5.5 Comparison of methods for different geometries in shear, contact law. 97
5.6 Contact law contours under normal and shear loads. 98
5.7 FE model geometry and loading. 100
5.8 FE mesh near the receded contact corner. 101
5.9 Mesh-convergence study. 102
5.10 Example loading history in P, Q and K_I, K_{II} spaces. 102
5.11 Comparison of methods, tractions at contact edges. 103
5.12 Relationship between infinitesimal change in external loads and near edge stress intensity factors. 106
5.13 Two-stage loading paths giving full stick or partial slip ($a/R = 10$). . 108
5.14 Transient tractions at the two edges for example loading paths. 110
5.15 Cyclic loading paths exhibiting partial slip ($a/R = 10$). 111
5.16 Steady-state shear tractions, unloaded to state (3). 112
5.17 Steady-state shear tractions, reloaded to state (2). 113

6.1 The two contact configurations matched in this chapter. 123
6.2 Equivalent experimental configurations for receded and Hertzian contacts. 123
6.3 Dislocation decomposition for remote tension on the receded contact. 130
6.4 Stress-intensity calibrations for an oscillatory normal load. 130
6.5 Stress-intensity calibrations for an oscillatory remote tension. 131
6.6 Stress-intensity calibrations for an oscillatory shear load. 131
6.7 Contact and stick–slip transition extents versus coefficient of friction. 132
6.8 Sign convention for positive stress intensity factors at contact edges. . 132
6.9 Finite-element validation of the receded-contact edge asymptotes. . . 134
6.10 Matched mean contact tractions for the receded and Hertzian contacts. 139
6.11 Matched cyclic shear tractions at the left contact edge. 140

7.1 Sliding contact edge behaviours and adhesion limit. 155
7.2 Eigensolution for a sliding 45^o wedge. 156
7.3 Separation and partial slip results for a 45^o wedge. 157

List of Symbols

β Dundurs' second constant

μ Coefficient of friction

ν Poisson's Ratio

ϕ Wedge angle

σ Bulk tension

$\sigma_{ij}(x)$ Stress

a Contacting body half-width, in Chapter 6: stick-zone half width

b Contacting body flat half-length

B_x, B_y Dislocation density

b_x, b_y Burgers vectors

c Thickness of strip

d Length of contact in rounded section of contacting geometry

E Young's Modulus

E^* Plane strain modulus

G_{ijk} Kernel

$K_{i[1/2]}$ or $\widetilde{K}_i$ Crack-tip stress intensity factor

$K_{i[3/4]}$ or K_i Wedge sense stress intensity factor

L_I Asymptotic multiplier at contact edge for normal traction

L_{II} Asymptotic multiplier at contact edge for shear traction

M	Moment
P	Normal load
$p(x)$	Normal traction
Q	Shear load
$q(x)$	Shear traction
R	Radius of curvature
T	Torque

Chapter 1

Introduction

Contents

1.1 Motivation **2**

1.2 Thesis Structure **4**

1.1 Motivation

Structural and mechanical assemblies rely on contacts to transmit load. In applications as varied as turbine blade roots, splines, clamped joints and subsea connectors, contacts are used to locate components and to carry large forces over small areas. Particularly when these contacts are under load with small perturbations, these interfaces can be common initiation sites for damage due to fretting fatigue; cracks can nucleate near the contact edges and grow under a highly non-uniform, mixed-mode and load-history-dependent stress state.

A striking difference between fretting fatigue and 'plain' fatigue is that the initiation site is not random in the former. Under plain fatigue, a component with mild stress gradients is, in effect, 'searching' over a large surface area for a weak point. Under fretting, the crack almost always initiates at (or very near) a contact edge. This observation immediately focuses attention on the mechanics local to the edge. It also suggests that it may be unhelpful to use standard S–N data to quantify fretting fatigue, as the near-surface stress environment is not simply a scaled version of a uniform stress field.

Furthermore, in plain fatigue, stress gradients are typically mild, and the transition from nucleation to early crack growth takes place in a nearly uniform stress field. The alternating stress that governs nucleation is, to a good approximation, the same σ that appears in the crack-tip stress intensity factor once a small crack forms, and the S–N framework (together with mean-stress corrections such as those of Goodman, Haigh and Soderberg) exploits this connection. At a contact edge, the situation is fundamentally different. The stress field has steep gradients, is mixed-mode, and controlled by the local contact mechanics. A crack nucleating at a contact edge grows into an environment whose intensity cannot be characterised by a single nominal stress, and the familiar mean-stress corrections become even less rigorous than they are in plain fatigue. For these reasons, it seems more productive to pursue a description of the contact-edge stress state that is rooted in the local mechanics, rather than to treat fretting as a perturbation of uniform-field fatigue data.

One of the challenges with fretting fatigue is that contact edges are difficult to model. The steep stress gradients can lead to changes in stick–slip behaviour over very small distances. In numerical models the same features that matter physically, such as sharp gradients and near-singular behaviour, are the features that cause mesh sensitivity and convergence difficulties. Meanwhile, the most widely used analytical description of frictional contacts, half-plane theory, is built on a powerful idealisation that both bodies can be treated as elastic half-planes. This gives elegant closed-form

solutions and, for many incomplete contacts, an excellent description of the behaviour very close to the contact edge.

However, the engineering contacts that motivate this thesis are often not well represented globally by a half-plane. In particular, many practical contacts have a flat face with rounded edges. When the flat segment is long compared to the edge radius, the nearby traction-free sides of the contacting component influence the stress state. In that regime, geometric coupling becomes important: normal loading can also induce shear traction, tangential loading can alter the normal traction, and the evolution of contact size can become asymmetric. These effects are absent from the uncoupled half-plane idealisation (when the bodies are elastically similar).

In a rounded-edge incomplete contact, the very near-edge behaviour is always governed by a local half-plane field (Flamant theory), so that the leading-order form of the tractions is square-root bounded in the distance from the edge. Yet the region of physical interest in fretting is not infinitesimal. Slip zones and steep stress gradients can extend a non-negligible distance from the edge, and the stress field in that region is influenced by the 'outer' geometry of the bodies. A useful mechanics description therefore needs to respect both facts:

1. locally, the edge looks like a half-plane problem, and

2. globally, the geometry and boundary conditions determine the correct outer field.

This is the central theme of the work presented in this thesis, constructing a tractable description of near-edge tractions and of the stick–slip state which is locally consistent with half-plane behaviour but correctly 'geared' to a realistic far field contact-defining body.

A further practical difficulty is that fretting fatigue is often investigated experimentally using standard pad-on-dogbone arrangements producing nominally Hertzian contacts. These tests are convenient and well controlled, but this geometry is, *prima facie*, not always most applicable to industry. For example, many contacts in fretting involve receding edges, combined normal, shear and bulk stresses, or other load-path effects. This raises a question of whether a complicated contact can be 'represented' in the laboratory by a simpler Hertzian test, provided that the relevant near-edge conditions such as the stick–slip behaviour and the local stress states are matched.

The work in this thesis is restricted to two-dimensional, linearly elastic contacts with Coulomb friction. This is not because three-dimensionality, wear and plasticity are unimportant; rather, it reflects a deliberate attempt to build a clean framework for

the contact edge behaviour first. The near-edge stress field is key to aid the eventual aim of predicting threshold behaviour, supplying boundary conditions for crack growth calculations, or embedding the work in broader component-scale simulations.

With this motivation, the thesis addresses four research questions:

1. **Can a closed-form representation of the stress state at a contact edge be obtained when geometric coupling is present?** In particular, can we retain the convenience of a half-plane local description while accounting for the influence of nearby traction-free boundaries?

2. **When is half-plane theory appropriate for flat-and-rounded contacts, and when is it not?** That is, can we give quantitative guidance in terms of geometry ratios and loading on the validity of the half-plane idealisation?

3. **Can the contact-edge stress state be matched to a crack-like description in a way that remains useful under partial slip and complex loading histories?** The aim here is not to claim that a contact edge *is* a crack, but to exploit the well-developed structure of crack-tip asymptotics to parameterise the near-edge stress field and to make contact-edge descriptions portable between geometries under small perturbative loading.

4. **Can the near-edge conditions of a plane receded contact under oscillatory loading be replicated by a Hertzian contact, enabling standard fretting experiments to characterise more complex configurations?** This requires matching the asymptotic edge parameters controlling stick–slip, edge motion and local stress state, not the external loading itself.

1.2 Thesis Structure

This thesis is presented as an integrated thesis built largely from published papers, with additional material to establish context, define scope and provide a coherent narrative.

Chapter 2: Literature review

Chapter 2 reviews partial slip solutions for elastic contacts and classifies contact problems according to how the contact edge is defined (for example, incomplete contacts with square-root bounded pressures and complete contacts whose edges

are set by geometry). Particular emphasis is placed on: (i) the distinction between coupled and uncoupled contacts, (ii) the construction of stick–slip solutions from full-sliding or full-stick states, and (iii) the limitations of classical half-plane descriptions when applied to geometries with nearby traction-free boundaries.

Chapter 3: Near-edge tractions with traction-free boundary effects

Chapter 3 addresses Research Question 1. It develops a hybrid description in which the local, square-root-bounded half-plane behaviour at a rounded contact edge is matched to an outer field that represents the true domain shape. In practice this is done by collocating a half-plane rounded-edge solution into a three-quarter-plane far field governed by Williams' eigensolutions. The chapter establishes that this procedure captures geometric coupling and gives improved traction fields over a physically meaningful region near the edge.

Chapter 4: Finite contacts and the validity of half-plane theory

Chapter 4 addresses Research Question 2 by applying the Chapter 3 approach to finite, flat-and-rounded contacts. Comparisons with finite element calculations are used to quantify when half-plane theory remains adequate and when it becomes misleading. The chapter shows how the quality of half-plane predictions deteriorates as the flat length becomes large compared to the edge radius, and it identifies regimes in which the rounded three-quarter-plane description provides a marked improvement in both traction distributions and contact laws.

Chapter 5: Partial slip in coupled, flat-and-rounded finite contacts

Chapter 5 addresses Research Question 3. It extends the coupled near-edge traction description to contacts with partial slip under multi-stage and cyclic loading. The chapter introduces a three-domain framework: an outer calibration for the sharp-cornered (monolithic) geometry, an intermediate three-quarter-plane problem incorporating a crack, and an inner domain of a half-plane rounded-edge contact. By expressing the near-edge field in terms of stress-intensity-factors instead of external loads, classical partial slip constructions can be applied in a setting where half-plane theory is not globally valid. A practical consequence is that the two edges of a

coupled contact can exhibit different slip states under the same external loading history.

Chapter 6: Matching the slip condition at two types of contact

Chapters 3–5 develop the near-edge traction framework in the context of flat-and-rounded contacts. Chapter 6 addresses Research Question 4 by demonstrating how the same class of asymptotic edge parameters can be used to design equivalence between a complicated contact and a standard laboratory test. A plane receded contact, formed by pressing an elastic strip onto an elastically similar half-plane, is subjected to fluctuating normal load, shear load and bulk tension. The edge response is described using a small set of asymptotic parameters: a bounded-pressure multiplier L_I and two stress-intensity factors K_I, K_{II}. By calibrating these parameters for both the receded contact and a Hertzian contact, and then equating them, explicit load relationships are obtained which define an equivalent Hertzian experiment. This enables complicated contact configurations to be characterised using standard pad–on–dogbone experiments, providing a practical route from the analytical framework developed in the preceding chapters to experimental fretting fatigue investigation.

Chapter 7: Conclusions and future work

Chapter 7 draws together the main findings, places them in the context of fretting fatigue, and outlines limitations and natural extensions. The emphasis is on what the developed near-edge traction framework enables, particularly for threshold problems, and on what must be addressed next to build finite-life predictive procedures.

Notation and conventions

Throughout, the analysis is restricted to two-dimensional, linearly elastic bodies and Coulomb friction. Unless stated otherwise, bodies are treated as elastically similar so that the normal and tangential problems decouple in the half-plane limit, and coupling effects discussed later are due to geometry. Sign conventions for shear tractions and loading are stated explicitly in Chapters 3–6 where edge asymmetry becomes important.

Chapter 2

Literature Review

Contents

2.1 Introduction 8

2.2 Elastic coupling and conditions for Slip and Stick 10

2.3 Half-plane problems - constant normal load 13

2.4 Half-plane problems - varying normal load 16

2.5 Partial slip half-plane solutions using edge dislocations . 21

2.6 Complete contacts 25

2.7 Complete, common-edge contact 28

2.8 Receding contacts 31

2.9 Shakedown 33

2.10 Conclusion 35

A Review of Partial Slip Solutions for Elastic Contacts

B Eames and D A Hills
Department of Engineering Science, University of Oxford, Parks Road, Oxford, OX1 3PJ, UK

Abstract

This review classifies contacts into their fundamental classes and provides basic properties of each type of contact. For both complete and incomplete contacts, the conditions for no-slip are identified, and the extent of slip, where it occurs, is determined. Limited data on other classes of contact are also presented. The question of 'coupling' - where the application of a normal load also induces interfacial shear, and a shear load modifies the contact pressure distribution - is also discussed. This study aims to provide a cohesive understanding of elastic contacts under partial slip, serving as a foundation for advancing theories and applications in the field.

2.1 Introduction

This paper focuses on the interface between elastic bodies, typically plane bodies, in contact. It examines situations where Amontons-Coulomb friction is present. The goal is to understand when the contact is fully stuck or in partial slip, and, when an oscillatory load is applied, when there are regions of reversing slip. In partial slip, some parts of the interface are stuck while others are slipping.

The Coulomb-Amontons law states that, when one body slides over another, the ratio of the shear force, Q, to the normal force, P, remains constant for a given pair of materials. This ratio is independent of the shape of the bodies and the speed at which they are sliding. It is given the symbol μ. It is assumed that this same ratio governs the ratio of the magnitude of the shear traction, $q(x)$ to the contact pressure, $p(x)$. This not only applies throughout the contact when the bodies are sliding, but also to the slipping regions of contact which are in partial slip.

The behaviour of contacts is best understood if they are classified, first, into the basic types, and also the concept of 'coupling' is discussed. Figure 1 shows five basic types of contact.

The contact class which has received most attention since the 1880s and Hertz' studies is depicted in Figure 1(a), which shows two cylinders pressed together. Hertz, who studied the 3-D form of the problem, assumed that the contact patch is so small

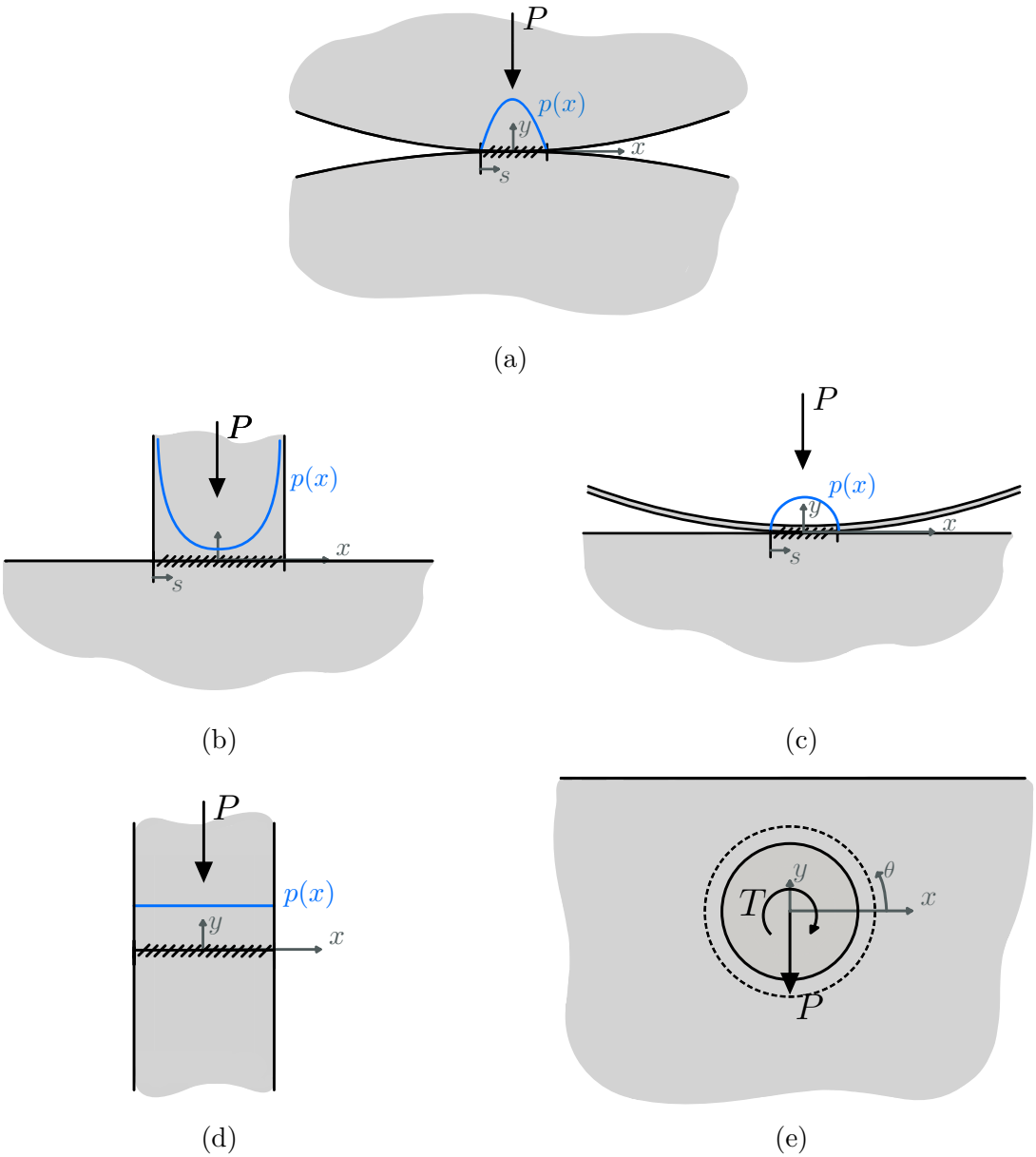


Figure 2.1: Five classes of two-dimensional elastically-similar contacts considered in this review: (a) a Hertzian incomplete contact between two cylinders, with square-root-bounded near-edge pressure; (b) a square punch pressed onto a half-plane, a complete contact with singular near-edge pressure controlled by Williams' eigensolution; (c) a thin elastic strip pressed onto a half-plane, a receding contact in which the contact ends short of the strip ends; (d) two identical square punches pressed together along a common edge, a complete common-edge contact with finite pressure to the edge; (e) a disk shrink-fitted into a hole, a contact without an end. In (a)–(c) the near-edge normal-traction asymptote $p(x)$ is sketched in blue.

compared with the radius of curvature that each component may be thought of as a half-space (or half-plane in this case), with just a small 'bump'. This defines the geometry of the body, here in the form of a parabola (approximating a circular arc),

but the theory applies also to shallow wedges and other slightly convex profiles. If we set up a second coordinate, s, measured inwards from the contact edge, and think of small values of this quantity compared with the width of the contact, we will reveal the nature of the contact pressure present near the edge. Here, it will fall smoothly to zero in a square root bounded fashion ($p(s) \sim \sqrt{s}$), as the edge is approached. We refer to this general class of contacts as *incomplete*. Here, we will largely restrict ourselves to problems in which the half-plane idealisation of the contacting bodies applies.

Figure 1(b) shows a square block being pressed onto an elastically similar half-plane. Barber refers to this type of problem as 'conforming' [1]; when the unloaded elements are placed in contact, their profiles naturally conform. When a normal load is applied, the contact patch size is determined by the dimension of the front-face edge of the block. In other words, it is defined by the discontinuity in the profile gradient at the corner of the block. In problems of this kind, the half-plane theory cannot be applied because of the presence of the traction-free faces at the sides of the block. It is not possible to produce an elasticity solution for the block on its own, other than by a series representation. The contact pressure adjacent to the ends of the contact varies in the form $p(s) \sim s^{\lambda-1}$, where usually $\lambda < 1$ so that the contact pressure is singular. We refer to these contacts as *complete*.

If a relatively thin layer is pressed against an elastically similar half-plane, Figure 1(c), the layer beyond the pressed region will lift off, provided that the contact pressure stops well short of the ends of the layer. The contact therefore *recedes*, and at the contact edge the contact pressure is again square root bounded in form.

In Figure 1(d) two bodies having the same front-face length (or having common edges) are pressed together. In this case, the edges of the contact are aligned and the contact pressure is finite right to the edge.

Lastly, Figure 1(e) shows a disk shrink-fitted into a hole within a half-plane, and possibly also subject to a torque and small radial force, insufficient to cause separation. In this contact *without end*, the contact pressure is also finite everywhere.

2.2 Elastic coupling and conditions for Slip and Stick

In general terms, the concept of coupling arises when the application of a normal contact load causes interfacial shear tractions to develop. The application of a subsequent shear force, or a tension in one body parallel with the free surface, also modifies the contact pressure distribution.

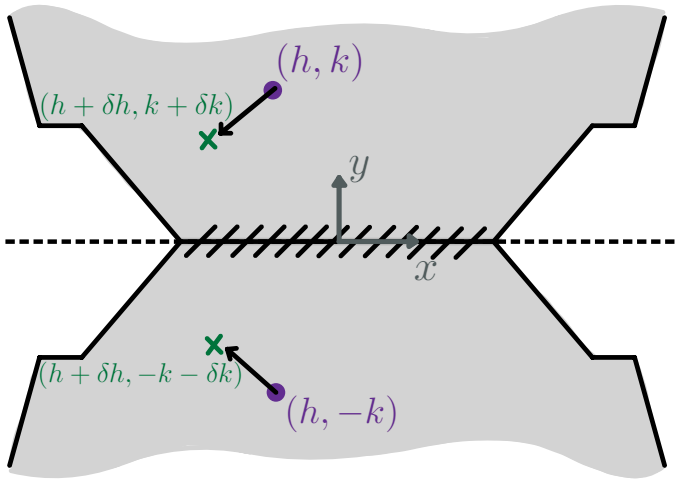


Figure 2.2: A fully stuck, complete contact between two bodies, symmetrical about the x axis. For an arbitrary load in compression, the purple points are displaced to their corresponding green points.

The phenomenon has two origins - geometry mismatch and elastic mismatch. First, we will consider the case where two bodies pressed normally together are of any general shape, but where the bodies are geometrically similar to each other. If one body is the mirror image of the other about the interface, particles at corresponding points will displace by equal amounts relative to the interface. For example, as seen in Figure 2.2, particles at corresponding points (h, k) in one body and $(h, -k)$ in the other body will displace in the y-direction by equal but opposite amounts relative to the interface, and in the x-direction by equal amounts, of the same sign, even if the interface is lubricated.

It follows that, in the absence of lubrication (i.e. in the presence of friction), no shear tractions will arise along the interface. However, if a hole, for example, is drilled in one of the components, so the bodies are no longer mirrored across the interface line, our remarks about the symmetry of displacements in the bodies will no longer apply; the geometric mismatch causes interfacial shear tractions to develop if the interface is free of lubricant. This is an example of geometric coupling.

For incomplete contacts where each body is idealised as a half-plane, there can be no geometric coupling. In the case of the complete contact shown in Figure 1(b) the bodies have very different domain shapes, and there is strong geometric coupling; as we will show, the shear traction is 54% of the contact pressure near the edge, if it is stuck, and independent of the orientation of the contact force, conditional only on the contact area extending to the edge of the block.

Now consider the effect of elastic mismatch between two bodies. Even when the two bodies have the reflection property described, if they are made from elastically

different materials they will exhibit coupling; for example, under a normal load, particles away from the centre line will be displaced laterally by different amounts, because of differing Poisson effects. An exhaustive discussion of this phenomenon is outside the scope of this article, but in general, the effects of mismatch will be controlled by two dimensionless elastic mismatch parameters (α, β) devised by Dundurs [2]. In the case of half-plane problems, there is a reduced dependence on only the second parameter, β.

This concept of coupling has been introduced for three reasons:

1. Most simply, the coupling means that when the contact is initially formed (even by a normal force), slip may arise if the coefficient of friction is insufficiently big.

2. Solving precisely the interfacial traction distribution is very complicated.

3. Coupling has a profound effect on the possibility of the problem becoming stuck under oscillatory loading - shakedown [3, 4].

We need to write down what the conditions for stick and slip are during any change of load. Time will enter the solution insofar as it defines the sequence of loading, but the solution is in no sense dynamic, and no inertial loads are present. A point, x, along the contact, will remain or become stuck if, after the load change [5],

$$|q(x)| < \mu p(x) \tag{2.1}$$

and, in addition, any slip displacement $\Delta u = u_1(x) - u_2(x)$ will be preserved. When a point slips, it does so when the shear traction at the point reaches the limiting value, i.e.

$$|q(x)| = \mu p(x) \tag{2.2}$$

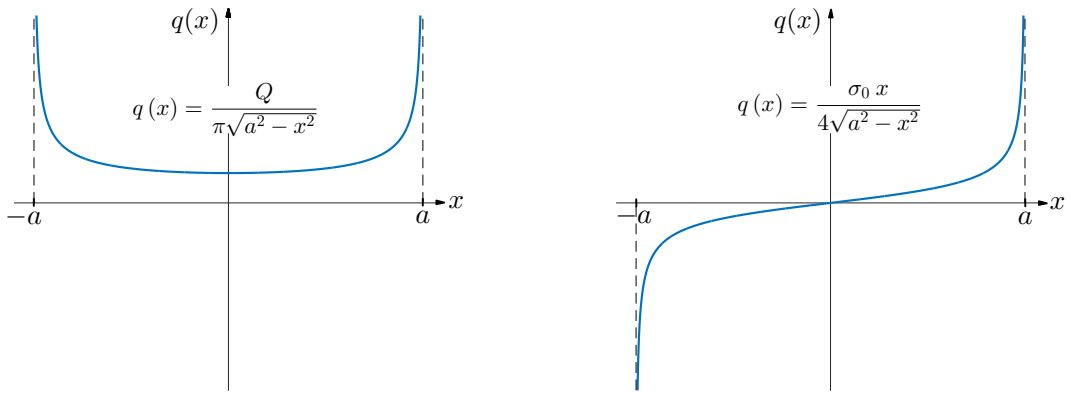
and the sense of the shear traction must be such as to oppose the sense of change in slip displacement, so that

$$\operatorname{sgn}(\Delta u(x)) = -\operatorname{sgn}(q(x)). \tag{2.3}$$

Work by Dini discusses how the coefficient of friction may change in the slip region throughout a component's life and he describes how we can numerically predict this change from measured mean values [6]. Although the results have been shown to be accurate for the Hertz contact, the change in coefficient of friction for flat and rounded geometries, where the slip zone sizes are small, is less accurately predicted.

2.3 Half-plane problems - constant normal load

We restrict ourselves to the case of contact between elastically similar half-planes, so that the contact is uncoupled; normal loads do not induce interfacial shear tractions, and similarly, induced changes in shear traction cause no change in the contact pressure distribution. With this provision, it means that the contact pressure is uniquely specified by the geometry and normal load, P, together with an applied moment, M, if the contact is capable of supporting a moment. On the other hand, the shear traction distribution, $q(x)$, is critically dependent on the load path taken. Shear tractions may be induced by the application of a shear force, Q, and/or differential tensions, $\sigma_0 = \sigma_1 - \sigma_2$ exerted parallel with the free surface. Fig.2.3 illustrates the shear tractions that arise due to each type of loading parallel to the contacting interface.



(a) Shear traction, $q(x)$, induced by a shear force, Q

(b) Shear traction, $q(x)$, induced by a differential bulk tension, σ_0

Figure 2.3: Shear traction distributions for a fully adhered complete contact of semi-width a [7].

Historically, the first solutions to frictional, stationary contact problems of this kind were obtained for three-dimensional Hertzian contacts, under a constant normal load by Cattaneo [8], and re-discovered by Mindlin [9]. The plane equivalent of these geometries, where cylinders are pressed together under a constant normal load with a monotonically increasing shear force, has been solved in many publications. Johnson's book on contact problems [10] solves this problem, although the solution had been known for quite some time by then. There are many ways to derive it, but the most informative way is to use the integral equation representation. If the plane strain modulus of the components is E^*, (equal to $E/(1-\nu^2)$), where E is Young's

modulus and ν Poisson's ratio, the contact pressure, $p(x)$, is related to the surface relative slope at any point, dh/dx, by

$$E^* \frac{dh}{dx} = \frac{2}{\pi} \int_{-a}^{a} \frac{p\,(\xi)\,d\xi}{x-\xi} \quad -a \leqslant x \leqslant a \tag{2.4}$$

where the contact spans $[-a \quad a]$, and dh/dx defines the relative gradient of the contacting profiles. In addition, when a bounded-both-ends solution for the contact pressure is sought, as it is for an incomplete contact, normal equilibrium must be imposed between the contact pressure and the external normal force, P, given by

$$P = \int_{-a}^{a} p\,(x)\,dx. \tag{2.5}$$

The integral equation representing the connection between the shear traction, $q\,(x)$ and the gradient of the relative surface tangential displacement, du/dx, which is also the difference in surface strain (ϵ_{xx}), is, generally

$$E^* \frac{du}{dx} = \frac{2}{\pi} \int_{-a}^{a} \frac{q\,(\xi)\,d\xi}{x-\xi} \quad -a \leqslant x \leqslant a. \tag{2.6}$$

After the contact is formed, and holding the normal load constant, a monotonically increasing shear force, Q is applied. We choose to represent the shear traction as the sum of two terms, viz., first a sliding shear traction $q_1\,(x) = \mu p(x)$ over the whole contact, i.e. $-a \leqslant x \leqslant a$, together with a corrective term, $q_2\,(x) \equiv \mu p_2\,(x)$, present only over the stick zone, which we assume spans $[-b \quad b]$, so that

$$E^* \frac{du}{dx} = \frac{2\mu}{\pi} \int_{-a}^{a} \frac{p\,(\xi)\,d\xi}{x-\xi} + \frac{2}{\pi} \int_{-b}^{b} \frac{q_2\,(\xi)\,d\xi}{x-\xi} \quad -a \leqslant x \leqslant a. \tag{2.7}$$

If no shear force was exerted before the contacting pair was formed, the relative strain within the stick zone is zero, i.e.

$$\frac{du}{dx} = 0 \quad -b \leqslant x \leqslant b, \tag{2.8}$$

and hence, as $a > b$,

$$E^* \frac{dh}{dx} = -\frac{2\mu}{\pi} \int_{-b}^{b} \frac{p_2\,(\xi)\,d\xi}{x-\xi} \quad -b \leqslant x \leqslant b \tag{2.9}$$

A comparison of Eqs.(2.4,2.9) shows that the integral equation for the corrective

shear, $p_2(x)$, is the same in form as the equation for contact pressure, but at a lower normal load. If we apply tangential equilibrium condition, Eq.(2.5), we have that, overall,

$$Q = \mu (P - P_2). \tag{2.10}$$

The size of the stick zone is the value of b sought in Eq.(2.7) and it is given by the contact law for a problem under consideration when it is loaded by a normal force P_2. It will be noted that the result just found has been derived without specifying the shape of the indenter, dh/dx. We have shown that, regardless of the shape of the contact, the corrective term has a distribution which is a scaled form of the pressure distribution corresponding to a lighter load, which is specified in equation (2.9). This result was not discovered until much later, separately by Jaeger [11] and Ciavarella [5]. It applies both to single contacts and multiply connected contacts, and approximately also to three-dimensional problems. The procedure is exact for three-dimensional contacts where the material from which the bodies are made exhibits no Poisson effect. Munisamy examined the 3-D problem when the bodies do show some Poisson effect [12].

Shear tractions may also be induced along the plane of the contact interface by the imposition of tensions exerted parallel with the contact surface. In general both bodies may be loaded in this way, and it is the difference between the tensions which is responsible for driving interfacial shear. The most general case of loading by σ_1 and σ_2 is shown schematically in Fig.2.4, where differential remote forces are applied at the contact sides giving rise to both tension and a shear force. This form of the problem practically arises in standard pad-on-dogbone fretting fatigue tests and was studied with this in mind by Nowell and Hills [13], for the case of a Hertzian contact. Fig.2.3 shows the interfacial shear traction distributions arising along the interface when fully stuck under (a) a shear force and (b) a differential bulk tension. It will be noted that first is symmetric about the centre line and the second is antisymmetric.

Analysing the contacting geometry of a flat and rounded punch pressed into a half-plane is relevant to match to pad-on-dogbone experiments with gas turbine dovetail roots. Vazquez produced explicit equations for the interfacial stresses and contact law for this geometry when the contact was first loaded normally, and then a shear force was introduced [14]. The internal state of stress can be found using Muskhelishvili potentials [15]. Ciavarella [16] and Vazquez [17] looked particularly at the case when tensions *alone* were present. In cases where a shear force is applied together with a small differential tension, so that the slip zones remain of the same sign, a similar formulation to that given above will apply, except that now the stick zone will be offset (say by c, to span the interval [-b+c b+c] as seen in Fig.2.4).

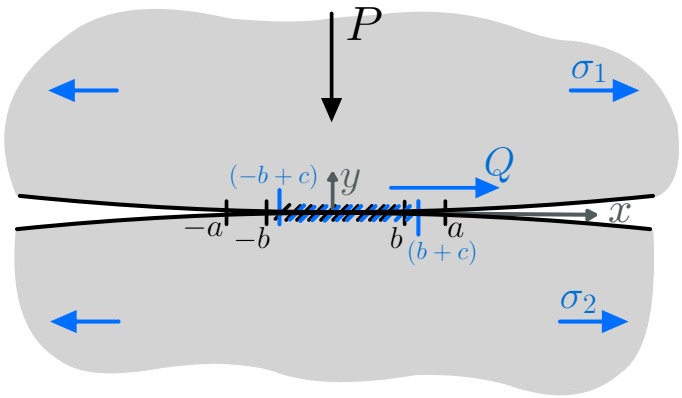


Figure 2.4: A Hertzian contact spanning the interval $[-a \quad a]$. Under normal load only, the stick zone region is $[-b \quad b]$. The introduction of shear load may offset the stick zone by c.

The strain in the stick region is no longer zero; instead, it is given by σ_0/E^*. The Jaeger-Ciavarella idea continues to apply but this time with the scaled form of the contact pressure offset. In cases where the applied tension is sufficiently large for the slip zones to be of opposite sign, the procedures described in this section, using superposition of two sliding shear traction distributions cannot be used and an alternative formulation starting from the stress state in two fully stuck contacts, must be used, and this procedure, using the solution for an edge dislocation as the kernel, is described later.

2.4 Half-plane problems - varying normal load

The previous section outlines solutions for half-plane problems, where the shear traction distribution and the location and size of the stick zone are to be determined. This is done by using a superposition of the shear traction from sliding (rigid body motion) with a similar, scaled corrective term over the stick region.

Early studies focused on Hertzian geometry, but later expanded to include other shapes where the half-plane idealization still applies, such as shallow wedges or punches with a flat central portion and rounded edges. The latter shapes are important in practical applications, such as the dovetail roots of fan blades or locking segments used in seabed riser connections. There is some doubt about the fidelity of a half-plane-based model when the central, conforming flat region is large relative to the rounded edge radius. The non-circular profiles also introduce the possibility of the contact supporting an applied moment (or, equivalently, an offset normal force), M. We now see that there are, generally, four quantities which affect the behaviour of the contact, viz. P, Q, M, σ_0. In an uncoupled half-plane contact problem with friction

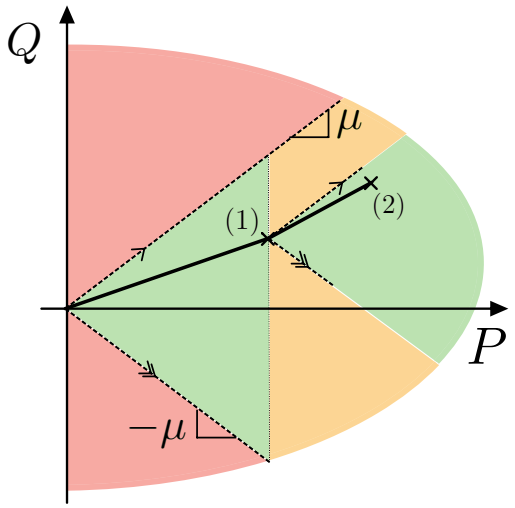


Figure 2.5: A graph of normal load P against shear load, Q. The dashed lines have a gradient with magnitude μ, the coefficient of friction. If, at any point, the contact is loaded to meet the dashed lines that border the red region, the contact will undergo full body sliding, i.e. $|Q|/P = \mu$. When the contact is loaded to a location within the green envelope, the contact will remain fully stuck, i.e. $\Delta Q/\Delta P < \mu$. For subsequent loading steps, the contact will undergo partial slip if $\Delta Q/\Delta P \geqslant \mu$. By following load steps (1) and (2), the contact remains fully stuck.

present, the contacting bodies must normally be elastically similar for the result to apply. The sequence of all four quantities P, M control the size of the contact and the pressure distribution, and all four quantities control the shear traction distribution when Q, σ_0 are non-zero, but they do not influence the normal contact problem. The proximity to sliding is controlled only by the ratio $|Q|/\mu P$, and is independent of both M, σ_0. To reiterate, the possibility of slip is controlled by all four quantities, and by the sequence in which they are applied.

In this section, we look at more general loading histories than in §3. A useful way to start is to think about a contact in which the only forces which arise are P, Q, and the loading history is neatly represented in a diagram having these axes, Figure 2.5.

If we draw two lines through the origin having gradients $\pm\mu$, we see that any loading trajectory which results in the force state arriving on one of those bounding lines will result in rigid body motion, that is, sliding. The force state may not be outside those bounding lines if the body is to be in equilibrium. If the load state lies within the green and orange sections shown it may be in either a state of full stick or partial slip, depending on the exact trajectory followed. The best way of understanding this is to use a representation of half-plane loading, originally devised by Mosakovskii but developed by Barber [18, 1]; the process of applying a smoothly increasing load is seen as the limit of applying small finite steps. The theory may

be used to form an Abel equation allowing the contact law to be solved, from the profile. Here, it is sufficient to note that an increase in the normal load, ΔP, gives rise to an increase in contact pressure, $\Delta p(x)$, given by [19]

$$\Delta p(x) = \frac{1}{\pi} \frac{\Delta P}{\sqrt{a^2 - x^2}} \tag{2.11}$$

where a is the current contact half-width and where the corresponding normal surface displacement is constant over x.

The similarity between the governing equations for normal and shear loading of a half-plane [1] means that a constant tangential displacement of the surface is produced by a change in shear traction, $\Delta q(x)$. In turn, the shear traction is given by a change in shear force ΔQ, and these are related by [19]

$$\Delta q(x) = \frac{1}{\pi} \frac{\Delta Q}{\sqrt{a^2 - x^2}}. \tag{2.12}$$

Suppose that we simultaneously increase the normal load by ΔP (>0) and the shear force by ΔQ. The contact will increase slightly in size and there will be a change in both shear and direct traction distributions which vary spatially with x in the same way. Therefore, the change in the ratio of the shear to direct traction is the same as the change in the ratio of the shear to normal force. It will now be fully adhered if

$$\frac{|\Delta Q|}{\Delta P} < \mu. \tag{2.13}$$

If we load along the trajectory shown in Fig.2.5, the contact will become fully stuck as it satisfies the condition in Eq.(2.13).

These concepts may be extended to problems where bulk tension is applied, a change of which induces a shear traction change given by [19]

$$\Delta q(x) = \frac{1}{4} \frac{\Delta \sigma_0 x}{\sqrt{a^2 - x^2}}. \tag{2.14}$$

Further, when there is a small change in applied moment, ΔM, the change in contact pressure is given by [20]

$$\Delta p(x) = \frac{2}{\pi} \frac{\Delta M x}{a^2 \sqrt{a^2 - x^2}}. \tag{2.15}$$

We are now in a position to see what happens when all four quantities vary at the same time. Provided that the magnitude of M is not too big, so that both edges of the contact advance (which will be dependent on the contact law), the most critical points will be at each edge of the contact. From Eqs.(2.11-2.15) we see that no slip

will occur provided that

$$\frac{\frac{\Delta Q}{\Delta P} \pm \frac{\pi a}{4}\frac{\Delta \sigma_0}{\Delta P}}{1 \mp \frac{2}{a}\frac{\Delta M}{\Delta P}} < \mu. \tag{2.16}$$

Note that we must check both sides of the contact and the inequality must be satisfied on both sides. The sign convention is that a positive moment is applied clockwise, upper signs apply at the left-hand side of the contact and the lower signs on the right-hand side.

When there is partial slip present the size and position of the stick zone may be found using one of two methods. The first is based, as earlier, on a shear traction distribution under sliding conditions, with a correction term to be found for what happens within the stick region. This general idea will, as earlier, work provided that the bulk tension is not too large and the slip zones are of the same sign. The second approach, which overcomes this difficulty, will be described in the next section.

The biggest step in obtaining a solution to problems in which the normal load changes was made by Barber [21]. He observed that the scaled sliding corrective term from the Jaeger-Ciavarella concept could be extended to problems well beyond those originally treated in the solutions from 'contacts with small bulk tension' papers. In [21], the problem of a half-plane contact subjected to varying normal and shear forces is explored through a complex loading cycle, including an arbitrary phase shift between the load components. The paper introduces two key new elements. The first relates to the similarity between the effects of changes in normal and shear forces, as suggested by Eqs.(2.11,2.12). This implies that, when moving along a contour $Q(P)$ where the normal load is increasing between two points, say A and B, Figure 2.6 under full stick. The shear traction distribution changes given by

$$q_B(x) = q_A(x) + \int_{P_A}^{P_B} \frac{\partial p(x,P)}{\partial P}\frac{dQ}{dP}dP, \tag{2.17}$$

where we adopt the notation developed by Barber [21], $p(x;P)$ denotes the contact pressure distribution corresponding to a normal load P and is non-zero over the interval $|x| < a(P)$, where a is the contact half-width.

If we follow the contour shown in Figure 2.6, the contact remains fully stuck until we reach point B, where inequality (2.13) is violated. As we move further along the contour, the contact will increase in size but a region of slip will develop. When we reach point C the shear traction will be described by

$$q_C(x) = \int_0^{P_A} \frac{\partial p(x,P)}{\partial P}\frac{dQ}{dP}dP + \mu\left(p(x,P_C) - p(x,P_A)\right). \tag{2.18}$$

where the second term represents the shear traction in the region of slip $a_B \leqslant |x| \leqslant a_C$.

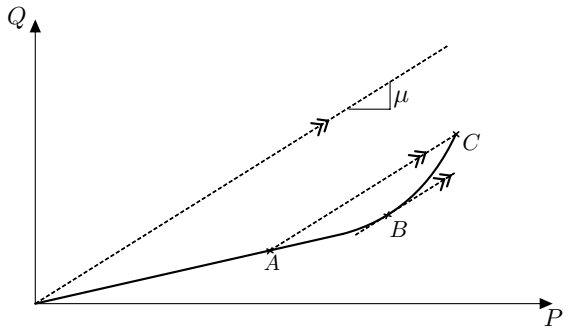


Figure 2.6: The solid line represents a loading trajectory in P, Q space, the dashed construction lines have gradient of the coefficient of friction, μ. The contact is fully stuck up to point B, after which undergoes partial slip. When the contact is loaded to point C, the contact is stuck within the interval $|x| \leqslant a_B$, and in slip over the intervals $a_B \leqslant |x| \leqslant a_C$.

The location of point A is undetermined. It must lie on the loading contour, and the imposition of tangential equilibrium shows that it is given by [21]

$$Q_C = Q_A + \mu \left(P_C - P_A \right) \tag{2.19}$$

Further aspects of this problem are covered in [21] including what happens when there is reverse slip and unloading ($\Delta P < 0$). This reference describes a very general loading case, including the possibility of phase shift. However, it is restricted to cases where the loading is defined by $Q(P)$ and M, σ do not enter the problem.

In many problems a single applied external force on an assembly excites both the normal load and a shear, which therefore develop in phase. At the same time, we note that there are two further relevant 'forces' which appear locally at the contact, viz differential tension, σ_0, and a moment, M. In a pair of papers where the loads are changed proportionally, the solutions were extended by the addition of these two extra effects. Only the steady-state solution was sought because this is of great practical relevance. However, a key limitation in these papers is that they rely on a superposing a sliding shear traction distribution, which is only appropriate when the slip zones are of the same size, meaning the bulk tension must be no more than modest. When this assumption does not hold, a different approach is necessary.

2.5 Partial slip half-plane solutions using edge dislocations

The Jaeger-Ciavarella principle and its generalisation is a very powerful result, enabling partial slip solutions, monotonic and cyclic, to be found for many problems. But, because the approach starts with a shear traction distribution for sliding contact (and inserts a correction for stick) it means that it can be used only for problems where the slip zones are of the same sign or, in practical terms, that any bulk tension present is of no more than moderate value.

It is perfectly possible to start from the opposite assumption, i.e. that the contact is fully stuck, and then distribute glide dislocations along the interface to represent the effect of slip [1]. It is probably worth making some introductory remarks about the technique generally. Most solutions to problems using the continuum theory of elasticity start with a simple configuration where the domain under consideration is loaded by a force, and the resulting stress and displacement fields found. This is the starting point when we look at half-plane problems, and it is the basis for equation (2.4). But it is not the only possible first step. We might instead use a dislocation — in plane problems, this would be an edge dislocation. These entities have the same mechanical properties as the well-known crystalline defect, but they are used as a 'strain nucleus', and there is no implication in their use of the presence of real (crystal defect) dislocations in the problem under consideration. An edge dislocation is formed by making path-cut from its core to a free surface (or an infinitely remote point), and making a constant displacement across that path cut (of magnitude equal to the Burgers vector). By having an array, or, in the limit, a distribution of dislocations, and making the path cuts follow, for example, a trace line along the line of a crack, the crack opening displacement or crack shear displacement may be found, and other relevant quantities in the solution. The starting point, however, is always the solution for a single edge dislocation in whatever domain is to be analysed, and it is this which limits the repertoire of solutions which may be found. A comprehensive introduction to the subject is given by Hills et al [23]. As stated above, no progress may be made without the solution for a single dislocation in the relevant domain, and it was Barber who showed that, if two elastically similar half-planes are bonded over the interval $[-a \quad a]$, a glide dislocation of Burgers vector b_x positioned at ξ will

[1] Edge dislocations, where the Burgers vector is normal to the interface, may also be used to solve the contact problem itself [22], but this will not be followed up here.

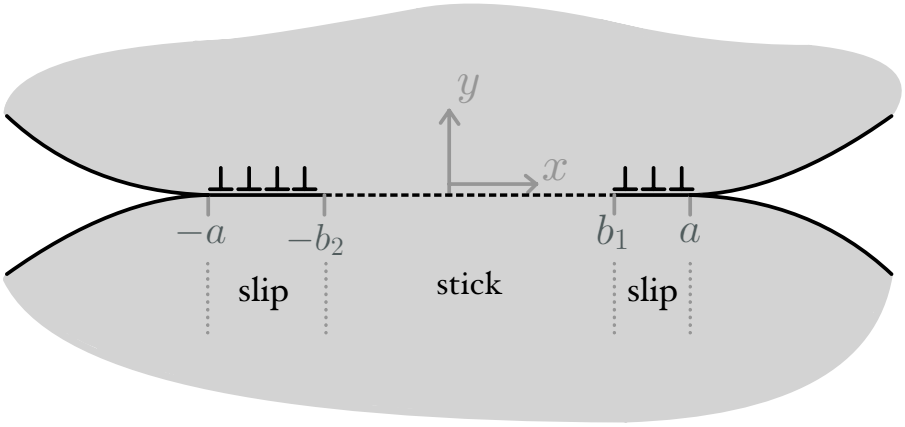


Figure 2.7: In partial slip, dislocations over the intervals $[-a \quad -b_2]$ and $[b_1 \quad a]$ model the slip regions of the contact. The centre region $[-b_2 \quad b_1]$ is fully adhered.

induce a shear traction, $q(x)$, given by [24]

$$q(x) = \frac{E^* b_x(\xi)}{2\pi\sqrt{a^2 - x^2}} \frac{\sqrt{a^2 - \xi^2}}{\xi - x}. \tag{2.20}$$

As expected, this displays singular behaviour both at the ends of the bonded interval and a Cauchy singularity at the location of the dislocation itself. For example, the distribution of such dislocations over intervals $[-a \quad -b_2]$ and $[b_1 \quad a]$ attached to the edges of an adhered contact, seen in Fig.2.7, will result in a shear traction distribution [24], $q_c(x)$ given by

$$q_c(x) = \frac{E^*}{2\pi\sqrt{a^2 - x^2}} \left[\int_{b_1}^{a} \frac{\sqrt{a^2 - \xi^2} B_x(\xi)\, d\xi}{\xi - x} + \int_{-a}^{-b_2} \frac{\sqrt{a^2 - \xi^2} B_x(\xi)\, d\xi}{\xi - x} \right] \tag{2.21}$$

where we have added the subscript c to denote that it will be used to form a correction. The dislocation density is $B_x(x) = db_x/dx$.

In a problem with a constant normal load, the full stick shear traction distribution, $q_{st}(x)$, under the influence of a shear force and differential bulk tension is given by

$$q_{st}(x) = \frac{Q}{\pi\sqrt{a^2 - x^2}} + \frac{\sigma_0 x}{4\sqrt{a^2 - x^2}} \tag{2.22}$$

so that, when the coefficient of friction is finite, and some slip is expected, the total traction is

$$q(x) = q_{st}(x) + q_c(x). \tag{2.23}$$

We now identify the intervals over which the dislocations are distributed as slip

regions. Consequently, we observe that

$$q(x) = \pm\mu p(x) \quad x \in [b_1 \quad a] \text{ and } [-b_2 \quad -a]. \tag{2.24}$$

These conditions provide an integral equation for the unknown dislocation density $B_x(x)$. However, to find the locations of the stick/slip boundaries [25], it is only the side conditions associated with the bounded nature of the inversion which must be evaluated.

When only a tangential shear force is applied the slip zones will be of the same sign, and $b_2 = b_1 = b$. One side condition is then automatically satisfied and the second gives

$$\int_b^a \frac{\xi p(\xi) d\xi}{\sqrt{\xi^2 - b^2}} = \frac{Q}{2\mu}. \tag{2.25}$$

Once $p(s)$ is known, the slip zone size may be found from this integral, highlighting the generalisability of this condition.

When only a differential tension is applied we see again that the slip zones are of opposite sign. The relevant side condition is

$$\int_b^a \frac{p(\xi) d\xi}{\sqrt{\xi^2 - b^2}} = \frac{\pi\sigma}{8\mu}. \tag{2.26}$$

For further details and explicit solutions when the contact is Hertzian please refer to [25].

In most practical problems the transient loading is not relevant. When periodic loading is applied, we are interested in the steady-state solution. First, we will briefly describe what happens when the normal load is constant, so that the contact patch is fixed in size. Imagine that we are moving between two points (Q_1, σ_1) and (Q_2, σ_2). Initially, as we start to move away from point 1, the shear traction there, $q_1(x)$, is locked in. As we move to point 2, where the shear traction, $q_2(x)$, is given by

$$\begin{aligned} q_2(x) = q_1(x) &+ \frac{Q_2 - Q_1}{\pi\sqrt{a^2 - x^2}} + \frac{(\sigma_{02} - \sigma_{01})\, x}{4\sqrt{a^2 - x^2}} \\ &+ \frac{E^*}{2\pi\sqrt{a^2 - x^2}} \left[\int_{b_1}^{a} \frac{\sqrt{a^2 - \xi^2}\, B_x^{\rightarrow}(\xi)\, d\xi}{\xi - x} + \int_{-a}^{-b_2} \frac{\sqrt{a^2 - \xi^2}\, B_x^{\rightarrow}(\xi)\, d\xi}{\xi - x} \right]. \end{aligned} \tag{2.27}$$

we expect there to be edge-of-contact slip zones occupying the intervals $[a \quad b_1]$ and $[-b_2 \quad -a]$. Hence, we anticipate having to distribute dislocations in those regions. The arrow superscript is added to denote loading from $1 \rightarrow 2$. As point 2 is

approached the slip zones will take their maximum extent. Just as the loading is reversed the shear traction, $q_2(x)$ becomes locked in. We now unload back to point 1, as that is approached we have

$$q_1(x) = q_2(x) - \frac{Q_2 - Q_1}{\pi\sqrt{a^2 - x^2}} - \frac{(\sigma_{02} - \sigma_{01})\, x}{4\sqrt{a^2 - x^2}} + \frac{E^*}{2\pi\sqrt{a^2 - x^2}} \left[\int_{b_1}^{a} \frac{\sqrt{a^2 - \xi^2}\, B_x^{\leftarrow}(\xi)\, d\xi}{\xi - x} + \int_{-a}^{-b_2} \frac{\sqrt{a^2 - \xi^2}\, B_x^{\leftarrow}(\xi)\, d\xi}{\xi - x} \right]. \quad (2.28)$$

We now subtract equation (2.27) from equation (2.28) and make several further observations.

First, within the slip intervals, the shear traction always reaches limiting friction, i.e.

$$q(x) = \pm \mu p(x). \quad (2.29)$$

Secondly, as in the steady state, all points must return to their original position. The dislocations inserted during the loading phase must precisely be annihilated by those inserted during the unloading phase, i.e

$$B_x^{\rightarrow}(x) = -B_x^{\leftarrow}(x). \quad (2.30)$$

These conditions, Eqs. (2.29,2.30) when combined with equations (2.27,2.28) enable us to write down a solitary integral equation for the steady state dislocation density during a loading change from $1 \rightarrow 2$ (or $2 \rightarrow 1$),

$$q_0(x) \equiv 2\mu p(x) \operatorname{sgn}(x) - \frac{Q_2 - Q_1}{\pi\sqrt{a^2 - x^2}} - \frac{(\sigma_{02} - \sigma_{01})\, x}{4\sqrt{a^2 - x^2}} \ldots = \frac{E^*}{2\pi\sqrt{a^2 - x^2}} \left[\int_{b_1}^{a} \frac{\sqrt{a^2 - \xi^2} B_x^{\rightarrow}(\xi)\, d\xi}{\xi - x} + \int_{-a}^{-b_2} \frac{\sqrt{a^2 - \xi^2} B_x^{\rightarrow}(\xi)\, d\xi}{\xi - x} \right]. \quad (2.31)$$

As with the simpler problems, frequently a full inversion is not needed - unless we wish to find the slip displacements - and the primary unknowns are the locations of the stick-slip interface points. These points may be determined from side conditions alone, arising from boundedness requirements, and correspond to Eqs. (2.25,2.26). We have introduced the quantity $q_0(x)$, and the side conditions are

$$\int_{b_1}^{a} \frac{q_0(\xi)\, d\xi}{\sqrt{(\xi - b_1)(\xi + b_2)}} = \int_{-a}^{-b_2} \frac{q_0(\xi)\, d\xi}{\sqrt{(\xi - b_1)(\xi + b_2)}} \quad (2.32)$$

and

$$\int_{b_1}^{a} \frac{q_0(\xi)\,\xi d\xi}{\sqrt{(\xi - b_1)(\xi + b_2)}} = \int_{-a}^{-b_2} \frac{q_0(\xi)\,\xi d\xi}{\sqrt{(\xi - b_1)(\xi + b_2)}} \tag{2.33}$$

These integrals are tractable [25, 26] when the contact pressure distribution is elliptical (the Hertz problem) and may be in other cases.

Although the formulation presented thus far expands the range of solutions that can be explored, it represents only a subset of the possibilities that the new technique enables. The approach remains neat and tractable in problems where the normal load varies, although, no solutions are known for contacts which may support a moment, and where the moment changes during loading variations. For this reason, the examples tackled to date are often based on a Hertzian contact, despite the formulation having greater applicability. We suppose that the contact moves in steady-state between two load states (P_1, Q_1, σ_1) and (P_2, Q_2, σ_2). Going from load state 1 to load state 2, in place of equation (2.27) we have

$$\begin{aligned} q_2(x) = q_1(x) &+ \left\{ \frac{Q_2 - Q_1}{P_2 - P_1} + \frac{\pi x}{4} \frac{\sigma_{02} - \sigma_{01}}{P_2 - P_1} \right\} \left[\, p(x; P_2) - p(x; P_1) \,\right] \\ &+ \frac{E^*}{2\pi\sqrt{a^2 - x^2}} \left[\int_{b_1}^{a} \frac{\sqrt{a^2 - \xi^2}\, B_x^{\rightarrow}(\xi)\, d\xi}{\xi - x} + \int_{-a}^{-b_2} \frac{\sqrt{a^2 - \xi^2}\, B_x^{\rightarrow}(\xi)\, d\xi}{\xi - x} \right]. \end{aligned} \tag{2.34}$$

which leads to a similar recipe to that given by equation (2.31), namely

$$\begin{aligned} q_0(x) \equiv\; & p(x; P_2) \left\{ \mu\ \mathrm{sgn}(x) + \frac{Q_2 - Q_1}{P_2 - P_1} + \frac{\pi x}{4} \frac{\sigma_{02} - \sigma_{01}}{P_2 - P_1} \right\} \\ & + p(x; P_1) \left\{ \mu\ \mathrm{sgn}(x) - \frac{Q_2 - Q_1}{P_2 - P_1} - \frac{\pi x}{4} \frac{\sigma_{02} - \sigma_{01}}{P_2 - P_1} \right\} \\ = \; & \frac{E^*}{2\pi\sqrt{a^2 - x^2}} \left[\int_{b_1}^{a} \frac{\sqrt{a^2 - \xi^2}\, B_x^{\rightarrow}(\xi)\, d\xi}{\xi - x} + \int_{-a}^{-b_2} \frac{\sqrt{a^2 - \xi^2}\, B_x^{\rightarrow}(\xi)\, d\xi}{\xi - x} \right]. \end{aligned} \tag{2.35}$$

2.6 Complete contacts

The first consideration of interfacial stick and slip conditions for complete contacts was carried out by Wright and O'Connor [27]. They considered the behaviour of a rectangular block pressed onto a dogbone specimen and carried out experiments with this configuration. In an attempt to inhibit slip in some tests, they used serrations, but the serrations formed were rather coarse. They also looked at the contact overall by the finite element method [28], but this was unsuccessful due to the computing power available to them at the time. Khadem and O'Connor [29, 30] had looked

analytically at the same problem using a series solution, but only conditions of full stick or zero friction could be treated.

The issues faced when attempting to analyse these types of contacts are two-fold. First, there is the difficulty of resolving slip zones using the standard linearisation methods of the stick-slip problems. Secondly, addressing these issues is complicated by the presence of an implied singularity in the state of stress near the contact edge. Note that we are interested in problems in which both bodies are elastic - usually with the same elastic constants. The solution sought is wholly different in character from those where the contact-defining body is made rigid [31].

Although we cannot analytically solve the tractions along the entire contact interface, we can focus on the edge behaviour local to the stress concentrations. By zooming-in to the contact edge, we can model the geometry as a semi-infinite wedge (of angle ϕ) pressed into a half-plane. Assuming that the coefficient of friction is sufficiently high to ensure the contact is fully adhered, we can treat the contact edge as a monolithic wedge of angle $2\alpha = \pi + \phi$. For example, the edge of a square punch has a semi-infinite wedge angle $\phi = \pi/2$ such that, when pressed into a half-plane, the overall wedge angle is $2\alpha = 3\pi/2$. Studying William's eigensolutions [32], we can solve for the near-edge stress state relative to the bisector of the wedge [33]. By defining the two general stress intensity factors that correspond to mode I (symmetric) and mode II (antisymmetric) loading, the stress state can be described by [7]

$$\sigma_{ij} = K_I r^{\lambda_I - 1} f_{ij}^I(\theta) + K_{II} r^{\lambda_{II} - 1} f_{ij}^{II}(\theta) \tag{2.36}$$

where r is the radius measured from the contact edge and θ is the angle measured anticlockwise from the wedge bisector. For the square block pressed into a half-plane, the eigenvalues are $\lambda_I = 0.5445$, $\lambda_{II} = 0.9085$. Therefore, as we approach the contact edge, the symmetric term dominates with just less than square-root singular behaviour.

Hills and Dini employed these eigensolutions to determine the critical coefficient of friction to maintain adhesion for complete contacts for various geometries. As the internal angle of the contacting body pressed into a half-plane decreases, the critical coefficient of friction increases. For a sharp square punch, the critical coefficient of friction is found to be $\mu = 0.543$ [34], shown in Fig.2.8. When the coefficient of friction is below this value, the edges of the contact slip (in an advancing contact sense) when the contact is formed. If a shear force is applied and the coefficient of friction quite large, the trailing edge of the contact is expected to separate. When separation occurs, normally following application of a shear force, the stresses no longer show singular behaviour, but are instead square-root bounded, as the trailing

edge (where it first occurs) is now incomplete in character.

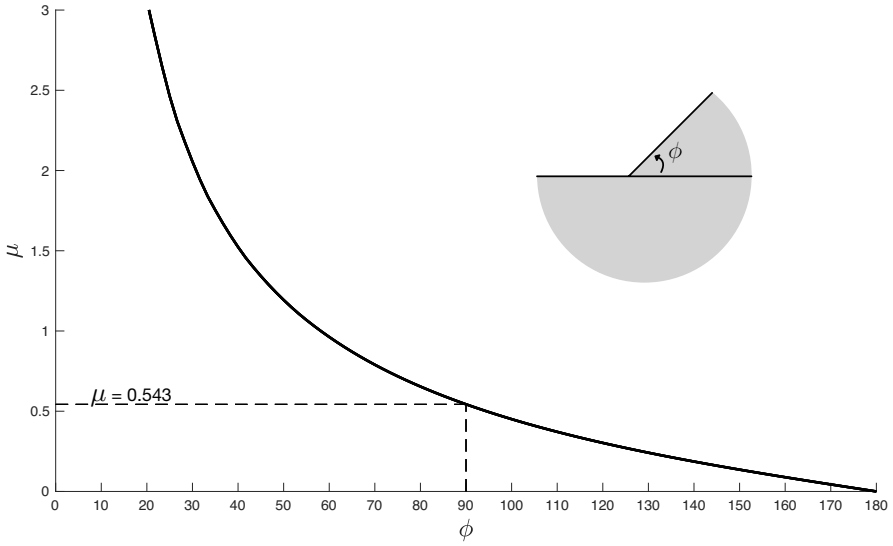


Figure 2.8: Critical coefficient of friction for a given internal wedge angle to maintain adhesion [34].

When a complete contact is subjected to shear loading and the coefficient of friction is both below the value needed to inhibit edge slip, but at the same time separation is averted, an analytical solution developed by Churchman and Hills can be employed to quantify the slip zone size [35]. This approach involves inserting glide dislocations along the adhered interface and solving the resulting stress integral equations. As anticipated, the slip zone length grows as the coefficient of friction decreases.

Fretting fatigue experiments in the 1960s were frequently carried out by having a rotating-bending dogbone with bridge-shaped pieces clamped to the sides. The feet of the bridge were invariably flat-faced, so that they produced conforming contacts. It was partly this which motivated Hattori [36, 37] to tackle the problem of the analysis of complete contacts. He recognised the presence of singular behaviour at the contact corners and was a proponent of using the boundary element method to analyse the contact overall. These ideas were also adopted by Dominguez and colleagues [38].

The sliding complete contact problem was first analyzed by Karuppanan, starting with the sharp square punch geometry [39]. In this case, the pressure distribution was shown to be strongly influenced by the coefficient of friction. Extending this analysis to other geometries, such as wedges with internal angles of 120° and 60°, it was found that both the wedge angle and coefficient of friction play a crucial role in determining the characteristic equation [40]. This equation governs the dominant

eigenvalue, which in turn defines the behaviour at the contact edges. The edges can fall into three categories of pressure distributions: fully stuck with singular edge behaviour, bounded behaviour, or edge separation characterised by subsequent square-root bounded behaviour. These distinctions are critical in understanding slip at the contact edges as the different types of edge behaviour significantly affect the pressure distributions.

2.7 Complete, common-edge contact

Our knowledge of common-edge contacts is limited, with little systematic evidence of what to expect generally, but a couple of examples, based on elementary beam and shaft theory, will tell us something. If we first consider two identical strips, or cylinders, to be fully adhered in contact, we can consider the equivalent problems of a monolithic beam or shaft, and obtain the bilateral solution across the cross-section, i.e. the interface, by using elementary beam/torsion theory.

First consider two identical strips in contact. When under a normal load, the normal traction across the width of the strip, and thus the interface, is a constant finite value equal to the normal load divided by the area of the cross section,

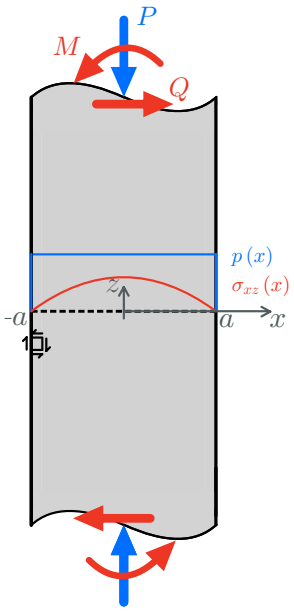
$$p(x) = \sigma_{zz}(x) = -\frac{P}{2at} \tag{2.37}$$

where a is the semi-width of the strip, t is the strip thickness, and the origin is measured from the centre of the interface, as seen in Fig.2.9. When under a shear load, Q, the shear traction across the interface falls to zero at both ends to satisfy the condition of free surfaces. If the coefficient of friction is great enough to prevent any slip along the interface, i.e. $q/p < \mu \ \forall r$, we can use beam theory to obtain the shear traction along the interface,

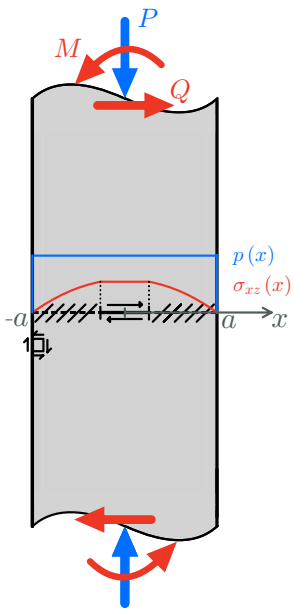
$$\sigma_{xz}(x) = \frac{3Q}{4at}\left(1 - \frac{x^2}{a^2}\right). \tag{2.38}$$

To keep the geometry in rotational equilibrium, a moment, M, must also be applied to the contacting bodies, but we can arrange for the interface to be positioned on the plane where the bending moment vanishes, for simplicity.

If the shear load is increased so that the coefficient of friction can no longer prevent slip, the central area of the contact will slip first, as shown in Fig. 2.9b. As the shear load increases, the slipping region expands outward, until the slipping region reaches the edges of the contact, at which point the interface enters full sliding.



(a) Two strips fully adhered.



(b) An interior region of slip.

Figure 2.9: Two identical strips, with semi-width a, loaded remotely by an axial force P, shear force Q, and corrective moment M to ensure equilibrium with no resultant moment along the interface. The normal and shear tractions along the interface are illustrated in blue and red, respectively. A shear surface element is drawn to show that the shear traction must be zero at the contact edges due to it being a traction-free surface.

The slip zone size can be found by using a corrective unilateral solution that alters the interfacial stress distribution until equilibrium conditions are met, this is carried out in detail in [41]. Note that the fully stuck interface is eroded from an interior point first, with slip extending to the free edges as sliding is approached.

If we now consider two identical cylinders in contact, each with radius a, the normal traction from a normal load P follows the same description as before,

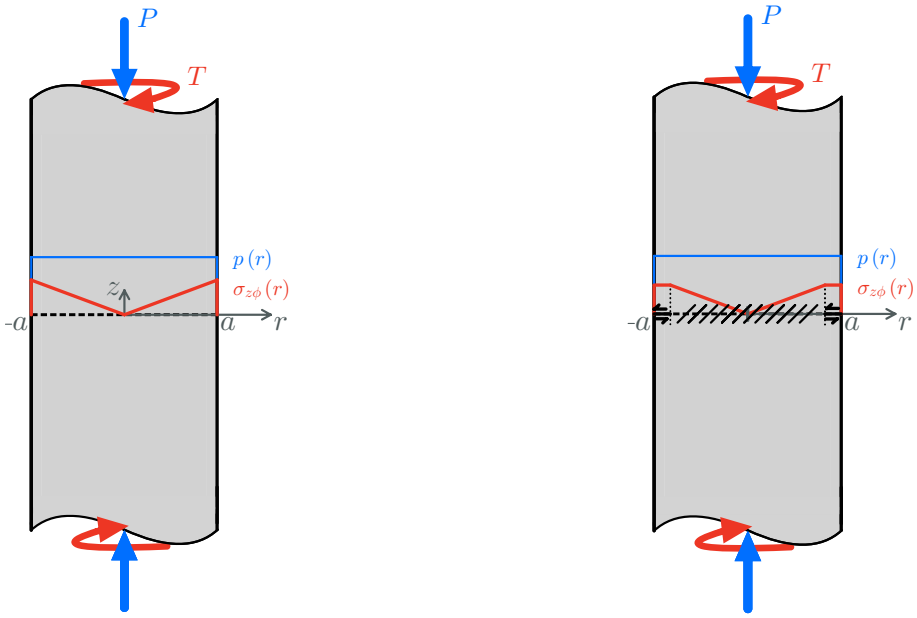
$$p(r) = \sigma_{zz}(r) = -\frac{P}{\pi a^2} \tag{2.39}$$

where a is the radius of the cylinders, and the origin is measured from the centre of the interface, as seen in Fig.2.10.

Provided the coefficient of friction is great enough to prevent any slip across the interface, when torsion is applied to the cylinder, as seen in Fig.2.10a, the shear stress can be described by

$$\sigma_{z\phi}(r) = \frac{2Tr}{\pi a^4}. \tag{2.40}$$

If the coefficient of friction is not high enough to inhibit slip, the outer edge of the contact will slip first as seen in Fig2.10b. In a 3-dimensional sense, the inner



(a) Fully adhered case; monolithic strip.

(b) Exterior regions of slip.

Figure 2.10: Two identical cylinders with semi-width a, loaded axially and under torsion. The normal and shear tractions along the interface are illustrated in blue and red, respectively.

core of the cylinder will be stuck and the outer annulus will slip. Increasing the torsional load increases the width of the slip regions until they meet in the centre and the cylinders undergo full-body sliding, manifested as spin. The extent of the slip zone regions can be found by introducing a corrective solution, as before, giving an implicit result where the applied torque can be found for any given slip zone size, treated in [42]. In the anti-plane (torsional) loading problem the fully stuck solution is eroded from the edges first, and the last point to slip is the centre of the cylinder.

When studying complete contacts experimentally, there can be many issues to be aware of, such as indenter misalignment, giving rise to a small edge step at the end of the interface, and therefore the contact behaves very locally in a complete (sharp edged) manner [43] and of course, wear in the contact can modify the contacting profile. In a plane problem, if slip extends to the free surface a step will inevitably be formed, whose size and significance will increase as the slip displacement increases. In the torsional problem and, indeed, more generally in problems which locally experience anti-plane slip, the profile will be preserved.

2.8 Receding contacts

Receding contacts also remain incompletely understood and there is no comprehensive approach for addressing all cases. Receding contact problems occur when the area of contact between two surfaces decreases under load [2]. These contacts can take various forms, such as a thin strip pressed against a surface, or a cylindrical pin loaded into a cylindrical hole of precisely the same diameter; the latter example merits a summary in Barber's book [1], however, in this review, we will focus on the former. We are interested in the problem of a point load pressing into a strip on a half-plane as it models the simplest form of a loaded layer on a surface, with many practical applications such as a bolted lap joints. When a layer is pressed onto a surface by an infinitesimal line load, the contact 'snaps' to a finite size. As the line load is increased, the contact size remains the same, independent of load, whilst the lift-off angle, displacements, strains and stresses are all proportional to the load [44].

To solve the semi-infinite strip pressed into a surface by a line force, we first centre the axes on the strip-surface interface, a distance equal to the thickness of the strip, c, below the half-plane surface. By applying a normal point load, P, at point $(0, c)$, as seen in Fig.2.11, we obtain the following bilateral solution for the normal traction $p(x, 0)$ and shear traction $q(x, 0)$ along the interface

$$p(x,0) = \frac{-2P}{\pi c}\frac{c^4}{(c^2+x^2)^2} \tag{2.41}$$

$$q(x,0) = \frac{2P}{\pi c}\frac{xc^3}{(c^2+x^2)^2}. \tag{2.42}$$

We note that these tractions are formulated on the assumption that there is no slip or separation along the interface. As we move along the infinite interface, at infinitely remote points, although both tractions decay to zero, the direct component does so more quickly than the shear component, so an infinitely high coefficient of friction is required to satisfy the condition of stick; for stick along the entire interface, $\mu = q(x,0)/p(x,0) = x/c$, thus $\mu c \leqslant |x| \leqslant \infty$. In reality, the coefficient of friction along the interface will be finite, resulting in slip over the intervals $a \leqslant |x| \leqslant \infty$ and we find in turn, separation over the interval $b \leqslant |x| \leqslant \infty$, where a and b are to be found. Chaise solves this problem by distributing glide dislocations to model slip, and climb dislocations to model the separation along the contact interface after an infinitesimal load is applied to restore the conventional unilateral (Signorini) contact inequalities [44], represented in Fig.2.12. It is found that the extent of slip and

[2] Dundurs included stationary contacts within this definition

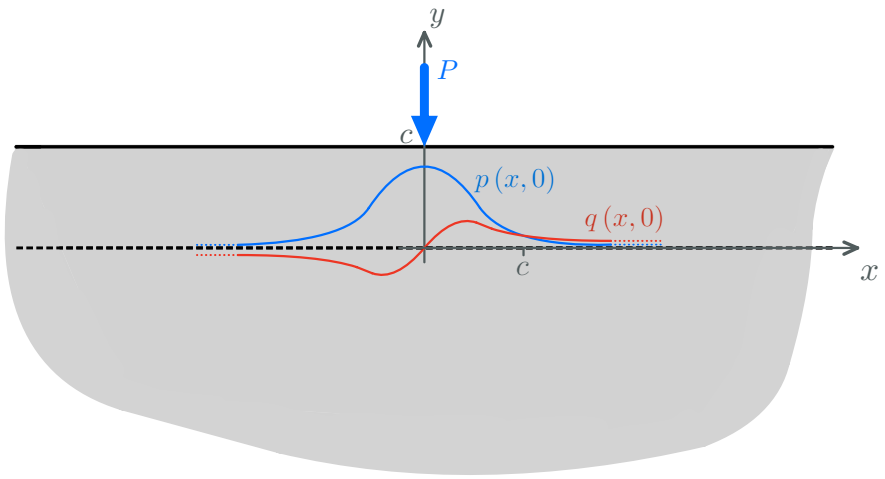


Figure 2.11: A depiction of the bilateral solution, obtained by a normal point load, P, pressed onto the surface of a half-plane. The semi-infinite strip is of thickness c and is fully adhered to the surface. The normal and shear tractions along the semi-infinite strip interface are illustrated by the blue and red lines, respectively.

intimate contact is a function of the coefficient of friction alone.

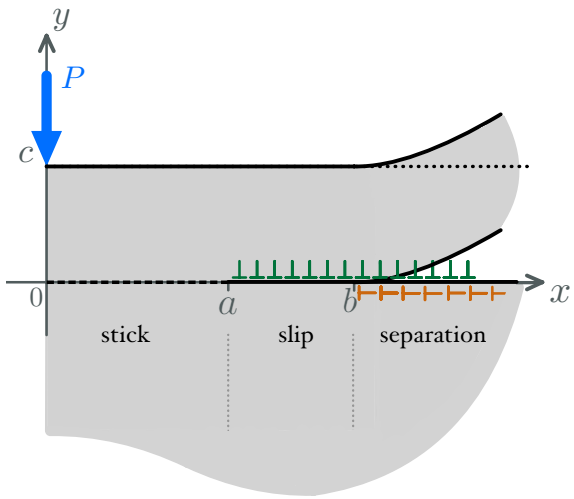


Figure 2.12: A semi-infinite strip, pressed onto a surface by a point load is fully stuck for $|x| \leqslant a$, in slip for $a \leqslant |x| \leqslant b$ and separated for all other values of x. The interface tractions follow the bilateral solution, corrected in the slip region by distributing glide dislocations (green), and in the separated region by distributing climb dislocations (orange).

For the receding contact problem of an elastic block pressed into a rigid surface, Ahn studied the effect of unloading and cyclic loading [45]. At the onset of decreasing the load, a stick zone initially forms at the edge of the contact, whilst the interior slip zones remain. As we continue to unload the contact, the edge stick zones advance to the centre of the contact. Reversing slip zones form at the contact edge and the

separation zones increase in size so that the overall contact continues to recede.

When the contact is reloaded, the contact behaviour changes from the initial loading phase; the contact size is no longer independent of load as it grows throughout the reloading stage. As cycles progress, the contact configuration continues to evolve such that many cycles are required to reach a steady-state condition [45]. By analysing this receding contact under oscillatory loading, it can be deduced that the contact experiences partial shakedown; the energy dissipated per cycle decreases with each successive cycle towards a steady state energy dissipation that is 56% of that from the initial cycle.

2.9 Shakedown

In each of the preceding sections we have described the partial slip state present in a range of contacts, usually found by a semi-analytical method (sometimes wholly analytical), because these problems continue to be very tricky to solve by commercial finite element codes, and achieve sufficient detail. In engineering practice, we would often like to understand what happens under some form of cyclic loading (perhaps excited by vibration), which may give rise to reversing cyclic slip. The underlying physical reasons for this are that the work done against friction gives rise to damping but, at the same time, it may also produce surface damage and hence promote the nucleation of a surface crack. Often, the transient problem will be irrelevant, and it is the steady state response which is of over-riding interest. The question therefore arises of whether we can obtain the steady state solution without tracking through the transient, and also whether the steady state solution depends on the loading path during the transient phase. Similar concepts apply to cyclically loaded elastic-plastic components: if, during the load cycle, the component enters the plastic state, when the load is removed again a residual state of stress will be left behind, and its character will be such that, during a subsequent cycle, the total stress state (due to both the applied loads and the residual stresses) will be milder than without the residual stress present. Thus, the self-developing residual stress state will drive the component towards behaving wholly elastically or *shaking down*.

In a contact problem the analogous process is that, during early transient cycles of load, if the contact is driven into a partial slip state, removing the loads again will not result in surface particles, once opposite each other, and displaced during slip, going back to their original positions. If we think of the 'dislocation' model of slip this is equivalent of saying that all the dislocations introduced during the loading cycle will not be annihilated - some will remain behind.

Returning to the plastic shakedown problem, one of the very useful theorems associated with the process is due to Melan [46] who, at its simplest, stated that if a body is loaded severely, cyclically, and initially into the plastic state is capable of attaining a residual state of stress such that it will become wholly elastic, then the body certainly will shake down. In other words, if some residual stress state can be postulated which, together with the applied elastic stresses at all points during the loading cycle is wholly elastic, the system certainly will shake down at at least the load where the calculation was undertaken. Thus, it may be possible to avoid having to track the evolving stress state during each cycle. The question is 'Does the Melan theorem apply to frictional contacts?' that is, do they inevitably move towards a fully stuck state and become fully stuck if possible. This question has been studied very extensively by Barber, Klarbring, Spagnoli and colleagues. The mathematical foundations are provided in Klarbring et al [3], and Barber et al [47]. A key result of their work is that contact problems which do not exhibit normal-tangential coupling follow Melan's theorem; that is, if shakedown is possible then it will be achieved, regardless of any transient loading path. On the other hand, systems which do exhibit coupling and which, for some transient paths, do achieve a shaken down (i.e. fully stuck) state may not do so in all cases. The concept of load factors was introduced in civil engineering many years ago in plastic design, and it has been borrowed for use in frictional contact problems. It is simply a dimensionless load, and the reference value might be taken as the force where the first particle slips. It is invariably given the symbol λ.

Early examples studied to demonstrate these principles often used discrete systems, rather than continuous contacts [48], in which a two-node problem is studied. Or, in Jang and Barber [49] a study was made of a solid containing small cracks, so that each might be open, or closed and stuck, or closed and slipping, and this displays a further property of coupled systems, via. a sequence of critical load factors that may be defined; (a) λ_1, below which shakedown will occur for all initial conditions, (b), λ_2, so that when $\lambda_1 < \lambda < \lambda_2$, shakedown will occur for some initial loading paths, but not for all, and when there is steady state slip the amount of energy dissipated will vary depending on the transient path taken, (c) λ_3, such that when $\lambda_2 < \lambda < \lambda_3$ the system will certainly not shake down, but the steady state dissipation of frictional energy per cycle will vary, and finally when $\lambda > \lambda_3$, not only will there be steady state frictional energy dissipation but its value is unique for a given value of λ, and independent of the transient path. The results were reviewed by Barber [50] and in this paper, a further system load factor, λ_4 was introduced. If $\lambda_3 < \lambda < \lambda_4$ the system could be expected asymptotically to approach a unique steady state

dissipative state, whereas at very high loads, $\lambda > \lambda_4$ a steady state condition is reached within a very small number of cycles, and every node (or point) in the system can be expected to slip at some stage (so there must be the possibility of relative rigid body motion). The effect of phase shift was explored by Jang and Barber [51]. The next stage in the development of our understanding came when the possibility of frictional slip along the contact interface together with plastic shakedown, for discrete systems, was formulated by Barber, Klarbring, Spagnoli and Terzano in two important papers [52, 53]. This was followed by a comprehensive numerical study in [54], and a review of the progress of all of the above was published by Ahn et al [55].

Continuous contacts displaying the properties analysed in the above paragraphs are relatively uncommon, but a 'contact without end', Figure 1(e) was studied by Cwiekala and others [56, 4, 57] in the form of a shrink fitted disk held in a cavity within an infinite plane, and subject to a radial force and torque. The radial force was not sufficiently large to cause separation, so that the entire edge of the disk was in contact, and hence the contact pressure was always finite at every point. This configuration, which displays coupling, enabled shakedown to be investigated in a moderately realistic setting.

2.10 Conclusion

This review has set out the established methods for analysing the partial-slip behaviour of two-dimensional elastic contacts, and identified where those methods break down. The starting point, due to Cattaneo [8] and Mindlin [9] and formalised in plane form by Jaeger [11] and Ciavarella [5], treats the contact as two half-planes pressed together under a constant normal load with a monotonically applied shear force. From this base, more general loading histories can be tackled, such as a varying normal load and bulk tension parallel with the interface, either by the superposition arguments of Barber and Truelove [58, 59] or by the edge-dislocation formulation expressed as coupled Cauchy singular integral equations [24, 25]. For complete contacts, where one or both contacting bodies have an abrupt corner against the interface, Williams' eigensolutions [32] characterise the near-edge stress field, and the calculations of Dini and Hills [34] give the critical coefficient of friction needed to maintain adhesion at the corner. Common-edge contacts and receding contacts have been treated separately, the former through elementary beam and torsion theory in the fully adhered case and through corrective unilateral analysis once slip occurs [41], the latter through Chaise's superposition of the normal-loading solution with a corrective dislocation-density field [44].

Each of these methods is built around a single assumption about the geometry of the contacting bodies, applied globally. Half-plane partial-slip solutions treat both bodies as half-planes throughout the contact, so that the half-plane integral relation applies at every point along the interface. Complete-contact analyses assume that the contact-defining body has a sharp corner at the contact edge, so that Williams' singular eigensolution describes the contact tractions along the interface. Receding-contact solutions assume a thin elastic strip pressed onto a half-plane, with the same square-root bounded edge field at both ends of the contact. Each method therefore takes its geometric assumption as a global statement that must hold across the entire contact, even when the real contact does not reflect this assumption along the entire interface.

This restricts the literature in a way that is particularly inconvenient for engineering practice. A great many of the contact geometries that matter in fretting-fatigue applications, such as the dovetail roots of turbine blades, friction-grip bolted joints, subsea locking segments, are flat-and-rounded contacts with vertical traction-free edges and a moderate flat-to-rounded length ratio. These cannot be represented globally as two half-planes, because the traction-free vertical faces violate the half-plane idealisation away from the curved edge; nor can they be represented as complete contacts, because the curved edges produce square-root bounded rather than singular near-edge fields. They therefore sit in the gap between the established methods. Existing analyses either treat the whole contact using half-plane theory, potentially incurring large errors in the near-edge stress state when the flat segment is long, or rely on case-by-case finite-element computation, which is computationally expensive and noisy in the very region (the contact edge) that controls fretting-fatigue crack nucleation. No closed-form framework currently exists for the partial-slip behaviour of these geometries, nor for the way in which the two edges of a single contact may exhibit different slip states under the same external loading because of geometric coupling between normal and shear.

The remainder of this thesis is directed at this gap. Chapter 3 introduces a wedge-and-half-plane matching technique that delivers closed-form near-edge tractions for a rounded quarter-plane pressed into an elastically similar half-plane, capturing the influence of an adjacent vertical free surface for the first time. Chapter 4 maps out the range of flat-and-rounded geometries for which this matched solution outperforms half-plane theory, providing quantitative guidance for practitioners. Chapter 5 extends the framework to partial slip under multi-stage and cyclic loading by expressing the near-edge behaviour in terms of stress intensity factors that quantify changes in contact-edge position and shear traction; this makes it possible to import

the half-plane partial-slip machinery reviewed above into geometries where half-plane theory is not globally valid. Chapter 6 shows that the same edge descriptors can be used to design experimental equivalence between a complicated contact configuration (a plane receded contact) and a standard Hertzian laboratory test, opening a practical route from analysis to experiment for fretting-fatigue characterisation.

References

[1] J.R. Barber. *Contact Mechanics*. Solid Mechanics and Its Applications. Springer International Publishing, 2018, 29–39. ISBN: 9783319709390. URL: https://books.google.co.uk/books?id=4GNLDwAAQBAJ.

[2] J. Dundurs. "Discussion of edge bonded dissimilar orthogonal elastic wedges under normal and shear loading". in *ASME Journal of Applied Mechanics* 36.3 (1969), 650–652.

[3] A. Klarbring, M. Ciavarella and J. R. Barber. "Shakedown in elastic contact problems with Coulomb friction". in *International Journal of Solids and Structures* 44 (2007), 8355–8365.

[4] N. Cwiekala, J. R. Barber and D. A. Hills. "Frictional shakedown of a coupled continuous contact". in *International Journal of Solids and Structures* 274 (2023), 112293.

[5] M. C. Ciavarella. "The generalised Cattaneo partial slip plane problem. Part 1: Theory, Part 2: Examples". in *International Journal of Solids and Structures* 35 (1998), 2349–2378. DOI: https://doi.org/10.1016/S0020-7683(97)00154-6. URL: https://www.sciencedirect.com/science/article/pii/S0020768397001546.

[6] Daniele Dini and David Nowell. "Prediction of the slip zone friction coefficient in flat and rounded contact". in *Wear* 254 (2003), 364–369. DOI: 10.1016/S0043-1648(03)00010-3.

[7] David A. Hills and Hendrik N. Andresen. *Mechanics of Fretting and Fretting Fatigue*. Solid Mechanics and Its Applications. Published: 25 April 2021. Springer Cham, 2021. ISBN: 978-3-030-70745-3. DOI: 10.1007/978-3-030-70746-0. URL: https://doi.org/10.1007/978-3-030-70746-0.

[8] C. Cattaneo. "Sul Contato di due corpi elastici". in *Atti Accad Naz Lincei, Cl Sci Fis, Mat Rend* 27 (1938), 342–348, 434–436, 474–478.

[9] R. D. Mindlin. "Compliance of Elastic Bodies in Contact". in *ASME Trans J Appl Mech* 16 (1949), 259–268.

[10] K. L. Johnson. *Contact Mechanics*. Cambridge University Press, 1985.

[11] J. Jaeger. "Ein Neues Prinzip der Kontaktmechnik". in *ZAMM* 77.S1 (1997), 143–144.

[12] Richard. Munisamy, David A. Hills and David Nowell. "Static Axisymmetric Hertzian Contacts Subject to Shearing Forces". in *Journal of Applied Mechanics* 61 (1994), 278–283. URL: https://api.semanticscholar.org/CorpusID:119835729.

[13] D. Nowell and D. A. Hills. "On the Mechanics of Fretting Fatigue". in *Wear* 125.1–2 (1988), 129–146.

[14] Jesús Vázquez, Carlos Navarro and Jaime Domínguez. "Explicit equations for the half-plane sub-surface stress field under a flat rounded contact". in *Proceedings of the Institution of Mechanical Engineers, Part J: Journal of Engineering Tribology* 228.10 (2014), 1164–1175.

[15] Nikolai Ivanovich Muskhelishvili. *Some basic problems of the mathematical theory of elasticity*. 2nd. Translated from Russian by J.R.M. Radok. Groningen, Netherlands: Noordhoff International Publishing, 1953.

[16] M Ciavarella and G Macina. "New results for the fretting-induced stress concentration on Hertzian and flat rounded contacts". in *International Journal of Mechanical Sciences* 45.3 (2003), 449–467. ISSN: 0020-7403. DOI: https://doi.org/10.1016/S0020-7403(03)00061-4. URL: https://www.sciencedirect.com/science/article/pii/S0020740303000614.

[17] Jesús Vázquez, Carlos Navarro and Jaime Domínguez. "Analytical solution for a cylindrical contact with reverse slip". in *The Journal of Strain Analysis for Engineering Design* 48.3 (2013), 189–197. DOI: 10.1177/0309324712466977. URL: https://doi.org/10.1177/0309324712466977.

[18] V. I. Mossakovskii. "Application of the reciprocity theorem to the determination of the resultant forces and moments in three-dimensional contact problems (in Russian)". in *PMM* 17 (1953), 477–482.

[19] D. A. Hills, M. Davies and J. R. Barber. "An incremental formulation for half-plane contact problems subject to varying normal load, shear and tension". in *Journal of Strain Analysis* 46 (2011), 436–443.

[20] A. Sackfield, C. Truman and D. A. Hills. "The tilted punch under normal and shear loads (with application to fretting tests)". in *International Journal of Mechanical Sciences* 43 (2001), 1881–1892.

[21] J. R. Barber, M. Davies and D. A. Hills. "Frictional Elastic Contact with periodic loading". in *International Journal of Solids and Structures* 48 (2011), 2041–2047.

[22] M. R. Moore and D. A. Hills. "Solution of half-plane problems using distributed climb dislocations". in *International Journal of Solids and Structures* 147 (2018), 61–66.

[23] D. A. Hills, P. A. Kelly, D. N. Dai and A. M. Korsunsky. *Solution of Crack Problems: The Distributed Dislocation Technique*. Solid Mechanics and Its Applications; 44. Springer Dordrecht, 2013. DOI: https://doi.org/10.1007/978-94-015-8648-1.

[24] D. A. Hills, R. Ramesh, J. R. Barber and M. R. Moore. "Methods to solve half-plane partial slip contact problems". in *International Journal of Solids and Structures* 155 (2018), 155–159.

[25] M. R. Moore, R. Ramesh, D. A. Hills and J. R. Barber. "Half-plane partial slip contact problems with a constant normal load subject to a shear force and differential bulk tension". in *Journal of the Mechanics and Physics of Solids* 118 (2018), 245–253.

[26] H. Andresen, D. A. Hills, J. Barber and J. Vázquez. "Steady state cyclic behaviour of a half-plane contact in partial slip subject to varying normal load, moment, shear load and moderate bulk tension". in *International Journal of Solids and Structures* 182 (2020), 156–161.

[27] G. P. Wright and J. J. O'Connor. "The influence of fretting and geometric stress concentrations on the fatigue strength of clamped joints". in *Proceedings of the Institution of Mechanical Engineers* 186 (1972), 827–835.

[28] G. P. Wright. "Studies in fretting fatigue with special reference to the effect of stress distributions on the fatigue strength of assembled components". DPhil thesis. University of Oxford, 1970.

[29] R. Khadem and J. J. O'Connor. "Adhesion or frictionless compression of an elastic rectangle between two identical half-spaces". in *International Journal of Engineering Science* 7 (1969), 153–168.

[30] R. Khadem and J. J. O'Connor. "Axial compression of an elastic cylinder in contact with two identical half-spaces". in *International Journal of Engineering Science* 7 (1969), 785–800.

[31] A. Mugadu and D. A. Hills. "The evolution of the process zone when a complete contact is subject to cyclically varying loads". in *International Journal of Solids and Structures* 40.18 (2003), 4417–4435.

[32] M. L. Williams. “Stress singularities resulting from various boundary conditions in angular corners of plates in extension”. in *Journal of Applied Mechanics* 19 (1952), 526–528.

[33] J. R. Barber. *Elasticity*. Dordrecht, MA: Kluwer Academic Publishers, 1992.

[34] D. A. Hills and D. Dini. “What level of friction guarantees adhesion in a complete contact?” in *The Journal of Strain Analysis for Engineering Design* 39.5 (2004), 549–551. DOI: 10.1243/0309324041896425.

[35] C.M. Churchman and D.A. Hills. “Slip zone length at the edge of a complete contact”. in *International Journal of Solids and Structures* 43.7-8 (2006), 2037–2049. DOI: 10.1016/j.ijsolstr.2005.06.099.

[36] T. Hattori, M. Nakamura and T. Watanabe. “Simulation of Fretting Fatigue life by using stress singularity parameters and fracture mechanics”. in *Tribology International* 36 (2003), 87–97.

[37] T. Hattori, V. Trung Kien and M. Tamashita. “Fretting fatigue life estimations based on fretting mechanisms”. in *Tribology International* 44 (2011), 1389–1393.

[38] L. Bohorquez and J. Dominguez. “Characterisation of the contact between a punch and a half-infinite substrate in a fretting situation”. in *International Journal of Mechanical Sciences* 49.5 (2007), 608–621.

[39] S Karuppanan, C Churchman, D Hills and E Giner. “Sliding frictional contact between a square block and an elastically similar half-plane”. in *European Journal of Mechanics A-Solids* 27.3 (2008), 443–459.

[40] S Karuppanan and D Hills. “Sliding of general frictional complete contacts”. in *International Journal of Mechanical Sciences* 50.9 (2008), 1404–1410.

[41] M. E. Kartal, J. R. Barber, D. A. Hills and D. Nowell. “Partial slip problem for two semi-infinite strips”. in *International Journal of Engineering Science* 49 (2011), 203–211. DOI: 10.1016/j.ijengsci.2010.11.007.

[42] M. Kartal, D. A. Hills, D. Nowell and J. R. Barber. “Torsional contact between elastically similar flat-ended cylinders”. in *International Journal of Solids and Structures* 47 (2010), 1375–1380. DOI: 10.1016/j.ijsolstr.2010.01.021.

[43] Zoë Clark, Rangarajan Ramesh and David A Hills. “Edge slip zone size of misaligned common edge contacts”. in *The Journal of Strain Analysis for Engineering Design* 52.7 (2017), 450–454. DOI: 10.1177/0309324717724261.

[44] T. Chaise, R.J.H. Paynter and D.A. Hills. "Contact analysis of a semi-infinite strip pressed onto a half plane by a line force". in *International Journal of Mechanical Sciences* 81 (2014), 60–64. ISSN: 0020-7403. DOI: https://doi.org/10.1016/j.ijmecsci.2014.02.001. URL: https://www.sciencedirect.com/science/article/pii/S0020740314000411.

[45] Young Ju Ahn and J. R. Barber. "Response of frictional receding contact problems to cyclic loading". in *International Journal of Mechanical Sciences* 50 (2008), 1519–1525. DOI: 10.1016/j.ijmecsci.2008.08.003.

[46] E. Melan. "Theorie statisch unbestimmter Systeme aus ideal-plastischem Baustoff". in *Sitz.Berl.Ak.Wiss* 145 (1936), 195–218.

[47] J. R. Barber, A. Klarbring and M. Ciavarella. "Shakedown in frictional contact problems for the continuum". in *Comptes Rendus Mecanique* 336 (2008), 34–41. DOI: 10.1016/j.crme.2007.10.008.

[48] Young Ju Ahn, Enrico Bertocchi and J. R. Barber. "Shakedown of coupled two-dimensional discrete frictional systems". in *Journal of the Mechanics and Physics of Solids* 56 (2008), 3433–3440. DOI: 10.1016/j.jmps.2008.09.003.

[49] Yong Hoon Jang and J. R. Barber. "Frictional energy dissipation in materials containing cracks". in *Journal of the Mechanics and Physics of Solids* 59 (2011), 583–594.

[50] J. R. Barber. "Nominally static frictional contacts under periodic loading". in *Journal of Strain Analysis* 51 (2016), 270–278. DOI: 10.1177/0309324715602844.

[51] Yong Hoon Jang and J. R. Barber. "Effect of phase on the frictional dissipation in systems subjected to harmonically varying loads". in *European Journal of Mechanics A/Solids* 30 (2011), 269–274.

[52] A. Klarbring, J. R. Barber, A. Spagnoli and M. Terzano. "Shakedown of discrete systems involving plasticity and friction". in *European Journal of Mechanics / A Solids* 64 (2017), 160–164. DOI: 10.1016/j.euromechsol.2017.02.006.

[53] A. Spagnoli, M. Terzano, J. R. Barber and A. Klarbring. "Non-linear programming in shakedown analysis with plasticity and friction". in *Journal of the Mechanics and Physics of Solids* 104 (2017), 71–83. DOI: 10.1016/j.jmps.2017.04.006.

[54] A. Spagnoli, G. Beccarelli, M. Terzano and J. R. Barber. "A numerical study on frictional shakedown in large-scale three-dimensional conforming elastic contacts". in *International Journal of Solids and Structures* 217 (2021), 1–14. DOI: 10.1016/j.ijsolstr.2021.01.024.

[55] Y. J. Ahn, A. Klarbring, A. Spagnoli and M. Terzano. "Shakedown in frictional contact of discrete elastic systems: A review". in *International Journal of Solids and Structures* 241 (2022).

[56] N. Cwiekala, J. R. Barber and D. A. Hills. "Memory-free loading paths for a coupled continuous contact problem with friction". in *Mechanics Research Communications* 124 (2022). DOI: 10.1016/j.mechrescom.2022.103958.

[57] N. Cwiekala, J. R. Barber and D. A. Hills. "Frictional shakedown of a coupled continuous contact". in *International Journal of Solids and Structures* 274 (2023).

[58] J.R. Barber, M. Davies and D.A. Hills. "Frictional elastic contact with periodic loading". in *International Journal of Solids and Structures* 48.13 (2011), 2041–2047. ISSN: 0020-7683. DOI: https://doi.org/10.1016/j.ijsolstr.2011.03.008. URL: https://www.sciencedirect.com/science/article/pii/S0020768311001041.

[59] J.P.J. Truelove, L.E. Blades and D.A. Hills. "Half-plane contact problems in partial slip with varying normal and tangential loads". in *European Journal of Mechanics - A/Solids* 94 (2022), 104590. ISSN: 0997-7538. DOI: https://doi.org/10.1016/j.euromechsol.2022.104590. URL: https://www.sciencedirect.com/science/article/pii/S0997753822000699.

Chapter 3

Near Edge Tractions for a Rounded Quarter-plane Pressed into an Elastically Similar Half-plane

Contents

3.1 Introduction 46

3.2 Asymptotic representation of the state of Stress 48

3.2.1 Finite (b/d finite) 50

3.2.2 Validity of the asymptotic series expansion 50

3.3 Semi-infinite flat punches with rounded edges 52

3.3.1 Half-plane formulation 52

3.3.2 Three-quarter plane formulation 55

3.3.3 Pure Mode I Loading 55

3.3.4 Pure Mode II Loading 58

3.4 Conclusion 61

The work presented in this chapter builds directly on the literature review in Chapter 2, and addresses the identified gap concerning non-conforming contacts that cannot be adequately represented using classical half-plane assumptions. In particular, conventional approaches are known to perform poorly when applied to contacting geometries involving a flat contact with rounded edges and vertical traction-free sides, as the stress field deviates from the idealised half-plane solution.

This chapter presents research published as:

> **B. Eames**, D.A. Hills, M.R. Moore, Near edge tractions for a rounded quarter-plane pressed into an elastically similar half-plane, *Tribology International*, Volume 186, 2023, 108582, ISSN 0301-679X, [https://doi.org/ 10.1016/j.triboint.2023.108582].

This paper represents a significant contribution to the literature by providing, for the first time, a closed-form representation of the contact tractions local to a non-conforming contact edge, while explicitly accounting for the presence of a nearby traction-free vertical boundary. The formulation captures the local stress behaviour with substantially greater fidelity than traditional half-plane methods, which neglect such geometric coupling effects.

The methodology developed herein forms the foundation for subsequent chapters, where the approach is extended to finite contacts and then to contacts subject to complex loading histories. Throughout, the predictions are compared to traditional half-plane solutions and Finite Element Analysis, thereby demonstrating both the accuracy and practical applicability of the proposed framework.

Near Edge Tractions for a Rounded Quarter-plane Pressed into an Elastically Similar Half-plane

B Eames[1], D A Hills[1] and M R Moore[2]

[1]*Department of Engineering Science, University of Oxford, Parks Road, Oxford, OX1 3PJ, UK*

[2]*Department of Mathematics, University of Hull, Kingston-upon-Hull, HU6 7RX, UK*

Abstract

Asymptotic forms are a useful way of representing the state of stress at a contact edge, allowing us to characterise the region in which cracks nucleate. The asymptotes must match the behaviour implied by the local geometry. In this paper, we study the behaviour of a flat contact with a circular arced edge (i.e. a flat and rounded contact); a geometry that has extensive applications. We show explicitly how the very convenient closed-form solution for this problem, derived from half-plane theory, may be collocated into the more realistic three-quarter plane far field solution, obtained from Williams' solution. This provides a closed-form representation of the edge, correctly geared to the far-field solution, for the first time.

3.1 Introduction

Our high-level goal is to produce a rigorous match between prototypical problems suffering from fretting fatigue and the conditions present in laboratory experiments measuring fretting strength, with the intention of applying the idea to a wide range of applications. Cracks invariably start at or very near the contact edge [1]. The general philosophy is to match by using a set of asymptotic forms to describe the hinterland, a method which we have developed here over several years [2, 3, 4], and which has also been independently developed [5, 6, 7], in a slightly different form. We restrict ourselves to problems in which the contact is convex in form, and hence incomplete in character. This means that very close to the edge of the contact, and regardless of whether or not the contact overall may be described using half-plane theory, local surface tractions and corresponding displacements will be related by Flamant (half-plane) theory. Hence the contact pressure, $p(x)$, and shear traction, $q(x)$ may always be approximated by a single term, square root bounded in form, defined by a multiplier, L_I and L_{II} respectively so that

$$p(x) = L_I\sqrt{x} + O(x^{3/2}) \quad \text{as} \quad x \to 0, \tag{3.1}$$

$$q(x) = L_{II}\sqrt{x} + O(x^{3/2}) \quad \text{as} \quad x \to 0, \tag{3.2}$$

where x measures distance from the left-hand contact edge, as depicted schematically in Fig. 3.1. In practice, this single term may only apply over a very small distance from the contact edge and it is the goal of this paper to both categorize this and offer a possible remedy.

Later in this paper, we will investigate the different formulations of the problem for both pure mode I and II loading, as in [8]. Mode I loading is when the stress is orthogonal, and mode II when the stress is parallel, to the bisector of the three-quarter plane. Fig. 3.1 is a schematic representation of the incomplete contact between a semi-infinite flat and rounded punch (Body 1) and a half-plane (Body 2). $K_{I[1/2]}$ and $K_{II[1/2]}$, displayed in Fig. 3.1, are the square-root singular multipliers on modes I and II loading which emerge from the half-plane formulation. For an observation point remote from the contact edge, the edge radius becomes insignificant, and, if there is no remote slip, the domain can resemble a three-quarter plane (i.e. a large wedge of angle $3\pi/2$). $K_{I[3/4]}$ and $K_{II[3/4]}$, also labelled in Fig. 3.1, are the generalised stress intensity factors, acting as multipliers on Williams' modes I and II eigensolutions, in a wedge sense (cf. [9, 10] for an extensive discussion of the Williams' solution).

Irreversibilities occur in the 'process zone'. The approach outlined hinges on the process zone being contained wholly within a hinterland in which the (L_I, K_{II}) fields dominate the character of the (elastic) state of stress. We have recently looked at the properties of series expansions of the near-edge fields, beyond the first term [11]. Here we will just repeat, briefly the results of a representation of the singular shear traction:

$$q_{\text{local}}(x) = \frac{K_{II}^{\pm}}{\sqrt{x}} + L_{II}^{\pm}\sqrt{x} + M_{II}^{\pm}(x)^{3/2} + O\left(x^{5/2}\right) \quad \text{as} \quad x \to 0, \tag{3.3}$$

where the multipliers are given in [11] and show that the first term alone captures the state of stress well for a significant fraction of the contact size in a Hertzian contact.

Many of the early tests on fretting fatigue strength, when our understanding of its mechanics was in its infancy, used the Hertzian contact. However, a great many practical contacts have a central flat form, say of half-length b, and end radii, R, such as the finite punch displayed schematically in Fig. 3.2a. Applications include contacts found in the root of gas turbine fan blade dovetails [12], or in the locking segments of riser-seabed connectors. Analysing these problems introduces several new features. The first is the question of how well the asymptotic expansion near the contact edge models the contact pressure. Assumptions include that, in this

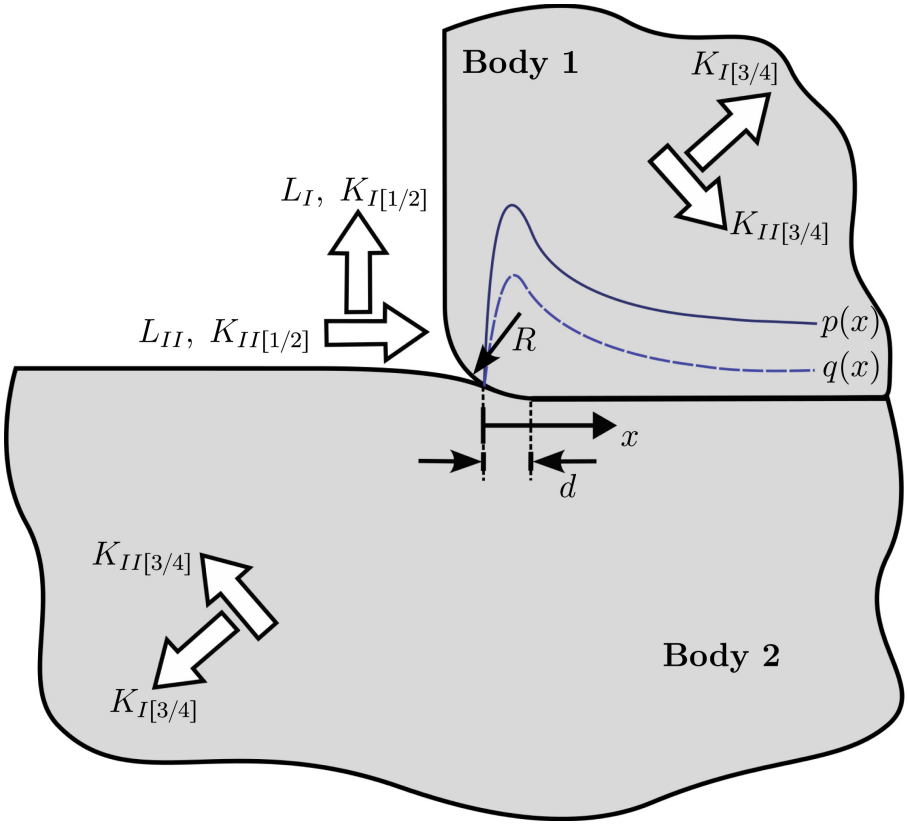


Figure 3.1: An undeformed schematic representation of a semi-infinite flat and rounded punch indenting a half-plane. Here, x denotes distance from the left-hand edge of the contact region, d denotes the length of the curved section in the contact, R the radius of curvature of the rounded part of the punch. $K_{I[3/4]}$, $K_{II[3/4]}$ and $K_{I[1/2]}$, $K_{II[1/2]}$ are the generalised stress intensity factors acting as multipliers for modes I and II, for a three-quarter plane and half-plane formulation, respectively. Illustrative profiles of the contact pressure $p(x)$ and shear tractions $q(x)$ are indicated for reference.

region, the contact is well represented by half-plane theory, which is treated in the next section. Secondly, a deeper question then surfaces of how interior properties of the contact, where half-plane theory does not apply, control the overall properties of the contact. In particular, what happens at the contact edge? This aspect is treated comprehensively in subsequent sections.

3.2 Asymptotic representation of the state of Stress

One method to improve the fidelity of the solitary term, Eq.(3.1), is to employ an asymptotic expansion, including higher-order terms in the asymptotic approximation.

Considering d, the contact length in the curved section, and $2b$, the flat length of the contact, permits us to have solutions for three different types of contacts:

- Hertzian contacts, $b/d \to 0$;
- finite contacts, b/d is finite;
- semi-infinite contacts, $b/d \to \infty$.

We discuss these in turn.

The exact solution for the normal contact pressure in the Hertz case [10] can be written as

$$p(x) = -\frac{2P\sqrt{d^2 - (x-d)^2}}{\pi d^2}, \tag{3.4}$$

where P is the constant downward normal force from the contact (see, for example, [10]). For the Hertz problem, we note that the entire contact length is curved: thus, d is also considered the half-length of the entire contact.

As seen in [13], the multiplier L_I may be shown to be

$$L_I = \frac{E^*}{R}\sqrt{\frac{d}{2}}, \tag{3.5}$$

where E^* is the plane strain modulus. In general, the normal force may be related to the contact half-width d via

$$-P(d) = \frac{\pi E^* d^2}{4R}. \tag{3.6}$$

As the normal force is uniform in the present analysis, i.e. $P(d) = P$, we can rewrite (3.4) to be in terms of L_I,

$$p(x) = \frac{L_I\sqrt{d}}{\sqrt{2}}\sqrt{1 - \left(\frac{x-d}{d}\right)^2}. \tag{3.7}$$

Hence, to find the asymptotic form of (3.7), we can assume x/d is small and take the Taylor expansion for $x/d \ll 1$,

$$p(x) = L_I\sqrt{x}\left(1 - \frac{x}{4d} - \frac{x^2}{32d^2} + O(x^3)\right), \tag{3.8}$$

so we readily obtain the next two terms in the approximation (as discussed previously in [11]).

3.2.1 Finite (b/d finite)

For the finite contact case, the exact solution is non-trivial and requires solving an integral equation, which can be found in [11] (see Eq.(20) therein). The expressions for the coefficients of the first three terms in the asymptotic expansion may also be found in [11] as Eqs.(4) and (21–23), respectively. We note here that, in [11], 'x' is defined as the coordinate measured from the centre of the contact, rather than the left contact edge. In this paper, we will continue to define 'x' as the coordinate measured from the left contact edge for consistency with the semi-infinite case.

Finally, for the semi-infinite case, when a normal load is applied, the exact solution for the contact pressure induced is given in [14]

$$p(x) = \frac{L_I}{4\sqrt{d}}\left[2\sqrt{dx} + (x-d)\ln\left|\frac{1-\sqrt{x/d}}{1+\sqrt{x/d}}\right|\right] \qquad x > 0. \tag{3.9}$$

Taking a Taylor series expansion of the full solution, we can write the asymptotic pressure distribution in the form

$$p(x) = L_I\sqrt{x}\left(1 - \frac{x}{3d} - \frac{x^2}{15d^2} + O(x^3)\right) \qquad \text{as} \quad x/d \to 0 \tag{3.10}$$

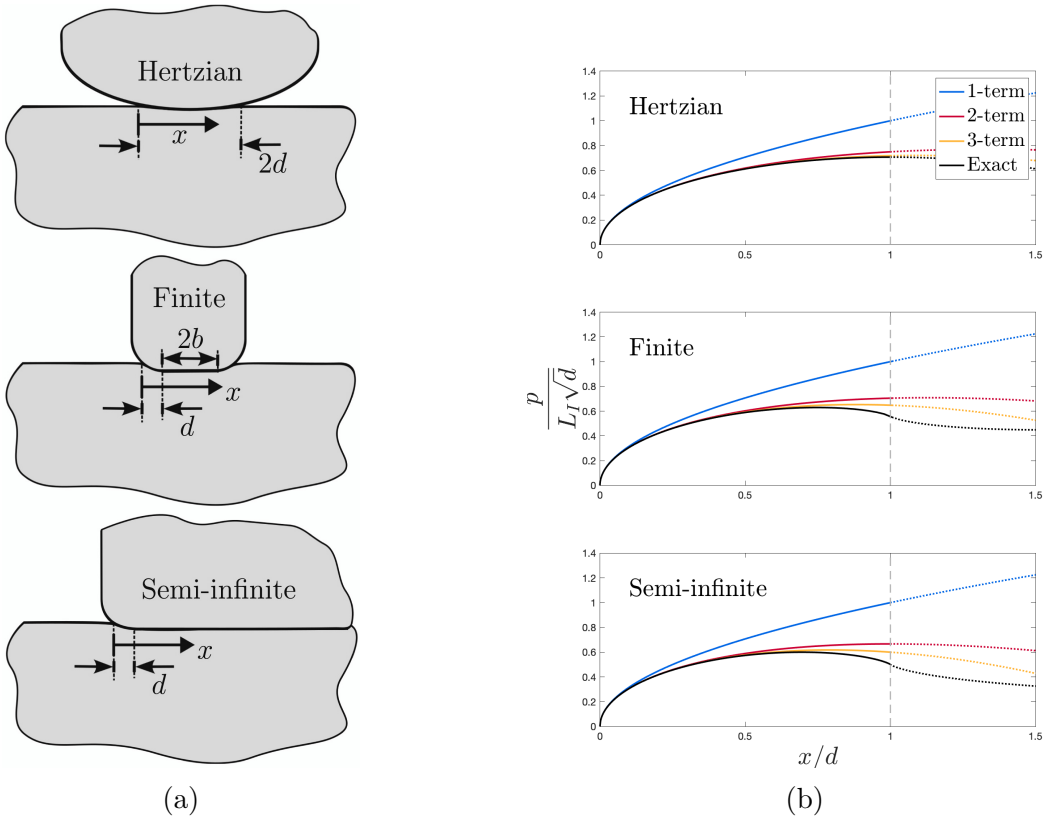
Here, the coefficients scale only with L_I and the contact size of the rounded section of the punch, d.

3.2.2 Validity of the asymptotic series expansion

In order to investigate the integrity of these asymptotic expansions in the vicinity of the contact edge, we may re-scale x by d and the asymptotic form of the pressure by $L_I\sqrt{d}$ to facilitate straightforward comparisons with the exact solution. We show these comparisons for the first three terms of the asymptotic expansions in Fig. 3.2.

We are interested in finding an accurate representation of the internal stress state as far as the slip region extends into the geometry. In practice, slip regions in Hertzian contacts will typically extend to just a small fraction of the contact half-width (here, d). On the other hand, in problems incorporating a flat, it is common for the slip region to extend to a significant fraction of the length d (and, in principle, it might extend beyond the curved region). Therefore, for flat and rounded problems, we may require an accurate representation of the internal stress state as far as $x/d = 1$ in from the contact edge.

For the Hertzian contact (top), even the two-term solution looks like a decent approximation of the exact solution; when $x/d = 1$, the error of the two-term



(a) (b)

Figure 3.2: Asymptotic expansion of the contact pressure for three contact classes pressed against a half-plane: Hertzian (top, $b/d \to 0$), finite flat-and-rounded (middle, $b/d = 0.515$), and semi-infinite flat-and-rounded (bottom, $b/d \to \infty$). (a) Geometry sketches indicating the curved-section length d, with x measured from the left contact edge. (b) Exact contact pressure (black) alongside one-term (blue), two-term (red) and three-term (orange) asymptotic approximations; dashed segments correspond to the flat portion of the contact, solid segments to the curved portion.

approximation is only 6.7%. Increasing the number of terms to three or more, improves the approximation even further; for the Hertzian contact, when $x/d = 1$, the error of the three-term approximation is only 1.7%

Unfortunately, this behaviour does not translate to finite (middle) and semi-infinite (bottom) contacts. When using three terms, the finite case approximation is slightly more accurate than the semi-infinite case, however, this is marginal: the errors of the three-term approximations at $x/d = 1$ are 17.5% (for a given finite ratio $b/d = 0.515$) and 20.0%, respectively. To consider a solution appropriate, we may look for errors $< 5\%$ throughout the extent of the slip zone. Therefore, even when using three-term solutions, the asymptotic approximations of finite and semi-infinite contacts are not valid as far as $x/d = 1$ in from the contact edge; asymptotic representations of flat and rounded contacts are poor in this region.

These findings encourage us to consider alternative approaches to finding

asymptotic approximations of the exact contact pressure and shear tractions that allow for greater scope and flexibility in problems containing geometries with both flat and rounded parts.

3.3 Semi-infinite flat punches with rounded edges

An alternative method to using an asymptotic expansion, alluded to in the previous section, is to consider an elastic contact between a half-plane and a semi-infinite indenter with a flat front face and rounded edge. This is attractive as it provides a possible vehicle for encapsulating rounded contact edge behaviour within a lifing procedure. We have made two attempts to find a solution to a contacting pair of this form. The first, [15], used a formulation based on uncoupled half-plane theory. The second, [8], employed a finite element analysis based on a three-quarter plane formulation with a rounded corner for the indenter radii. Before looking at these approaches and showing how they may be employed in tandem, some aspects of the half-plane solution and its attributes merit consideration.

3.3.1 Half-plane formulation

In a half-plane analysis, the surface tractions and surface normal displacement are related by the following integral equation of the second kind, which stems from Flamant's solution,

$$\frac{dg}{dx} = \frac{2}{\pi E^*} \int_{contact} \frac{p\,(\xi)\,d\xi}{x-\xi} - \beta q(x), \tag{3.11}$$

where $p(x)$ is the contact pressure, $q(x)$ is the shear traction present, and $g(x)$ is the relative surface profile. In this equation, the composite plane strain modulus, E^*, is given by

$$\frac{1}{E^*} = \frac{1-\nu_1^2}{E_1} + \frac{1-\nu_2^2}{E_2} \tag{3.12}$$

where E_i, ν_i are, respectively, the Young's modulus and Poisson's ratio of body i, and β, Dundurs' second constant, is given in [13] by

$$\beta = \frac{E^*}{2}\left[\frac{(1+\nu_1)\,(1-2\nu_1)}{E_1} - \frac{(1+\nu_2)\,(1-2\nu_2)}{E_2}\right]. \tag{3.13}$$

The solution to the contact problem, therefore, depends on the composite modulus. The mix of stiffness between the two bodies is unimportant in the first (integral) term in Eq.(3.11), but it is relevant in the second term. This second term physically represents the effect of shear traction on the solution.

We have already alluded to the concept of 'coupling', where the presence of shear tractions causes a change in the relative normal displacement of the contacting surfaces, and, consequently, the contact pressure. To derive a solution from half-plane theory, we are implicitly assuming the contact is 'uncoupled'. For this assumption to be valid, we must agree with two important criteria:

(a) both bodies can be appropriately represented by half-plane domain shapes,

(b) and, the second term in the integral Eq.(3.11) vanishes.

For the flat and rounded geometry, criteria (a) is only satisfied very close to the contact edge. For this analysis, criteria (b) can only be satisfied by setting $\beta = 0$ as we require a moderate coefficient of friction between the contacting bodies to avoid slip, $q(x) \neq 0$.

To conclude the discussion of 'coupling', in this paper we are only interested in the case where both bodies are elastically similar[1] ($E_1 = E_2$, $\nu_1 = \nu_2 \implies \beta = 0$); the solution derived from half-plane theory will be valid, but only when the observation point is very close to the contact edge, where both domains can be appropriately represented by a half-plane.

As a means of analysing, in practical terms, how far the uncoupled solution deviates from the true coupled solution for the flat and rounded geometry, we will now derive the uncoupled solution from half-plane theory, for a semi-infinite flat punch with a rounded edge, pressed into an elastically similar half-plane. The uncoupled nature of the solution means that a normal load will induce a contact pressure alone, given in Eq.(3.9), which takes the asymptotic forms

$$p(x) = \frac{L_I d}{3\sqrt{x}} \equiv \frac{K_{I[1/2]}}{\sqrt{x}} \qquad x \gg d, \tag{3.14}$$

$$p(x) = L_I \sqrt{x} \qquad x \ll d, \tag{3.15}$$

and where the contact law is given by

$$\frac{\pi R L_I}{2E^*} = \sqrt{d}, \tag{3.16}$$

or

$$\frac{d}{R} = \frac{\pi^2}{4} \widetilde{L_I}^2 \tag{3.17}$$

[1]For a different area of study, if the contact-defining body was rigid, its shape outside the contact patch would not figure in the solution; the solution would be the same whether the contact-defining body was a half-plane with a small rounded corner step, or a semi-infinite flat and rounded punch. Therefore, for the unique case where body 1 in Fig. 3.1 is rigid ($\nu = 0$) and body 2 is incompressible ($\nu = 0.5$): we could bypass criteria (a), and criteria (b) would be satisfied as $\beta = 0$; the uncoupled half-plane formulation would be valid for the entirety of the contact.

where $\widetilde{L_I} = RL_I/E^*$.

In addition, the solution derived in the half-plane formulation has the desirable property of being closed-form with a number of useful attributes, such as a contact law, Eqs.(3.16,3.17). For example, it is straightforward to show that the maximum contact pressure is given by

$$\frac{p_0}{E^*} \simeq \sqrt[3]{1.24\frac{\pi^4}{144}}\widetilde{L_I}^2. \tag{3.18}$$

Moreover, owing to the uncoupled nature of the solution, the same construction applies to a shear load that induces an isolated shear traction. By analogy, the near-edge shear traction takes the square-root-bounded form

$$q(x) = L_{II}\sqrt{x} \qquad x \ll d, \tag{3.19}$$

where L_{II} is the asymptotic multiplier for the shear traction. The closed-form half-plane shear distribution corresponding to this asymptote is

$$q(x) = \frac{L_{II}}{4\sqrt{d}}\left[2\sqrt{dx} + (x-d)\ln\left|\frac{1-\sqrt{x/d}}{1+\sqrt{x/d}}\right|\right] \qquad x > 0. \tag{3.20}$$

As expected, the asymptotic approximation given by Eq.(3.1) takes the correct form when close to the contact edge, $x \ll d$, where the contact problem is appropriately represented by half-plane theory. However, the difficulty in using this solution is when the observation point is remote from the edge. As we see from Eq.(3.14), the contact pressure is seen to decay in an inverse square-root fashion. If we consider the geometry in Fig. 3.1, where both bodies are elastically similar, far from the edge of the contact, the geometry looks like a wedge of angle $3\pi/2$ radians, not two half-planes. Therefore, we would expect the actual contact pressure decay along the interface to correlate with that found in the classical Williams' solution [9], which is not inverse square-root bounded. Here, the half-plane solution breaks down, away from the contact edge.

In summary, the pressure distribution displayed in this section is considered valid when the observation point is near the contact edge, i.e. we can be confident that Eq.(3.9) accurately represents the contact pressure between a pair of contacting elastically similar bodies for small values of x/d. However, the solution falls apart as the observation point moves away from the contact edge; the decay rate is not what we would expect from consideration of Fig. 3.1 if the interface has remotely adhered

due to the introduction of coupling.

As a result, it is justified to compare the half-plane formulation with an alternative formulation that is bounded by Williams' solution far from the contact edge to analyse the extent to which they diverge.

3.3.2 Three-quarter plane formulation

To overcome the problem that arises far from the contact edge, we must define the domain shape of the rounded edge body more rigorously.

Referring to Fig. 3.1, looking from an observation point well away from the contact edge, the pair of bodies behave like a square-edged quarter plane pressing onto an elastically similar half-plane. To permit the domain to be thought of as a three-quarter plane, - a bonded half-plane and quarter plane, or a wedge of angle $3\pi/2$, we must make the following assumptions: the bodies are both elastic and made from the same material (elastically similar), and the coefficient of friction is sufficiently large for the interface to be stuck away from the contact edge [2, 16]. The eigenvector to Williams' solution dictates the ratio of shear to direct traction; the contact will be stuck provided the coefficient of friction is at least as big as this ratio. The ratio for a wedge of angle $3\pi/2$ radians is 0.543, and it is assumed, in the analysis, that the coefficient of friction is at least as big as this. [2]

When these considerations apply, the solution far from the contact edge should, instead of displaying a square root decay, follow Williams' solution [9, 10]; for example, for the pure mode 1 loading case — relative to the bisector line — we should find $p \sim x^{\lambda_I - 1}$, where $\lambda_I = 0.5445$.

We constructed a finite element three-quarter plane model with a rounded corner for the indenter, following the assumptions outlined above, based on the approach in [8, 17]. In the finite element model, we apply displacement boundary conditions from Williams' solution, for a wedge of angle $3\pi/2$ radians, far from the contact edge [13].

3.3.3 Pure Mode I Loading

As a first step in understanding how the two solutions compare, we excite pure mode I loading only, in the wedge sense. We denote the corresponding stress intensity

[2] At the outset, it is not clear that this condition will also maintain stick at the contact edge where the theory does not apply; but, in anticipation of results found later, we state that if the friction is sufficiently high to ensure stick in the interior it will also ensure stick at the edge under proportional loading conditions; other load paths are outside the scope of the current analysis.

factor by $K_{I[3/4]}$, seen in Fig 3.1.

Looking near the contact edge, as we change the normal loading and shear loading in proportion, the contact edge moves slightly due to the growth in contact size, and a bounded shear traction results. Therefore, when $x/d \ll 1$, we see each traction is described well by the following square root bounded asymptotes

$$p(x) = L_I\sqrt{x}, \tag{3.21}$$

$$q(x) = L_{II}\sqrt{x}. \tag{3.22}$$

The calibrations for the asymptote coefficients L_I and L_{II} are given in [17] (see Eqs.(3,8) therein), viz.

$$L_I = \left(\frac{-0.93K_{I[3/4]}}{E^*R^{1-\lambda_I}}\right)^{1/3}\frac{E^*}{\sqrt{R}}, \tag{3.23}$$

$$L_{II} = \left(\frac{-0.04K_{I[3/4]}}{E^*R^{1-\lambda_I}}\right)^{1/3}\frac{E^*}{\sqrt{R}}, \tag{3.24}$$

where we have set $K_{II[3/4]} = 0$ as we are considering pure mode I loading, and the mode I eigenvalue, $\lambda_I = 0.5445$, for the case of a $3\pi/2$ radians wedge [8].

These curves plotted in Fig. 3.3, coloured blue (broken) for pressure and orange (broken) for shear, are the point of commonality between the rounded three-quarter plane solution and the half-plane solution. With the multipliers, L_I and L_{II}, fixed at the contact edge, the traction distributions may be plotted from the closed-form equation for a half-plane Eqs.(3.9,3.20). These are the smooth solid lines coloured blue (contact pressure) and orange (shear traction).

Theoretically, the half-plane formulation should only be valid when $x/d \ll 1$. However, as may be seen over the interval of Fig. 3.3, $0 < x/d < 4$, these lines are almost coincident with those from the numerical three-quarter plane analysis. This gives us confidence that we now have, for practical purposes, solutions for the tractions at the contact edge in closed form; the only multipliers on the solution are numerically determined for pure mode I loading, L_I and L_{II}.

Now, looking away from the contact edge, we must first check the two formulations fall to their asymptotic forms, and then analyse the extent to which the two solutions diverge from each other along the interface.

If we multiply the stress intensity factor, $K_{I[3/4]}$, by its corresponding eigenvector,

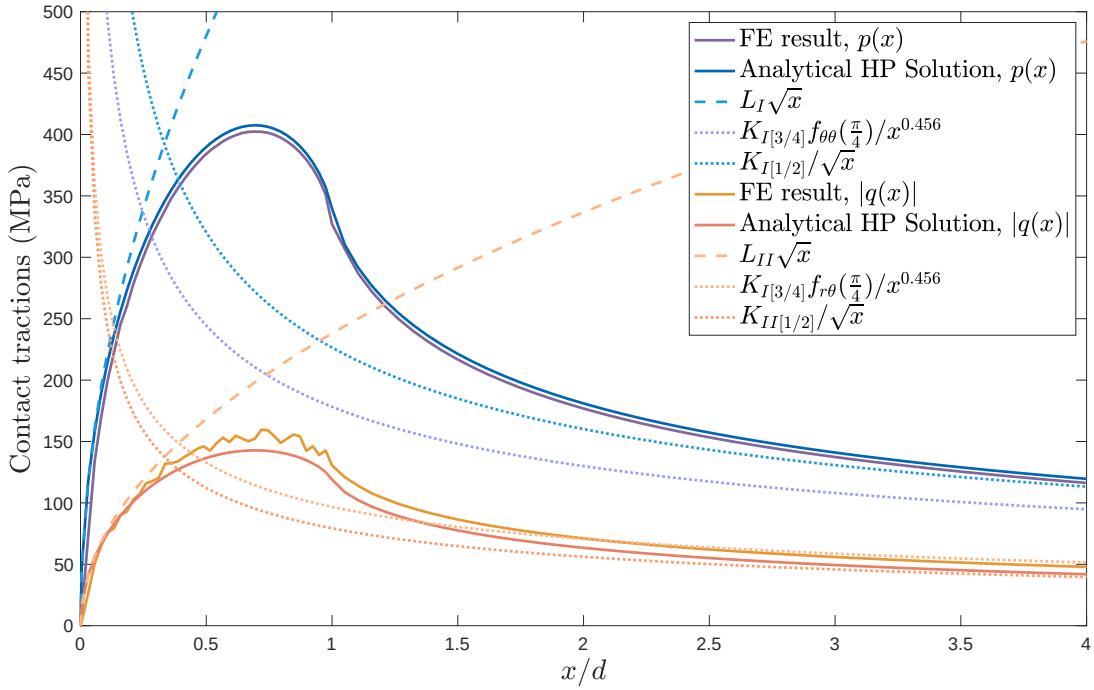


Figure 3.3: Pure mode 1 normal and shear tractions calculated using a three-quarter plane (FE result), and half-plane (analytical half-plane solution) formulations. These tractions are plotted alongside their near (broken line) and far (dotted line) asymptotes.

we can easily find the tractions appearing along the interface. When $x/d \gg 1$ these solutions will apply. Fig. 3.4 shows these asymptotes by a dotted purple line (contact pressure) and a dotted yellow line (shear traction). The actual traction distributions along the interface in the rounded three-quarter plane analysis, extracted from the finite element simulations, are coloured solid purple (contact pressure) and solid yellow line (shear traction). In the same figure, we show the tractions from the half-plane analysis as given by Eqs.(3.9,3.20): solid blue line (contact pressure) and solid orange line (shear tractions), are also plotted together with their square-root decay forms: dotted blue line (contact pressure) and dotted orange line (shear tractions) in Fig. 3.4.

We can infer two important points from Fig. 3.4. Firstly, we may be reassured that the distributions go to the correct asymptotic forms when $x/d \gg 1$, i.e. the tractions for both the half-plane and the finite element formulation approach their corresponding asymptotic forms as $x/d \to \infty$. Secondly, and more importantly, it is clear that the asymptotes for the half-plane formulation are quite distinct from those implied by the three-quarter plane analysis, particularly in the case of the

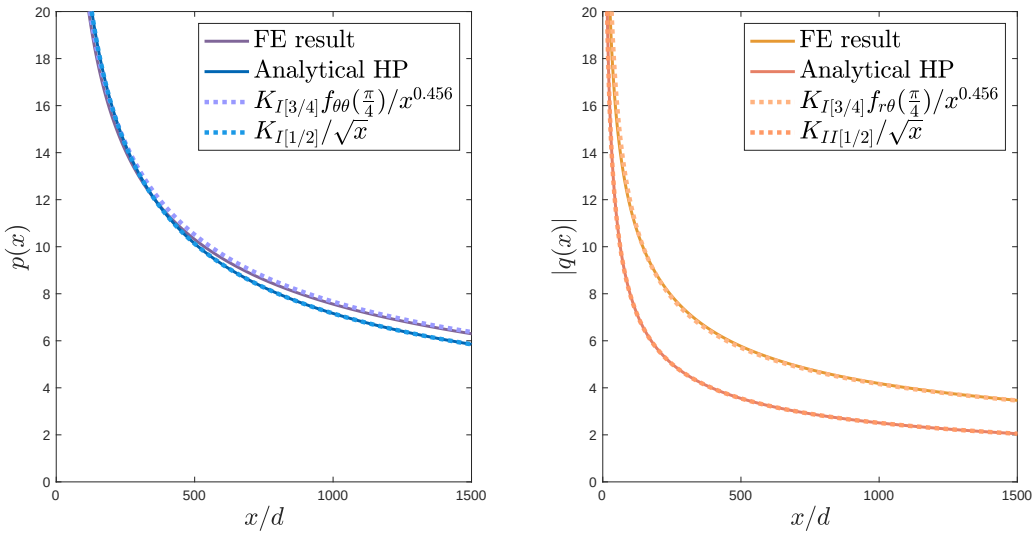


Figure 3.4: Normal (left) and shear (right) tractions (solid lines) plotted against the half-plane and three-quarter plane decay asymptotes (dotted lines), far from the contact edge.

shear tractions. For example, at the arbitrary far distance of $x/d = 1500$ from the contact edge, the magnitude of the error of the half-plane formulation compared to the three-quarter plane (Williams') solution, is 8.23% and 40.8% for the normal and shear tractions, respectively. The large errors here again illustrate the limitations of relying solely on half-plane theory in our approximations.

3.3.4 Pure Mode II Loading

This section provides an equivalent commentary to that given previously for pure mode II loading. Here, we reworked the finite-element model used in [8] for pure mode II loading only, in the wedge sense. The corresponding stress intensity factor is denoted by $K_{II[3/4]}$, seen in Fig. 3.1.

To begin with, we will study the tractions resulting near the edge of the contact. As mentioned previously, proportional loading of the contact results in a bounded shear traction at the contact edge; when $x/d \ll 1$, the tractions are well described by the square root bounded asymptotes, Eqs.(3.21,3.22). For pure mode II loading, $K_{I[3/4]} = 0$, the calibrations from [17] can be written in the form

$$L_I = \left(\frac{0.981 K_{II[3/4]}}{E^* R^{1-\lambda_{II}}} \right)^{1/3} \frac{E^*}{\sqrt{R}} \tag{3.25}$$

$$L_{II} = \left(\frac{0.04K_{II[3/4]}}{E^*R^{1-\lambda_{II}}}\right)^{1/3} \frac{E^*}{\sqrt{R}}, \tag{3.26}$$

where $\lambda_{II} = 0.9082$ is the mode II eigenvalue for the case of a $3\pi/2$ radians wedge [8].

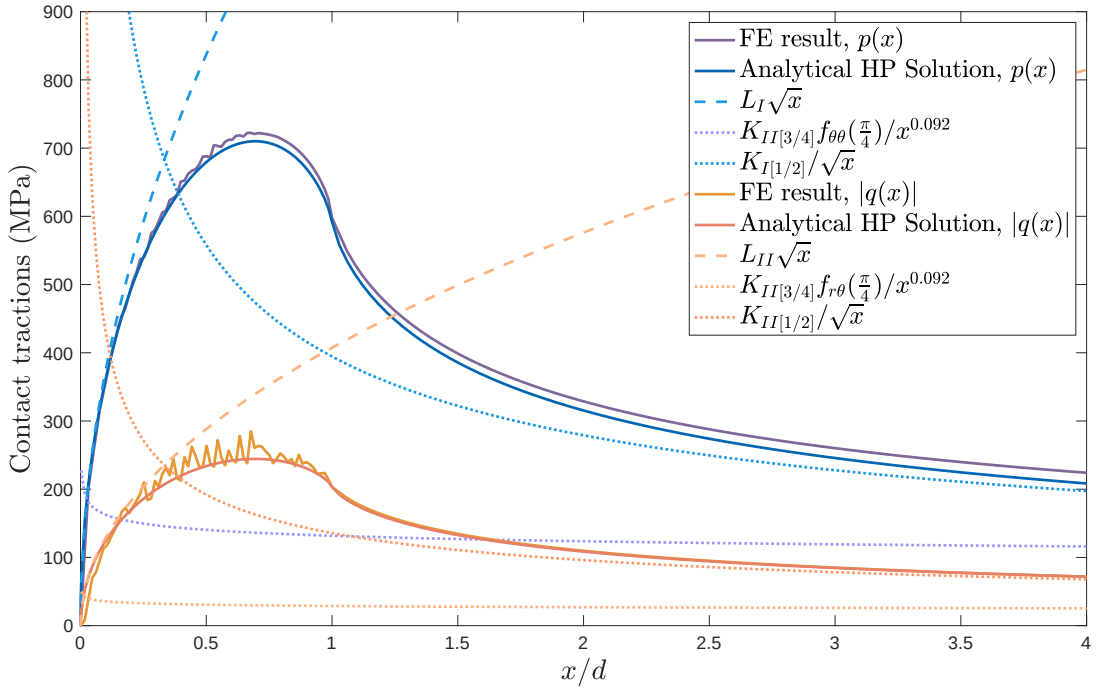


Figure 3.5: Pure mode 2 normal and shear tractions calculated using a three-quarter plane (FE result), and half-plane (analytical half-plane solution) formulations. These tractions are plotted alongside their near (broken line) and far (dotted line) asymptotes.

As for pure mode I loading, Eqs.(3.21,3.22), are the point of commonality between the rounded three-quarter plane solution and the half-plane solution. Fig. 3.5 displays these near-edge asymptotes, coloured blue (broken) for pressure and orange (broken) for shear. With the multipliers fixed at the contact edge, the normal and equivalent shear tractions are plotted from the closed-form half-plane solution, Eqs.(3.9,3.20). These are shown in Fig. 3.5 by the smooth solid blue (contact pressure) and orange (shear traction) lines, alongside the tractions which emerge from the rounded three-quarter plane formulation, plotted in solid purple (contact pressure) and yellow (shear traction).

Theoretically, the half-plane formulation should only be valid when $x/d \ll 1$. However, as seen in Fig. 3.5, the half-plane solution is, again, almost coincident

with the distributions obtained from the numerical three-quarter plane analysis for $0 < x/d < 4$. This is very encouraging, for practical purposes; it implies that we now have closed-form solutions for the tractions at the contact edge, with only the multipliers numerically determined, for both pure mode I and II loading.

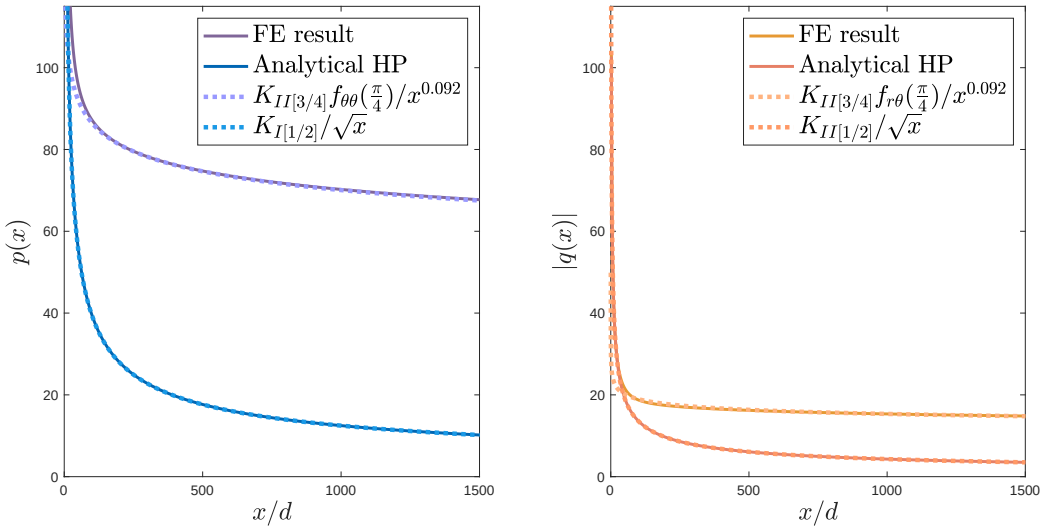


Figure 3.6: Normal (left) and shear (right) tractions (solid lines) plotted against the half-plane and three-quarter plane decay asymptotes (dotted lines), far from the contact edge.

As before, looking away from the contact edge (i.e. for $x/d \gg 1$), we must study two key areas: 1) that the two formulations fall to their corresponding asymptotic forms, and 2) the extent to which the two formulations diverge from each other. We address this in Fig. 3.6. For $x/d \gg 1$, the tractions along the interface for the half-plane formulation, are inverse square-root bounded, Eq.(3.14) and these are illustrated by the blue dotted line (contact pressure) and the orange dotted line (shear traction). However, the tractions far from the contact edge, along the interface, can be correctly described by Williams' solution. In pure mode II loading, this asymptotic decay can be found by multiplying the stress intensity factor, $K_{II[3/4]}$, by its corresponding eigenvector. These decay asymptotes are plotted in Fig. 3.6 by a dotted purple line (contact pressure) and dotted yellow line (shear traction).

As encountered for pure mode I loading, we can use Fig. 3.6 to infer two key points. First of all, Fig. 3.6 provides clear evidence that, for each case, the exact solutions (solid lines) approach their expected asymptotic forms (dotted lines) when $x/d \gg 1$. Moreover, we can see that the tractions arising along the interface when using a

half-plane formulation are significantly different to those implied by a three-quarter plane analysis. This difference is even starker than the previous example: in pure mode II loading, the difference is distinct for both normal and shear tractions; at the arbitrary far distance of $x/d = 1500$ from the contact edge, the magnitude of the error of the half-plane formulation compared to the three-quarter plane solution is 84.8% and 76.1% for the normal and shear tractions, respectively. These results highlight the deficiency of relying, exclusively, on the half-plane formulation when observing the contact tractions far from the contact edge.

3.4 Conclusion

In this analysis, we have demonstrated the limitations of using an asymptotic representation of the state of stress for flat and rounded contacts. In such contacts, the regions of interest — typically slip zones — may extend a significant distance from the edge of the contact, well beyond the range of validity of such asymptotic approximations.

Aiming to solve this problem, we first turned to a half-plane formulation, aware that using the half-plane model in isolation may be poor due to the misleading representation of the contact-defining body. We noted that the decay of the state of stress implied by this solution, at remote points, was not of the correct form. This meant that we could not collocate the solution into any finite, slightly rounded contact problem.

We then looked at an FE solution to the geometrically exact slightly rounded three-quarter plane problem. We matched the very near-edge solution with that derived from half-plane theory, mentioned in the previous paragraph. The results from this analysis are very promising; the closed-form solution lies very close to the exact solution up to approximately $x/d = 5$ for both pure mode I and II loading. However, the poor assumptions implicit in the half-plane model become an issue when $x/d \gg 1$, as the model diverges from the exact solution in both loading cases, as expected.

The formulation developed in this paper sets up the framework for a number of strands of investigation of the properties of slightly rounded contacts - here limited to those in which the contact-defining body has a free surface normal to the contacting surface. We can now describe near-contact edge behaviour analytically, using Eqs.(3.9,3.20), where the multipliers, L_I and L_{II} are rigorously, if numerically, related to the remote fields, Eqs.(3.23–3.26).

At the moment the remote fields have been chosen to be pure mode I and pure

mode II only; the extension of the solution to other combinations or remote loading trajectories will form the next step. This extension has been foreshadowed in [18], but at that time, our understanding of the behaviour of incomplete frictional contact behaviour under varying normal loads was less well advanced. In particular, for such cases, we anticipate the closed-form half-plane solution will form an accurate asymptote for the mixed-mode finite element solution. This will permit us to find clean solutions for edge partial slip for this domain. Practical applications of these findings include fan blade dovetails in the root of a gas turbine and locking segments of riser-seabed connectors.

References

[1] Olof Vingsbo and Staffan Söderberg. “On fretting maps”. in *Wear* 126.2 (1988), 131–147.

[2] C. Churchman, A. Mugadu and D. Hills. “Asymptotic results for slipping complete frictional contacts”. in *European Journal of Mechanics - A/Solids* 22 (2003), 793–800. DOI: 10.1016/S0997-7538(03)00074-3.

[3] Anthony Sackfield, A. Mugadu, James Barber and D. Hills. “The application of asymptotic solutions to characterizing the process zone in almost complete frictionless contacts”. in *Journal of The Mechanics and Physics of Solids* 51 (2003), 1333–1346. DOI: 10.1016/S0022-5096(03)00020-6.

[4] A. Mugadu, D. Hills, James Barber and Anthony Sackfield. “The application of asymptotic solutions to characterising the process zone in almost complete frictional contacts”. in *International Journal of Solids and Structures* 41 (2004), 385–397. DOI: 10.1016/j.ijsolstr.2003.09.038.

[5] Claudio Montebello, Sylvie Pommier, Demmou Karim, J. Leroux and Jean Meriaux. “Analysis of the stress gradient effect in Fretting-Fatigue through nonlocal intensity factors”. in *International Journal of Fatigue* 82 (2015). DOI: 10.1016/j.ijfatigue.2015.02.009.

[6] Barbara Ferry, José Araújo, Sylvie Pommier and Demmou Karim. “Life of a Ti-6Al-4V alloy under fretting fatigue: Study of new nonlocal parameters”. in *Tribology International* 108 (2016). DOI: 10.1016/j.triboint.2016.11.003.

[7] Raphael Cardoso, B. Ferry, Claudio Montebello, Jean Meriaux, Sylvie Pommier and José Araújo. “Study of size effects in fretting fatigue”. in *Tribology International* 143 (2019), 106087. DOI: 10.1016/j.triboint.2019.106087.

[8] Rodolfo Fleury, D. Hills and James Barber. “A corrective solution for finding the effects of edge-rounding on complete contact between elastically similar bodies. Part I: Contact law and normal contact considerations”. in *International Journal of Solids and Structures* 85 (2016). DOI: 10.1016/j.ijsolstr.2015.11.031.

[9] M. L. Williams. “Stress singularities resulting from various boundary conditions in angular corners of plates in extension”. in *Journal of Applied Mechanics* 19 (1952), 526–528.

[10] J. R. Barber. *Elasticity*. Solid Mechanics and Its Applications. Springer Dordrecht, 2009. **chapter** 12.5.3. ISBN: 978-90-481-3809-8. DOI: https://doi.org/10.1007/978-90-481-3809-8.

[11] M.R. Moore and D.A. Hills. "Analysing the accuracy of asymptotic approximations in incomplete contact problems". in *International Journal of Solids and Structures* 253 (2022), 111557. DOI: 10.1016/j.ijsolstr.2022.111557.

[12] H. Andresen, D.A. Hills and M.R. Moore. "Representation of incomplete contact problems by half-planes". in *European Journal of Mechanics - A/Solids* 85 (2021), 104138. ISSN: 0997-7538. DOI: https://doi.org/10.1016/j.euromechsol.2020.104138. URL: https://www.sciencedirect.com/science/article/pii/S099775382030526X.

[13] David Hills and Hendrik Andresen. "Mechanics of Fretting and Fretting Fatigue". in. 2021, 21–129. ISBN: 978-3-030-70745-3. DOI: 10.1007/978-3-030-70746-0.

[14] A. Mugadu, D. Hills, James Barber and Anthony Sackfield. "The application of asymptotic solutions to characterising the process zone in almost complete frictional contacts". in *International Journal of Solids and Structures* 41 (2004), 385–397. DOI: 10.1016/j.ijsolstr.2003.09.038.

[15] A. Sackfield, A. Mugadu, J.R. Barber and D.A. Hills. "The application of asymptotic solutions to characterising the process zone in almost complete frictionless contacts". in *Journal of the Mechanics and Physics of Solids* 51.7 (2003), 1333–1346. ISSN: 0022-5096. DOI: https://doi.org/10.1016/S0022-5096(03)00020-6. URL: https://www.sciencedirect.com/science/article/pii/S0022509603000206.

[16] D. Hills, A. Thaitirarot, James Barber and Daniele Dini. "Correlation of fretting fatigue experimental results using an asymptotic approach". in *International Journal of Fatigue* 43 (2012), 62–75. DOI: 10.1016/j.ijfatigue.2012.02.006.

[17] Rodolfo Fleury, D. Hills and James Barber. "A corrective solution for finding the effects of edge-rounding on complete contact between elastically similar bodies. Part II: Near-edge asymptotes and the effect of shear". in *International Journal of Solids and Structures* 85 (2016). DOI: 10.1016/j.ijsolstr.2015.11.032.

[18] R.M.N Fleury. "Investigation of fretting fatigue in turbine fir tree blade to disc joints at high temperature (DPhil thesis, University of Oxford)". phdthesis. 2015, 176.

Chapter 4

Elastic, Flat and Rounded Finite Contacts: When Should We Use Half-Plane Theory?

Contents

4.1 Introduction 67

4.2 Half-plane formulation of a flat and rounded contact . . 69

4.3 Rounded, three-quarter plane formulation of a flat and rounded contact 70

4.4 Application of the rounded, three-quarter plane solution to the finite contact 72

4.5 Comparison of solutions 74

4.5.1 Contact tractions 74

4.5.2 Contact Laws 77

4.6 Conclusion 81

In Chapter 3, it was shown that the closed-form half-plane solution for contact tractions in a semi-infinite flat - rounded contact can be modified using wedge-theory derived multipliers to account for a nearby vertical traction-free edge, yielding a strong approximation of the traction field local to the contact edge. In this chapter, we will study finite contacts and consider for what ratios of flat length to edge radius the novel method is preferred over traditional half-plane theory analysis. It would be expected that as the ratio is minimised we tend to a contact that looks like two half-planes, and therefore the traditional half-plane theory will dominate, yet, as the ratio is increased, the novel method would be preferred as the contact looks more like the semi-infinite flat and rounded contact analysed in the previous chapter. The question for this chapter is, for what ratio of flat to rounded section should we use each method?

This chapter presents research published as:

> **B. Eames**, D.A. Hills, M.R. Moore, Elastic, flat and rounded finite contacts: When should we use half-plane theory?, *European Journal of Mechanics - A/Solids,* Volume 106, 2024, 105306, ISSN 0997-7538, https://doi.org/10.1016/j.euromechsol.2024.105306.

This paper provides a key practical contribution to the literature, as we explain when solutions for contacting geometries solved using the new method developed in the previous chapter out-performs previous methods.

Once we know what range of flat and rounded contacting geometries are best solved by the new method, we are able to build on the method itself in the subsequent chapters, and so apply it to contacts experiencing a complicated loading history.

Elastic, Flat and Rounded Finite Contacts: When Should We Use Half-Plane Theory?

B Eames[1], D A Hills[1] and M R Moore[2]

[1]*Department of Engineering Science, University of Oxford, Parks Road, Oxford, OX1 3PJ, UK*

[2]*Department of Mathematics, University of Hull, Kingston-upon-Hull, HU6 7RX, UK*

Abstract

For a flat contact with radiused edges, it is shown that when the flat portion of the contact is small compared to the radius portion of the contact, half-plane theory may confidently be used, and the amount of coupling present is extremely small. When the flat region is large a good quality solution may be used by a different route, using the solution for a square-ended punch together with a corrective solution formed from a three-quarter plane problem but with a radius at the corner. The degree of coupling is captured well. Intermediate geometries are discussed in the text. A further, important, refinement is the fitting of a third solution, developed using half-plane theory for a slightly rounded, flat semi-infinite contact, as this provides an analytical description of the near-edge tractions, and is rigorously fitted into the edge of the three-quarter plane solution.

4.1 Introduction

The contact problem shown in Figure 4.1 represents the arrangement of a flat, conforming face, with edge radii pressed into a half-plane. This is an idealisation of an arrangement which frequently occurs in practical applications, such as in the dovetail roots of fan blades and the locking segments of riser connectors used for oil recovery from the seabed. Several solutions in the literature to this contact problem are based on half-plane theory. The original solution by Steuerman [1] was developed by Ciaveralla and Hills [2], and later by Ciavarella [3]. These papers provide closed-form implicit solutions to the problem but are based on the assumption that the contacting bodies may each be idealised as a half-plane. If this were true the problem would be uncoupled in the sense that, if friction were present along the interface no shear tractions would arise under the application of a normal load, as surface particles in the bodies would each tend to displace laterally by the same amount. Beyond that, there is the more general question of how good the quality of the solution is when the presence of the traction-free faces, i.e. the vertical sides of the body, are ignored.

Hertz's seminal work, found in [4] is based on the assumption that two contacting spherical surfaces can each be represented as a half-space. This assumption may appear unreasonable, however, it has been proved fully justified within the scope of linear elasticity [5].

Following from the above, we would expect that, when the flat section of the contact is very small relative to the radiused edge, a solution founded on half-plane theory would work well. Equally, when the converse is true, a solution based on half-plane theory may be expected to founder; the influence of the vertical sides of the punch is no longer negligible when considering the contact region.

We are interested in contacts with a flat segment, of half-length b, edged by circular arcs, of radius R, shown in Fig. 4.1a. Note the contacting body half-width, a, is dependent on these two variables alone as $a = b + R$.

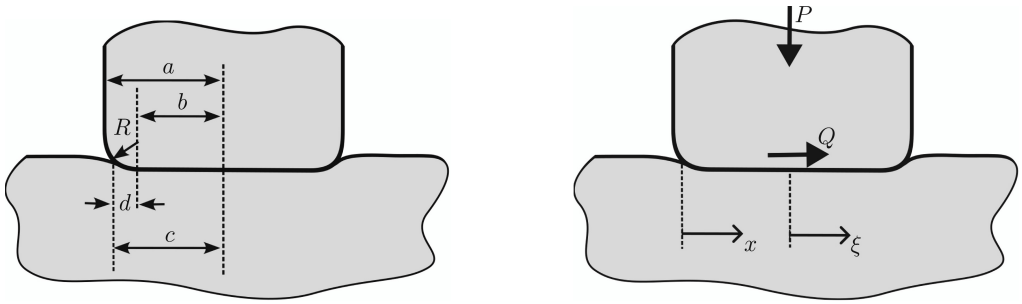
The half-plane formulation is only valid either when looking at the very edge of the contact, or when $b/R \to 0$, i.e. Hertz contacts. To get a better understanding of how the tractions change as we vary the geometry, a/R, we first investigate how to form a solution when starting from the opposite limit, $b/R \to \infty$. To this end, we turn to the rounded, three-quarter plane solution outlined in [6]. This solution matches the far-field Williams' wedge solution, formed from a rounded quarter plane pressing into an elastically similar half-plane — or, with interior stick, a solution which may be thought of as a rounded three-quarter plane —, to the near-field tractions, to obtain a closed-form solution. In doing this we note the formulation assumes that the effect of the far contact boundary is negligible, equivalent to requiring the flat length to be large, i.e. $b/R \gg 1$.

Previously, we have seen that this solution gives an accurate closed-form solution for a semi-infinite flat and rounded contact, as, unlike the half-plane solution, it correctly represents the adjacent normal free boundary. However, up until now, this solution has never been applied to contacts with a finite flat length, but where the presence of the opposite edge may be felt.

Our goal is to find an efficient, accurate solution to the problem of Fig. 4.1a for any ratio b/R, and at any load. We have three potential methods;

1. One possibility is to model the problem using the finite element method which is capable of representing the exact domain shape, where the elastic formulation is appropriate to that domain, and the limit of accuracy is imposed by the mesh density of the finite element discretisation and the intrinsic shape function chosen therein. We will use a finite element model as a guide later in the paper.

2. We have mentioned an analytical method - that is based on the half-plane representation of both bodies - which we expect will be correct for small b/R.



(a) (b)

Figure 4.1: Geometry, loading and coordinate system for a finite flat-and-rounded body pressed onto a half-plane. (a) Geometry: a is the body half-width, b the flat half-length, c the contact half-length, d the length of the curved section in contact and R the edge radius. (b) Applied normal load P and shear load Q; the coordinate x is measured from the left contact edge and ξ from the contact centre.

3. For very large b/R we will use a method employing the rounded three-quarter plane solution developed in [6].

The question we address in this study is, 'For which intermediate values of b/R do at least one of the analytical approaches (2) and (3) prove to be sufficiently accurate for practical engineering or industrial purposes?'. Analysing this problem will allow us to use the most accurate closed-form solution for any given application, i.e. for any ratio of flat and rounded sections of the contacting body.

4.2 Half-plane formulation of a flat and rounded contact

In this section, we provide the closed-form solution from [2] in which it is assumed that both bodies behave like half-planes. Half-plane theory negates the existence of coupling, so that, when loading the contact under a normal load, P, it will induce a normal traction alone.

The dimensionless contact half-width, c/R, where $c = b + d$ in Fig. 4.1a, can be defined implicitly as a function of the relative size of the flat section, b/R and an angle, ϕ_0, [2]

$$\left(\frac{c}{R}\right) = \left(\frac{b}{R}\right) \frac{1}{\sin\phi_0} \tag{4.1}$$

Using this definition of geometry, the closed-form contact law can be solved implicitly,

$$2\left(\frac{P}{E^*R}\right) = \left(\frac{b}{R}\right)^2 \left[\frac{\pi - 2\phi_0}{4\sin^2\phi_0} - \frac{\cot\phi_0}{2}\right], \tag{4.2}$$

where E^* is the plane strain modulus and P/E^*R is the dimensionless normal load on the contacting body.

The implicit form of the normal contact traction is as follows

$$\frac{c\,p(\phi)}{P} = \frac{2/\pi}{\pi - 2\phi_0 - \sin 2\phi_0} \times \left\{ (\pi - 2\phi_0)\cos\phi + \ln\left[\left| \frac{\sin(\phi+\phi_0)}{\sin(\phi-\phi_0)} \right|^{\sin\phi} \left| \tan\tfrac{\phi+\phi_0}{2}\, \tan\tfrac{\phi-\phi_0}{2} \right|^{\sin\phi_0} \right] \right\}. \quad (4.3)$$

where ϕ is a mapping described as $\sin\phi = \frac{\xi}{a}\sin\phi_0$.

Due to the nature of implicit solutions, we can easily solve Eq.(4.3) for the normal load, given a known contact width, c/R. Typically, however, in most applications, the load P will be the known input, with the contact half-width c the desired output. Thus, in most contexts, we will need to use Eq.(4.2) to numerically define an inverse function $c(P)$ that is able to provide this functionality.

4.3 Rounded, three-quarter plane formulation of a flat and rounded contact

A different formulation of the problem is needed for contacts with large geometry ratios, i.e. $b/R \gg 1$. Ideally, the domain shape would include the interface and 'normal' free surfaces in the contact-defining body, but this could only be achieved using a series solution [7] and this model has no rounding. Series solutions are undesirable due to their cumbersome nature and inability to capture the 'crisp formula' favoured to be practical usefulness. Instead, we adopt the following approach: consider, first, the limiting case when the edge radii become vanishingly small, and 'zoom in' towards an edge of the contact. For this geometry there will always be a region sufficiently local to the contact edge for the presence of the adjacent free boundary to be felt, whereas the opposite corner of the contact will be sufficiently remote for it to have a negligible effect. In this region, provided that the interfacial coefficient of friction were sufficiently large to prevent slip, the state of stress would approach that of a three-quarter plane, or, in other words, Williams' solution [8] specialised to a wedge of internal angle $3\pi/2$ radians, appropriately scaled. Now re-introduce a small edge radius, both in the actual contact and into the Williams' model. Provided that this is small compared with the overall size of the contact, there may be a region sufficiently remote from the very edge for Williams' solution still to establish itself, but which is also sufficiently far from the

opposite edge of the contact for the opposite free boundaries not to influence things. This is the approach which was successfully adopted in [4,5]. Here we provide a summary of the results found.

Consider a model of a three-quarter plane — this is appropriate because the interior of the contact is stuck and the displacements are continuous across the interface — with a radius at the corner. The outer boundary of the model is intended to represent infinitely remote points, and hence the loading there may be excited by using the displacement fields corresponding to Williams' eigensolutions, with multipliers on them in the form of stress intensity factors, K_I and K_{II}.

Looking, now, at the innermost points of the model, the contact region is locally incomplete because of the edge radius, and thus the tractions present very close to the contact edge will be square root bounded in character. Hence, we may represent the contact pressure in the form $p(x) = L_I\sqrt{x}$ and the shear traction as $q(x) = L_{II}\sqrt{x}$. These quantities (L_I, L_{II}) scale the tractions present near the contact edge.

To conclude this solution, we must understand how the far-field stress state controls the near-field stress state. We solve the resulting problem using the finite element package, Abaqus [9]. We can calibrate the associated near edge multipliers (L_I, L_{II}) for proportional loading, as in [10],

$$\left(\frac{L_I\sqrt{R}}{E^*}\right) = 0.9\left(-K_I^N + 1.09K_{II}^N\right), \tag{4.4}$$

$$\left(\frac{L_{II}\sqrt{R}}{E^*}\right) = 0.048\frac{(1.09K_{II}^N + K_I^N)}{(1.09K_{II}^N + K_I^N + 0.0004)} \tag{4.5}$$

where $K_i^N = \frac{K_i}{E^* R^{1-\lambda_i}}$, and λ_i are the corresponding eigenvalues of Williams' solution.

The corresponding contact law can be written explicitly [9, 10] as

$$\left(\frac{c}{R}\right)^3 = 13.08\left[-K_I^N + 1.09K_{II}^N\right]. \tag{4.6}$$

A refinement of the Fleury solution is possible. Very close indeed to the contact edge half-plane theory must apply, because very locally the problem looks Hertzian, and Flamant's solution [11] relates the surface tractions and displacements. In this neighbourhood, the outermost part of the solution derived in [12] is used which is another attempt at solving the rounded quarter plane pressing into a half-plane problem, but one where the influence of the free boundary on the interior contact pressure distribution is neglected. The original form of Mugadu's solution was scaled

by a stress intensity factor matched to the interior decay, but it is perfectly possible to re-scale those solutions in terms of the square root bounded traction decay at the very edge. We can then use the calibrated values of L_I and L_{II}, Eqs.(4.4,4.5), and the contact law, to scale the closed form, half-plane solution for a semi-infinite flat and rounded contact by taking the limits of Eq.4.3 as $b/R \to \infty$ [2],

$$p(x) = \frac{L_I}{4\sqrt{d}} \left[2\sqrt{dx} + (x-d) \ln \left| \frac{1-\sqrt{x/d}}{1+\sqrt{x/d}} \right| \right] \qquad x > 0 \tag{4.7}$$

and the equivalent equation for the shear traction

$$q(x) = \frac{L_{II}}{L_I} p(x) \qquad x > 0. \tag{4.8}$$

Since the calibrations of the multipliers, L_I and L_{II} come from the intermediate Williams' solution, the tractions account for the effect of coupling between the punch and the half-plane.

As seen in [6], the shape of the near-edge tractions from the half-plane solution, Eqs.(4.7,4.8), when scaled by the far-field calibrations, Eqs.(4.4,4.5), lie directly on top of the finite element output relatively far along the contacting interface (see Figs.3–6 of [6]). This means, going forward, we can use the loads on our problem to calibrate the stress intensity factors in the far field, and hence the multipliers that scale the tractions present relatively near to the contact edge; this model provides an explicit relationship between the stress intensity factors on the outer field and the multipliers on the innermost region.

4.4 Application of the rounded, three-quarter plane solution to the finite contact

The solution derived in Section 4.3 might be applied to find the effect of a small amount of rounding on any number of problems, for example, a cylindrical elastic punch pressed onto an elastically similar half-plane, but here we wish to use it to study the plane version of the problem, as seen in Fig. 4.1a for the first time. To do this, we first analyse the problem of a square elastic block, side length $2a$, pressed onto a frictional elastically similar half-plane. In principle, this arrangement might be subject to four kinds of load: a normal force, P, a shear force, Q, an applied moment, M, and tension within the half-plane, σ. A full analysis incorporating all four kinds of load was conducted by Riddoch [13] but in the preliminary investigation

we restrict ourselves to the case where the block is subject simply to a normal force and a shear force. The calibrations to move from (P, Q) space $\rightarrow$ (K_I, K_{II}) space are found in [9] as seen below,

$$\begin{Bmatrix} K_I/a^{1-\lambda_I} \\ K_{II}/a^{1-\lambda_{II}} \end{Bmatrix} = \begin{bmatrix} -0.4245 & 0.5057 \\ 0.2480 & 0.5032 \end{bmatrix} \begin{Bmatrix} P/2a \\ Q/2a \end{Bmatrix}. \tag{4.9}$$

Note that we restrict our attention to problems with intimate contact along the whole face. To inhibit corner lift-off, this requires $K_I < 0$ and therefore, from Eq.4.9, $|Q|/P < 0.8394$.

Fig. 4.2 plots various proportional loading paths for the flat and rounded contact as we look between the different loading spaces: normalised (P, Q), (K_I, K_{II}) and (L_I, L_{II}). The loads, P, Q, are bound by gradients that would cause separation at either contact edge. The term 'leading edge' refers to the edge aligned with the positive shear load direction, while the 'trailing edge' denotes the opposite edge aligned with the negative shear direction. With positive shear force applied from left to right, the leading edge is the right-hand edge, and the trailing edge is the left-hand edge. In this paper, we are particularly interested in normal loading (purple line), which causes mixed mode loading in (K_I, K_{II}) space, and, due to coupling, a non-zero multiplier on the near-edge shear traction, L_{II}.

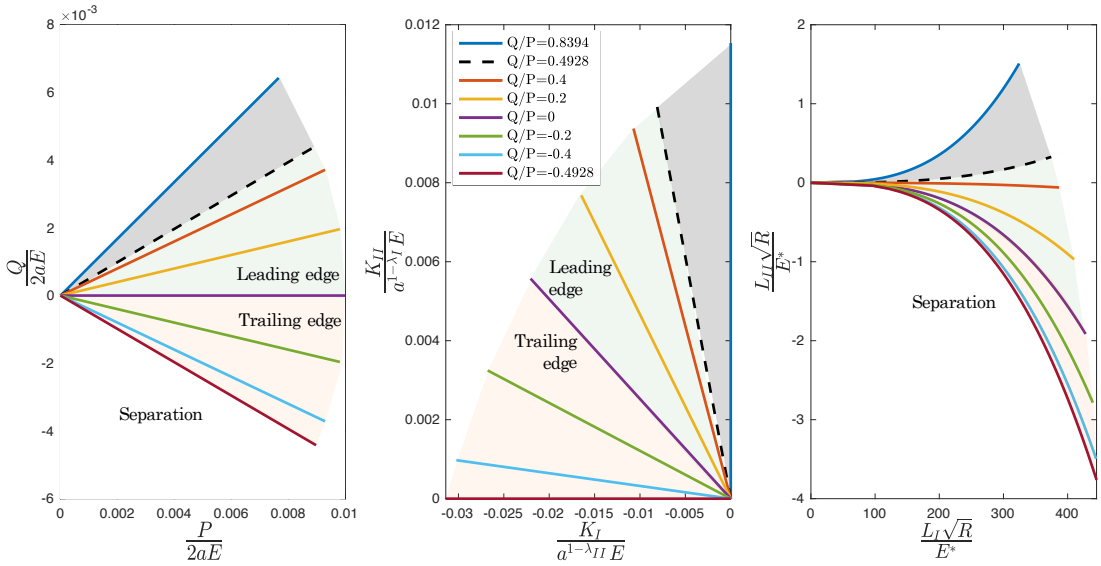


Figure 4.2: This plot shows the transformation of spaces for the flat-and-rounded contact with geometry ratio $a/R = 10$ for a range of load paths. The green-shaded area and the orange-shaded area display the loading at the leading edge and trailing edge of the contact, respectively. Any loading in the grey-shaded area represents moderate separation at the trailing edge of the contact.

When applying the rounded, three-quarter plane solution to the flat-and-rounded contact from Fig. 4.1a, we must do so with care. Since the calibrations of the stress-intensity factors are modelled on the sharp square contact, the solution will be most accurate when the geometry ratio, a/R, is large.

At both contact edges, the formulation of the closed-form solution will be as described in Section 4.3, and be referred to as the 'near-edge solution'.

As we move away from the contact edges, we will consider a 'centre solution'. At the centre of the contact, the tractions will be able to 'feel' the presence of both contact edges. Bounding the decay with Williams' solution, as seen in previous work [6], will not suffice for this geometry as it only considers the presence of one contact edge. Instead, to plot the contact tractions along the centre of the contact, we will use finite element analysis to analyse a sharp-edged, square contact, of width $2a$, on a half-plane.

4.5 Comparison of solutions

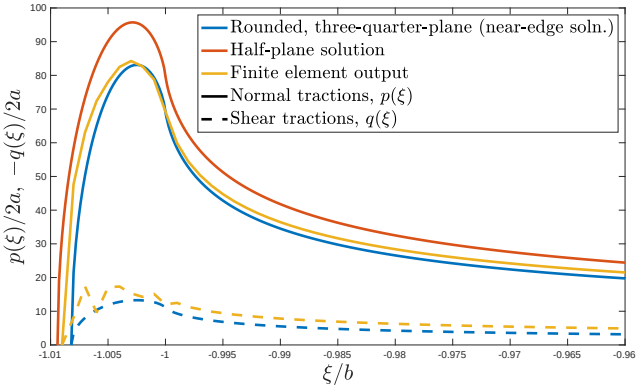
Comparisons of the contact tractions and contact laws below are given to analyse the suitability of each of the solutions: the half-plane solution and the rounded three-quarter plane solution, in the context of the finite flat-and-rounded contact of different geometry ratios.

4.5.1 Contact tractions

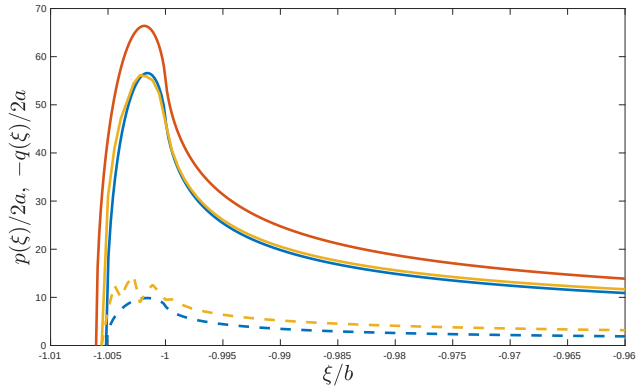
As discussed up Section 4.2, we predict the half-plane solution to be most accurate when b/R is small due to the assumptions made during its formulation. Similarly, the rounded, three-quarter plane solution, presented in Sections 4.3 & 4.4, ought to be most accurate when b/R is large.

In this section, we will compare each model to the output of finite element simulations for salient values of a/R. We will treat the numerical output as an 'exact' solution for the normal and shear tractions to enable this analysis. We will first do this by looking locally at the contact edge, Fig. 4.3.

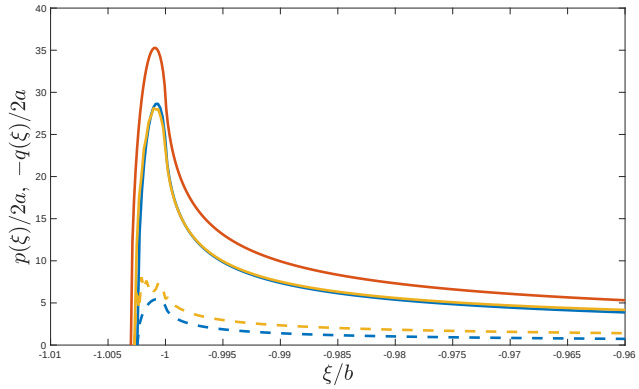
Firstly, we will analyse the normal tractions near the contact edge when $a/R = 6$ as shown in Fig. 4.3a. Very close to the contact edge ($-1.01 < \xi/b < 1.005$), the finite element normal traction (solid yellow) lies between the rounded, three-quarter plane solution (Eq.(4.7) in solid blue) and the half-plane solution (Eq.(4.3) in solid red). Throughout this region, the half-plane solution is as much of an overestimate as the rounded, three-quarter plane solution is an underestimate. For the following



(a) $a/R = 6$



(b) $a/R = 10$



(c) $a/R = 25$

Figure 4.3: Here we have plotted the normal (solid) and shear (dashed) tractions for the three types of solutions: rounded, three-quarter Plane solution (blue), Half-plane solution (red) and FEA output (yellow). The geometry of the punch is: (a) $a/R = 6$, (b) $a/R = 10$, (c) $a/R = 25$.

section of the contact ($-1.005 < \xi/b < -0.96$), the finite element solution falls close to the rounded, three-quarter plane solution.

Looking at the normal tractions near the contact edge when $a/R = 10$ and

$a/R = 25$, Fig. 4.3b,4.3c, we see that the finite element output lies increasingly close to the rounded, three-quarter plane solution. This is the outcome we would expect; as a/R increases, the rounded, three-quarter formulation becomes a more accurate representation of the true problem. In summary, we can see that this formulation gives a vast improvement over the half-plane representation of the normal tractions close to the contact edge when $a/R > 6$ under normal-only loading.

It is also important to study the shear tractions, displayed in Fig. 4.3. Since the half-plane formulation excludes the presence of coupling, under a pure normal load, no shear traction arises along the contact. Clearly, however, when we see the results of the finite element simulations, a pure normal load does indeed excite shear tractions. The rounded, three-quarter plane solution does allow for the presence of coupling, and thus both normal and shear tractions arise under a pure normal load and we see favourable comparisons to the simulations. The rounded, three-quarter plane solution is a significant improvement over the half-plane's representation of the shear tractions for all three geometry ratios. As a side note for the reader, the fluctuations in the finite element output (yellow dashed line) at the contact edges indicate that the solution has not fully converged. We accept this fact, considering the significant changes in traction over very small distances, and having utilized the finest mesh feasible with our computational power. The true shear traction will follow a smooth line by averaging these points.

To summarise, the key findings when comparing the solutions close to the contact edge are as follows.

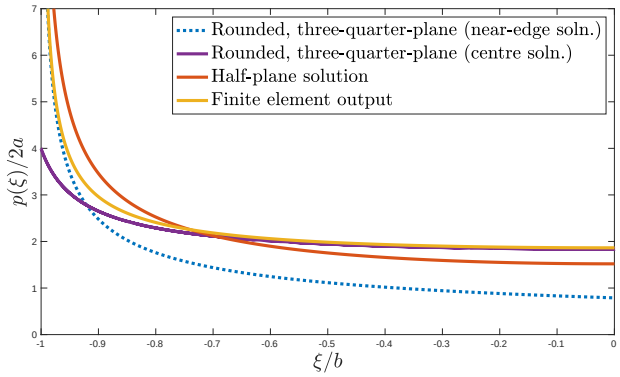
1. The normal tractions from the rounded, three-quarter plane solution become increasingly accurate as we increase the relative size of the flat region, b/R and hence a/R.

2. The rounded, three-quarter plane solution allows for the presence of coupling in the contact, thus it provides a far more accurate representation of shear traction compared to the half-plane formulation for all three values of a/R tested.

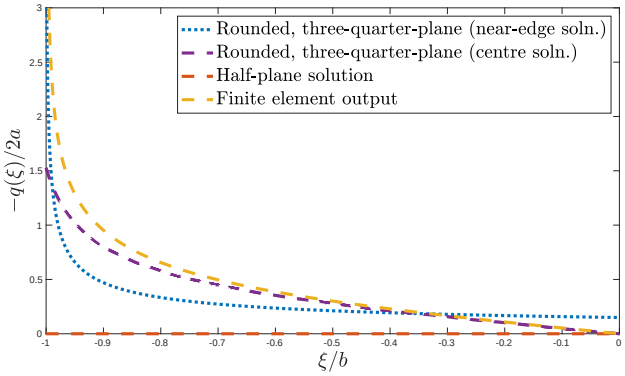
3. For all geometry ratios $a/R > 6$, the rounded, three-quarter plane solution is a significant improvement over the half-plane formulation.

To analyse how the solutions compare further into the contact region, we display the normal and shear tractions for $a/R = 25$ along the left half of the contact in Fig. 4.4. Fig. 4.4a demonstrates that the normal traction from the rounded, three-quarter plane centre solution tracks the finite element output very closely along the centre of the contact. The transition from the near-edge solution to the

centre solution takes place close to the intersection point between the two models, at $\xi/b \sim -0.88$. Throughout the centre section of the contact, the rounded, three-quarter plane solution is a better representation of the normal traction than the half-plane solution. Fig. 4.4b demonstrates the same is true for the shear tractions except the transition from the rounded, three-quarter plane near-edge solution to centre solution is much closer to the contact edge, at $\xi/b \sim -0.99$.



(a) Normal tractions.



(b) Shear tractions.

Figure 4.4: The normal (a) and shear (b) tractions for a flat-and rounded punch with $a/R = 25$. Here, ξ/b measures distance from the centre of the contact region. We display results for the: rounded, three-quarter plane solution (near-edge solution, blue, centre solution, purple), half-plane solution (red) and finite element output (yellow). The geometry ratio is $a/R = 25$.

4.5.2 Contact Laws

The contact law describes the relationship between the applied load and the size of the contact. To further investigate the suitability of each solution, we will analyse the contact law for the configuration of Fig. 4.5 for varying loads. In reality, both shear

and normal loading will contribute to the contact size due to geometric coupling, so for this section, we will introduce a shear load, Q, alongside the normal load, P. As with the previous analysis, all contacts are considered fully stuck unless stated otherwise.

Since there is no coupling in half-plane theory, the contact law using this formulation is independent of shear load; when loaded in shear, the contact size does not change and shear traction singularities grow at the edges of the contact. By contrast, the rounded, three-quarter-plane solution allows for the presence of geometric coupling; the contact law for this formulation is dependent on both shear and normal load.

Comparing the contact laws for varying Q/P loads will allow us to analyse the impact of geometric coupling on the contact law, and thus the suitability of the half-plane solution. In particular, if the geometric coupling has a significant impact on the contact law, we may consider the half-plane solution an unsuitable representation of the problem.

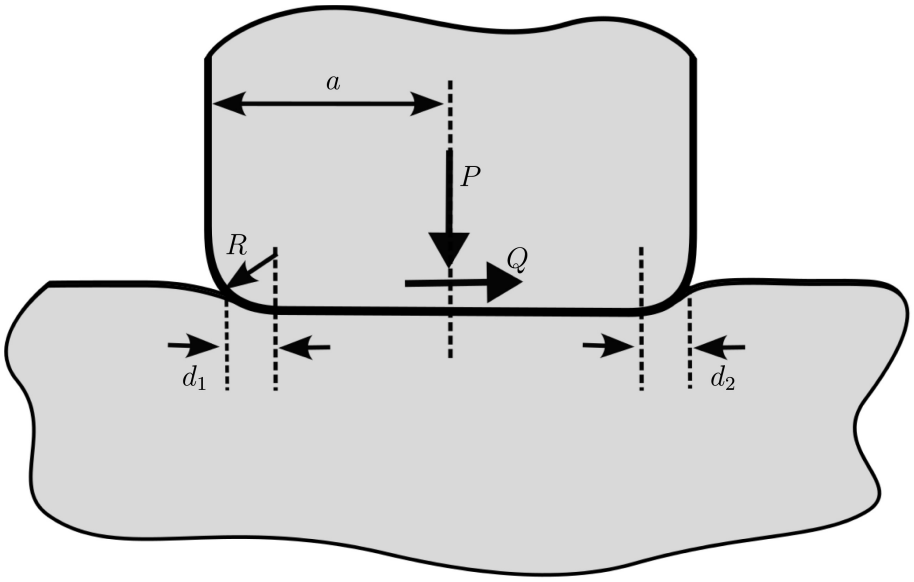


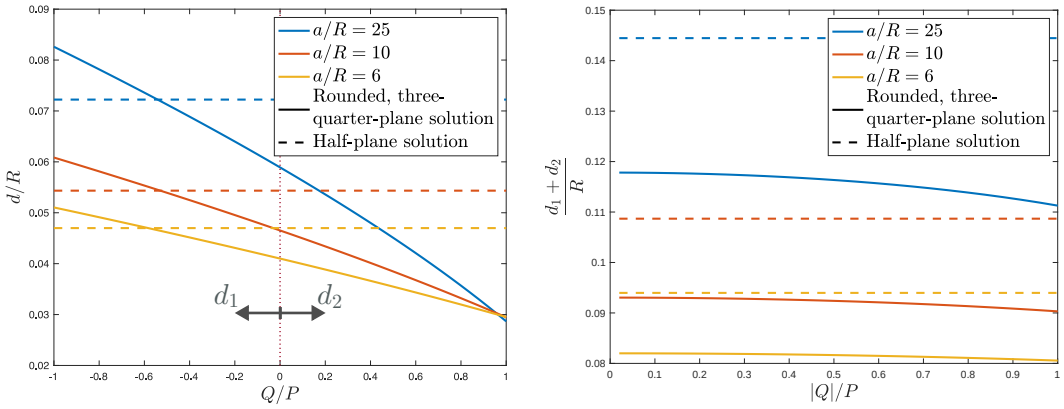
Figure 4.5: Flat and rounded contact loaded with a normal force, P and shear force, Q onto half-plane. The curved contact length on the left side, d_1 and right side, d_2 are defined for the contact law analysis to follow.

Fig. 4.6 displays the contact law from the half-plane formulation (dotted lines) and the rounded, three-quarter plane formulation (solid lines) under various loads, Q/P. To achieve this, the magnitude of the normal distributed load was held constant for all geometries considered, while the shear force was varied to achieve the desired loading ratios.

The rounded, three-quarter plane results in Fig. 4.6a are highest for large negative

loading ratios and lowest for large positive loading ratios. This shows that geometric coupling causes the leading edge of the contact (i.e. when $Q/P < 0$) to increase in length, and the trailing edge of the contact (i.e. when $Q/P > 0$) to decrease. As a result, we can expect the overall contact to shift toward the leading edge.

Clearly, we see a deviation of the rounded, three-quarter plane results from the constant prediction of half-plane theory, and, we expect the overall contact size to change as we increase the loading ratio. To analyse this further, we turn to Fig. 4.6b which displays the total length of the contact, in the two rounded portions of the contact, for both solutions. As may be seen, the rounded, three-quarter plane results are initially insensitive to the shear force, but begin to dip as the magnitude of Q/P increases; geometric coupling causes the total contact length to decrease as the magnitude of Q/P, increases.



(a) (b)

Figure 4.6: Two views of the contact law from the rounded three-quarter-plane solution (solid) and the half-plane solution (dotted) for different geometries. (a) Edge-specific contact length: for $Q/P > 0$ the leading-edge half-length d_2 is plotted; for $Q/P < 0$ the trailing-edge half-length d_1. (b) Total curved contact length as a normalised sum of the leading- and trailing-edge contact lengths.

In Fig. 4.6, as anticipated, the contact law using half-plane theory is constant for all values of Q/P (horizontal dashed lines) as it is only dependent on geometry, a/R and normal load, P. In Fig. 4.6b, the contact law using the rounded, three-quarter plane solution decreases at a non-constant rate as Q/P increases in magnitude. This results in the overall contact size decreasing as the magnitude of the external loads increases. Further, as the magnitude of the loading ratio increases, the rate of decrease of the contact size increases. The divergence is accounted for by the presence of geometric coupling, which is ignored in the half-plane solution, thus implying the unsuitability of the half-plane solution for this problem for increasing

values of geometric ratio ($\sim a/R > 6$).

To confirm our predictions for the suitability of the contact laws arising from half-plane and rounded, three-quarter plane formulations, we will compare these solutions with the finite element output. Within this paper, we have the numerical results for three discrete geometry ratios: $a/R = 6$, 10 and 25. Fig. 4.7 compares the solution found using half-plane theory as described in §4.2 and rounded, three-quarter plane solution described in §4.3, relative to the finite element output for the given geometries. The closer the contact law ratio, $d_{\text{theory}}/d_{\text{FE}}$, is to unity, the closer the solution is to the 'exact solution' represented by finite element analysis. We recognise that this plot is very sparse because obtaining fully converged finite element solutions is time-consuming and tedious; three discrete points per solution should only be used to give an indication of how the solutions' contact laws vary as we change the geometry. We can not justifiably extrapolate, or comment on the linearity of the relationship. However, as expected for the geometries trialled, Fig. 4.7 shows that the half-plane solution deviates from the numerical solution as we increase a/R, whilst the rounded, three-quarter plane solution becomes increasingly accurate. This is evidence that the rounded, three-quarter plane contact law is an improvement on the half-plane solution for $a/R \geqslant 10$. Also, the half-plane solution always over estimates the contact size, whereas the three-quarter plane method under estimates it.

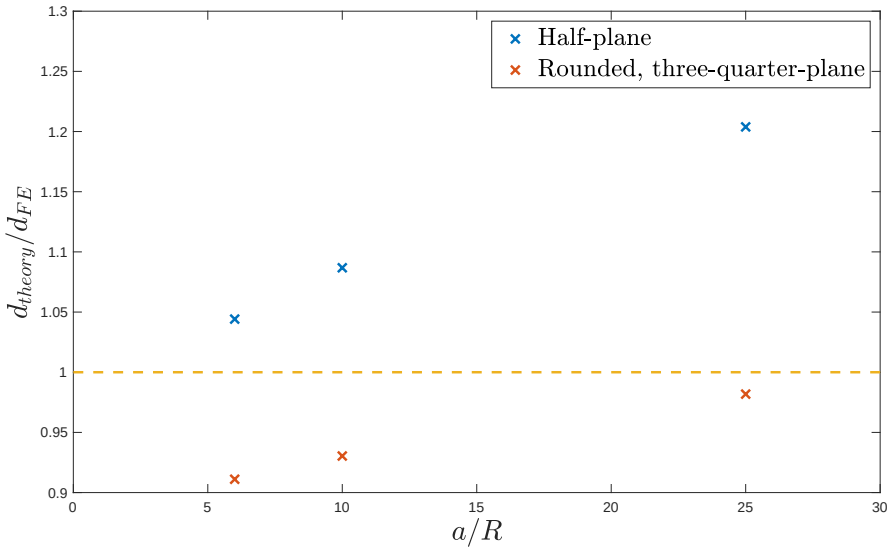


Figure 4.7: Comparing the contact law from the rounded, three-quarter plane solution (solid lines) and the half-plane solution (dotted lines) relative to the finite element output for three distinct geometries.

4.6 Conclusion

In this analysis, we have investigated the applicability and limitations of two models for incomplete contacts, namely one based on half-plane theory and a second derived from the rounded, three-quarter plane formulation. We first considered the limitations of applying half-plane theory to the flat-and-rounded contact pressed into a half-plane. We successfully applied the rounded, three-quarter plane solution [6] to the industrially relevant flat-and-rounded contact, where both contact edges may be felt. However, this solution in turn gives rise to its own limitations.

To investigate which solution is most appropriate for a given flat and rounded contact geometry, we solved the problem for three discrete geometries using a finite element model to provide an 'exact' solution.

These demonstrated that the rounded, three-quarter plane formulation is a big improvement on the half-plane solution for moderate to large geometry ratios, $a/R > 6$. The novel formulation presented herein gives a much better representation of the contact tractions along a flat and rounded contact for these geometries, whilst retaining a closed-form explicit solution. Further to this, it has improved our understanding of the impact of geometric coupling. This has major implications for practical applications such as fan blade dovetails in the root of a gas turbine and locking segments of riser-seabed connectors.

In this study, we have only considered proportional loading in (P, Q)-space. The calibrations for the near-edge multipliers, L_I and L_{II} may not hold for different loading trajectories, as we know the near-edge shear tractions are path dependent. Going forward we aim to apply this approach to problems with varying load paths, allowing for this path dependency.

Statement of Authorship

Author Contributions

B. Eames: [Writing - review & editing, Writing - original draft, Visualisation, Validation, Project administration, Methodology, Investigation, Formal analysis.] **D.A. Hills:** [Writing - review & editing, Writing - original draft, Visualisation, Validation, Supervision, Resources, Investigation, Formal analysis, Conceptualisation.] **M.R. Moore** [Writing - review & editing.]

References

[1] I. Ya. Steuerman. *Contact Problem of the Theory of Elasticity*. Available from the British Library in an English translation by Foreign Technology Division, FTD-MT-24-61-70, 1970.

[2] M Ciavarella, D A Hills and G Monno. "The influence of rounded edges on indentation by a flat punch". in *Proceedings of the Institution of Mechanical Engineers, Part C: Journal of Mechanical Engineering Science* 212.4 (1998), 319–327. DOI: 10.1243/0954406981521259. eprint: https://doi.org/10.1243/0954406981521259. URL: https://doi.org/10.1243/0954406981521259.

[3] Michele Ciavarella. "Indentation by nominally flat or conical indenters with rounded corners". in *International Journal of Solids and Structures* 36.27 (1999), 4149–4181.

[4] J.R. Barber. *Contact Mechanics*. Solid Mechanics and Its Applications. Springer International Publishing, 2018, 29–39. ISBN: 9783319709390. URL: https://books.google.co.uk/books?id=4GNLDwAAQBAJ.

[5] L.E. Goodman and L.M. Keer. "The contact stress problem for an elastic sphere indenting an elastic cavity". in *International Journal of Solids and Structures* 1.4 (1965), 407–415. ISSN: 0020-7683. DOI: https://doi.org/10.1016/0020-7683(65)90005-3. URL: https://www.sciencedirect.com/science/article/pii/0020768365900053.

[6] B. Eames, D.A. Hills and M.R. Moore. "Near edge tractions for a rounded quarter-plane pressed into an elastically similar half-plane". in *Tribology International* 186 (2023), 108582. ISSN: 0301-679X. DOI: https://doi.org/10.1016/j.triboint.2023.108582. URL: https://www.sciencedirect.com/science/article/pii/S0301679X23003699.

[7] R. Khadem and J.J. O'Connor. "Adhesive or frictionless compression of an elastic rectangle between two identical elastic half-spaces". in *International Journal of Engineering Science* 7.2 (1969), 153–168. ISSN: 0020-7225. DOI: https://doi.org/10.1016/0020-7225(69)90054-8. URL: https://www.sciencedirect.com/science/article/pii/0020722569900548.

[8] M. L. Williams. "Stress singularities resulting from various boundary conditions in angular corners of plates in extension". in *Journal of Applied Mechanics* 19 (1952), 526–528.

[9] Rodolfo Fleury, D. Hills and James Barber. “A corrective solution for finding the effects of edge-rounding on complete contact between elastically similar bodies. Part I: Contact law and normal contact considerations”. in *International Journal of Solids and Structures* 85 (2016). DOI: 10.1016/j.ijsolstr.2015.11.031.

[10] Rodolfo Fleury, D. Hills and James Barber. “A corrective solution for finding the effects of edge-rounding on complete contact between elastically similar bodies. Part II: Near-edge asymptotes and the effect of shear”. in *International Journal of Solids and Structures* 85 (2016). DOI: 10.1016/j.ijsolstr.2015.11.032.

[11] J. R. Barber. *Elasticity*. Solid Mechanics and Its Applications. Springer Dordrecht, 2009. **chapter** 12.5.3. ISBN: 978-90-481-3809-8. DOI: https://doi.org/10.1007/978-90-481-3809-8.

[12] A. Mugadu, D. Hills, James Barber and Anthony Sackfield. “The application of asymptotic solutions to characterising the process zone in almost complete frictional contacts”. in *International Journal of Solids and Structures* 41 (2004), 385–397. DOI: 10.1016/j.ijsolstr.2003.09.038.

[13] Daniel J Riddoch and David A Hills. “Necessary conditions for near-edge stick of complete contacts”. in *The Journal of Strain Analysis for Engineering Design* 55.5-6 (2020), 172–180. DOI: 10.1177/0309324720902873. eprint: https://doi.org/10.1177/0309324720902873. URL: https://doi.org/10.1177/0309324720902873.

Chapter 5

Elastic, Flat and Rounded Finite Contacts in Partial Slip: a novel solution based on wedge and half-plane formulations

Contents

5.1 Introduction 86

5.2 Summary of half-plane formulation for contact edge - *Phase (3)* 91

5.3 Three-quarter plane formulation: Calibrations - *Phase (2)* 93

5.4 Geometry specific calibration: External loads to Williams' Solution - *Phase (1)* 94

5.5 Combining the phases: Contact law 95

5.6 Combining the phases: Tractions under full stick 98

5.7 Comparison of methods under full stick 99

5.7.1 Finite-element reference solution 99

5.7.2 Validation 101

5.8 Condition for partial slip 105

5.9 Shear tractions with partial slip 107

5.10 Conclusion 114

The work presented in this chapter refines the method first developed in Chapter 3 such that it can be applied to contacts with complicated loading histories, and as a result, identify whether either edge of a flat and rounded contact experiences partial slip. This chapter serves as another significant step in our understanding of conforming contacts that cannot be appropriately represented as two half-planes as we are able to find cases when one edge may be in partial slip whilst the other is stuck.

This chapter presents research published as:

B. Eames, D.A. Hills, J.R. Barber, Elastic, flat and rounded finite contacts in partial slip: A novel solution based on wedge and half-plane formulations, *International Journal of Solids and Structures*, Volume 321, 2025, 113543, ISSN 0020-7683, https://doi.org/10.1016/j.ijsolstr.2025.113543.

Elastic, Flat and Rounded Finite Contacts in Partial Slip: a novel solution based on wedge and half-plane formulations

B Eames[1], D A Hills[1] and J.R. Barber[2]

[1]*Department of Engineering Science, University of Oxford, Parks Road, Oxford, OX1 3PJ, UK*

[2]*Department of Mechanical Engineering, University of Michigan, Ann Arbor MI 48109-2125, USA*

Abstract

The accurate modelling of elastic, flat and rounded contacts is critical for several engineering applications, such as turbine fanblade roots and seabed riser connections. This paper introduces a refined hybrid three-quarter plane / half-plane formulation that addresses the limitations of traditional half-plane theory by incorporating the effects of the traction-free surfaces. The refined method extends previous work that uses a combination of numerical and analytical techniques to solve for tractions and slip behaviour at the contact edges under multi-stage loading. Incorporating the effect of geometric coupling allows us to differentiate between the stress and slip conditions at each contact edge, for the first time.

Validating the results against finite element analysis demonstrates that the proposed approach achieves greater accuracy than half-plane theory for geometries with relatively large flat lengths.

5.1 Introduction

This paper advances the analysis of elastic, flat and rounded contacts that contribute to many high-value systems in engineering, such as turbine blade roots and subsea riser connections. The safety-critical applications of these contacts demand the best possible analysis.

A widely used approach involves the half-plane formulation; each body is thought of as a half-plane, but with a minor perturbation that represents the contact profile. Aside from the free surfaces either side of the contact, no other free surfaces are present in the model. Ignoring the vertical traction-free surfaces of the flat and rounded contact geometries, as illustrated in Fig. 5.1, can lead to inaccurate predictions of tractions and slip behaviour, with potentially serious consequences.

A new method has been developed to improve the representation of flat and rounded contacts, such as that illustrated in Figure 5.1, where the traction-free sides normal to the contact surface are taken into account, and which is relevant when the geometry has a flat length-to-radius ratio greater than $a/R \sim 6$. The goal is to

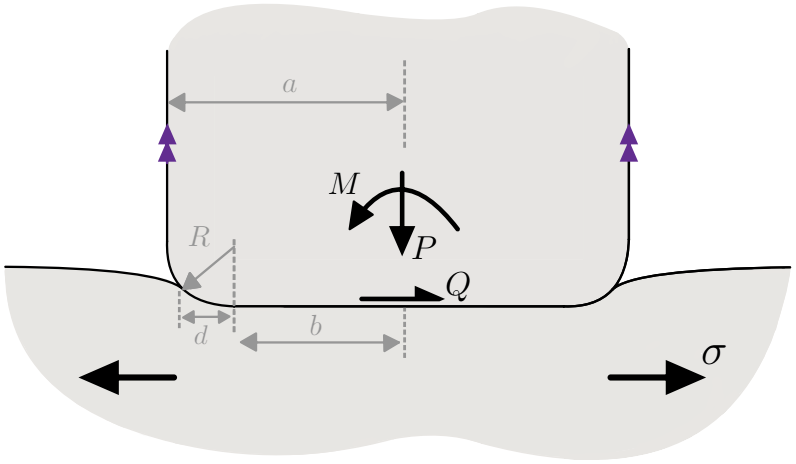


Figure 5.1: Flat and rounded punch pressed into a half plane under loads: normal force P, shear force Q, moment M, and bulk tension σ. The traction-free edges are indicated by purple markers. The geometry of the contact is defined by the ratio a/R, where a is the contact half width, R is the radius of the rounded section. b is the half flat length of the contact.

derive a reasonably straightforward method to solve for the contact law and near edge-of-contact tractions in a better way than using the half-plane based solution. The trade off is that the new method involves more steps than using the half-plane solution, and it provides information only about what arises at or quite near to the contact edge. But this is the region in which slip is most likely to occur, and hence surface damage is incurred, and it is also the region in which experiments (and practice) have shown that all cracks nucleate, and once some preliminary work is done, various loading histories may be analysed very easily. This is important because, in the examples cited, a single remote load excites both normal and tangential contact loading, and typically we will want to know the steady state stick-slip solution when the load state oscillates between two given points in P (normal load), Q (shear load) space. The formulation makes use of three phases, illustrated in Figure 5.2:

1. A simplified form of the actual contact, in which the edges of the contact are assumed sharp, is analysed using finite elements (or another numerical method). This model incorporates the free normal surfaces of the contacting bodies and could include other features, such as holes, but the function of the solution is to find a calibration between the loads applied and, assuming that the contact edge is adhered, the multipliers on the Williams' Solution for a three quarter plane, located at the contact corner.

2. An elasticity solution based on a wedge formulation, here specialised to a three-quarter plane, and with some feature (to be specified, but it could be

either slight rounding, as in our earlier formulation or, here, a crack) at the wedge corner. The function of this phase of the calculation is to specify the calibration between the Williams' 'wedge' calibration constants and the scaling factors for the half-plane rounded feature problem, very close to the contact edge (*phase (3)*).

3. The third solution is one derived from half-plane theory, and is for a semi-infinite rounded contact. It applies close to the edge of rounding.

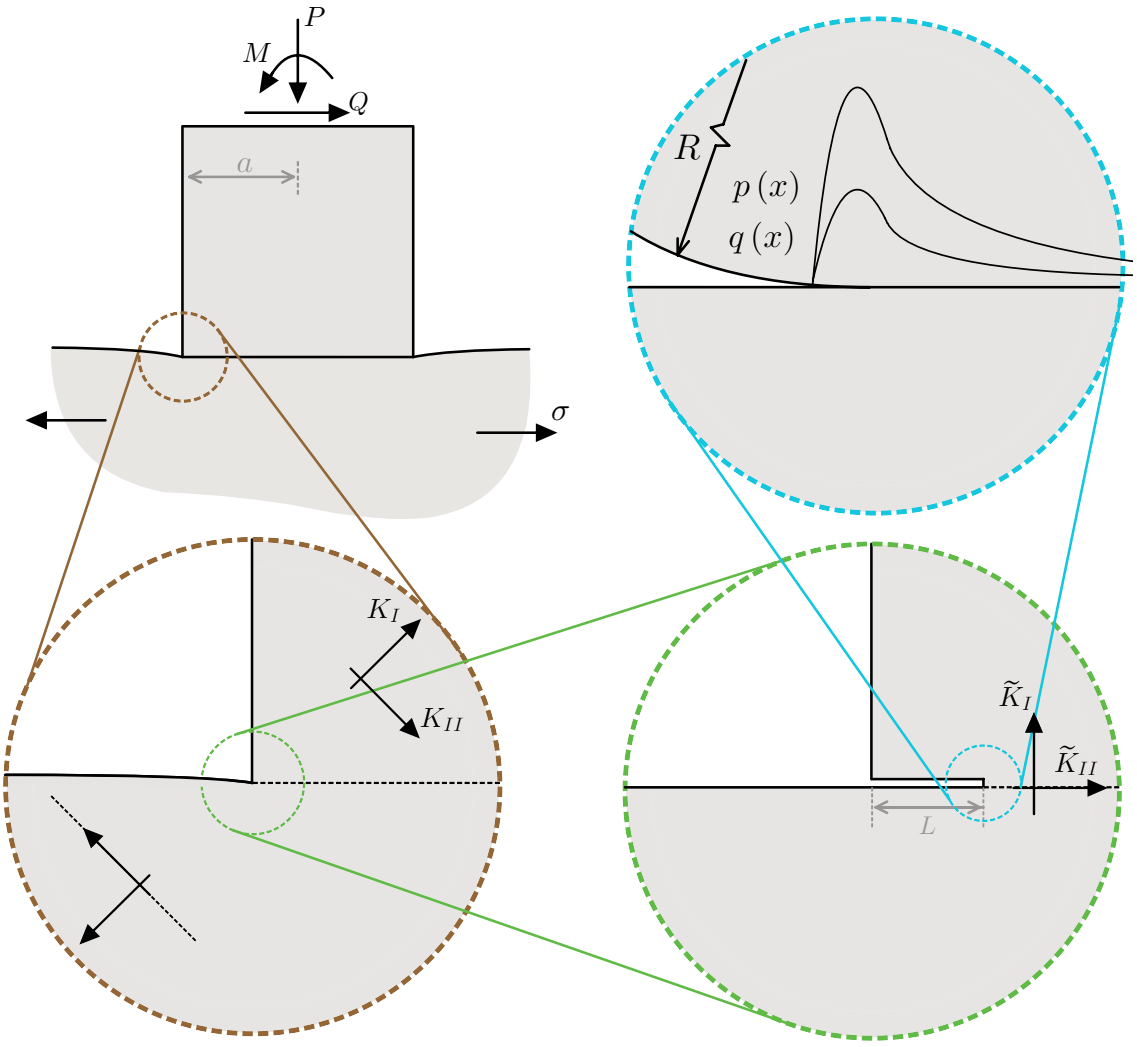


Figure 5.2: An illustration of the refined, three-quarter plane formulation. The formulation consists of three key phases: the first is a sharp square contacting body loaded onto a half-plane. The second phase (dashed brown and green circles) isolates one corner of the contact, modelling it as a wedge solved by Williams' solution with a crack inserted colinear to the contact interface. The final phase (blue dashed circle) applies half-plane theory to obtain the normal and shear tractions close to the rounded contact edge.

While FE can model the full geometry directly, achieving convergence and reliable edge-of-contact slip predictions remains challenging. The proposed method addresses this limitation by simplifying the demand on FE analysis to provide only the outer multipliers on the Williams' solution for a wedge (*phase (2)* above). As noted above, the FE model might incorporate any number of other features present in the prototype, including holes and other features away from the contact surface. In this paper, we will concentrate on the case where the basic geometry contains no other features and the block height is equal to the block width.

Once the calibration is known, attention will move to *phase (2)*, which comprises a three-quarter plane incorporating a feature at the internal corner. In our recent paper [1], this was a radius whose value was set equal to the actual radius of the contact edge, but here we will use a different feature, viz. a crack of length L whose length is chosen to be the distance from the free normal surface of the block to the flat-to-round transition point of the contact front face. The crack surfaces are assumed devoid of tractions, and the function of this phase of the calculation is to provide the calibration between the Williams' wedge multipliers (K_I, K_{II}) and the crack tip stress intensity factors $(\widetilde{K}_I, \widetilde{K}_{II})$.

The third element of the solution (*phase (3)* above) provides us with both the contact law and the contact edge tractions. These aspects are derived in [2] and is analytically straightforward, but, since it is based on half-plane theory, it is formally correct *only* at small distances from the contact edge. It has the properties that;

(a) as the extreme edge of the contact is approached the tractions decay in a square root bounded form (as expected, blue dashed line in Fig. 5.3)

(b) at remote points the tractions decay is a square root form (which is not what one would infer from a Williams' wedge solution, green dashed line in Fig. 5.3).

In previous work [3, 1], the calibration between *phase (2)* and *phase (3)* relied on matching the generalised stress intensity factors found from a model based on a slightly rounded wedge form of Williams' solution to the multiplier on the extreme-edge square-root-bounded tractions (*part (a)* above) of the Mugadu solution [2]. This piece of work showed very convincingly that the Mugadu solution penetrated a very long way in from the contact edge (up to at least $x/d \sim 10$). However, the limitations of the procedure were that (i) it relied on accurate calibrations of Fleury solution [4] that were very close to the limit of the precision of the original paper, and (ii), more restrictively, the method would work only when the loading trajectory was such that the contact remained adhered up to the edge. Both of these limitations are avoided in the current paper, which opens up our ability to pursue problems for any number

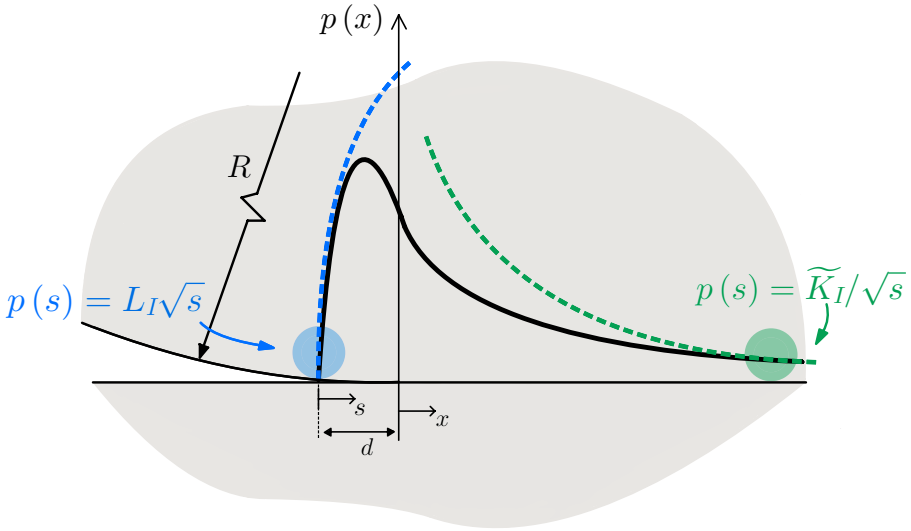


Figure 5.3: Coordinate x is measured from the flat and round transition point, and s is measured in from the contact edge such that $s = x + d$. The contact traction from Mugadu's solution using half-plane theory (solid black line) can be scaled by either the rising (*part (a)*) or decaying (*part (b)*) asymptotes, illustrated by the blue dashed and green dashed lines, respectively. The multiplier on the far-field asymptote, $\widetilde{K}_I$, is the stress intensity factor on the crack tip problem, seen in Fig. 5.2.

of contact loading histories, including those where edge slip occurs.

The key innovation is shown in Figure (5.3) in which we assume that the material in the rounded portion of the three-quarter plane, adjacent to the contact edge, sustains very little stress and therefore appears exactly like an edge crack. Inserting a crack into the three-quarter plane, co-linear with the contact interface, and of length equal to distance from the free surface to the flat-round transition point, L, Fig. 5.2, will yield conventional (square root singular) crack-tip stress intensity factors. Note that L may be set equal to the edge radius, R, if the edge radius is exactly a quarter-circle, but it may be less if the arc subtended by the edge radius is less than 90 degrees.

Because the solution for tractions for a semi-infinite rounded contact [5] decay in a square root manner, by setting their values ($\widetilde{K}_I$ for contact pressure, $\widetilde{K}_{II}$ for shear traction) to those derived from the intermediate problem, *phase (2)*, a solution to the original contact problem is derived. In addition, as the solution is now controlled by the value of the remote-from-edge multipliers, it means that slipping solutions are readily analysed using the techniques described fully in [6] for half-plane problems subject to complicated loading histories. This work improves the analysis of flat and rounded contacts, addressing the critical limitations of other formulations.

5.2 Summary of half-plane formulation for contact edge - *Phase (3)*

A solution for the contact problem under consideration, Figure 5.1, has been known for some considerable time, and it is this which has been used in industry for a number of problems. As stated earlier, the actual domain shape assumed for each contacting body is a half-plane, so that the free surfaces normal to the contact depicted in Figure 5.1 are not represented, and the purpose of this article is to remedy this limitation. The original solution goes back to a paper by Steuerman published in the late 1940s, and this was resurrected in an accessible form by Ciavarella et al [7]. If we let

$$\frac{sin\phi}{sin\phi_0} = \frac{x}{c}, \tag{5.1}$$

where c is the contact half-width, and $sin\,(\phi_0) = b/c$, the contact law is given by

$$\frac{2PR}{E^*} = b^2 \left(\frac{\pi - 2\phi_0}{2sin^2\phi_0} - cot\phi_0 \right), \tag{5.2}$$

where $E^*$is the plane strain modulus. The pressure distribution is given by

$$\frac{c\,p(\phi)}{P} = -\frac{2/\pi}{\pi - 2\phi_0 - \sin 2\phi_0} \times \left[(\pi - 2\phi_0)\cos\phi + \ln\left\{ \left| \frac{\sin(\phi + \phi_0)}{\sin(\phi - \phi_0)} \right|^{\sin\phi} \left| \tan\tfrac{\phi+\phi_0}{2}\, \tan\tfrac{\phi-\phi_0}{2} \right|^{\sin\phi_0} \right\} \right]. \tag{5.3}$$

Clearly, when the flat length, b, becomes vanishingly small, the contact recovers a cylindrical form. Hence, recovers the classic Hertz problem in two dimensional form, where the idealisation of both bodies as half-planes is known to be legitimate at loads in the elastic regime. Equally, when b is very large it is clear that the contact-defining body looks more and more like a square-ended punch, and its idealisation as a half-plane is not appropriate. As an aside, half-plane theory can be validly applied to the geometry of Fig. 5.1, but only when the contact-defining body is rigid, and when the contact is uncoupled, which can only be achieved in the absence of lubrication, if the half-plane is incompressible.

We have earlier referred to '*phase (3)*', which is the configuration which results if the solution just derived is taken and the ends moved infinitely far apart. The uncoupled nature of the solution means that a normal load will induce a contact

pressure alone, and this is given by [2, 8]

$$p(s) = \frac{3K_I}{4\sqrt{d^3}}\left[2\sqrt{ds} + (s-d)\,ln\left|\frac{1-\sqrt{s/d}}{1+\sqrt{s/d}}\right|\right] \qquad s > 0 \tag{5.4}$$

where s is a coordinate measured inwards from the contact edge, and which takes the simplified form

$$p(s) = \frac{K_I}{\sqrt{s}} \qquad s \gg d \tag{5.5}$$

when the observation point is very remote. In the solution being developed in this paper it is this quantity which will be used to scale the solution but for completeness we note that we may take the opposite limit, $s \to 0$ in equation (5.4) where the contact pressure is square root bounded in form and we have

$$p(s) = L_I\sqrt{s} \qquad L_I = \frac{3\widetilde{K}_I}{d} \qquad s \ll d. \tag{5.6}$$

The contact law is given by

$$\frac{3\pi R\widetilde{K}_I}{2E^*} = \sqrt{d^3}, \tag{5.7}$$

or, letting $\widehat{K}_I = \frac{\widetilde{K}_I}{E^*\sqrt{R}}$

$$\left(\frac{d}{R}\right)^3 = \left(\frac{3\pi\widehat{K}_I}{2}\right)^2, \tag{5.8}$$

and the peak contact pressure, p_0, which is at about $x/d \simeq 0.7$, is

$$\left(\frac{p_0}{E^*}\right)^3 = 1.24\widetilde{K}_I^2 \tag{5.9}$$

The material in the contact which is very close to the edge, just as we have analysed, *does* behave like a half-plane, because in this region the surface tractions and displacements are related by the Flamant solution. We have shown [3], that although strictly speaking the form of the contact pressure given by equation (5.4) is valid only very close to the contact edge, in practice it remains a very good approximation up to significant values of s/d, certainly beyond 10.

5.3 Three-quarter plane formulation: Calibrations - *Phase (2)*

In previous work [3], we made use of a finite element model developed by Fleury [4], consisting of a three-quarter plane, representing the sum of the contacting bodies, near to one corner, and incorporating a radius near the apex, illustrated in the intermediate phase in Figure 5.2. Details of this finite element model can be found in [4]. This enabled us to find the relationship between, on the one hand, the stress intensity factors for Williams' solution, specialised to a three quarter plane, K_I, K_{II}, and, on the other, the very near-edge multipliers on the contact pressure and shear traction, which are square root bounded in character, L_I, L_{II}. The latter may be matched up with the multipliers on Mugadu's half-plane solution, illustrated for the normal traction case in blue in Figure 5.3. However, the calibration for the shear traction (L_{II}) is only valid when the contact is fully stuck and loaded proportionally from the origin. In reality, many applications of the flat and rounded contact experience multiple step loading with partial slip, so, to avoid this limitation, we seek an alternative calibration for the near-edge half-plane *phase (3)*.

Very near the contact edge, both bodies can be appropriately modelled as half-planes, and the solution we have designated to *phase (3)* applies. Local to this region, the solution is governed by two distinct sets of multipliers - L_I, L_{II} which scale the tractions at the very contact edge, and $\widetilde{K}_I, \widetilde{K}_{II}$, which scale the traction decay as the observation point moves away from the contact edge, as seen in Fig. 5.3 and explained in the previous section. In this paper, we will use only the latter calibrations. Aside from the greater precision of the calibration, we note that this is the only feasible way to scale solutions if we expect there to be finite edge-of-contact slip zones present, as they are defined in a region where there will certainly be stick.

By inserting a crack at the edge of the three-quarter plane, colinear with the contact interface, the crack tip stress intensity factors represent the multipliers on the traction decay of the half-plane-based model when loaded, and, locally, $p \sim \widetilde{K}_I/\sqrt{x}$, $q \sim \widetilde{K}_{II}/\sqrt{x}$.

We define all stress intensity factors in this paper *without* the factor of $\sqrt{2\pi}$ which customarily appears in the definition of crack-tip intensity factors. The definition is

$$\widetilde{K}_I = \sigma_{\theta\theta}\left(r, 0\right)\sqrt{r}_{Lt\ r\to 0}, \tag{5.10}$$

and similarly for mode II, for both the multipliers on the Williams' solution and for the crack tip multipliers. Allowing for this scaling, we have in [5] the calibration for

the crack tip stress intensity factors, $\widetilde{K}_I, \widetilde{K}_{II}$, for a crack of length L, collinear with the contact interface and emanating from the corner of a three quarter plane,

$$\frac{1}{\sqrt{L}} \left\{ \begin{array}{c} \widetilde{K}_I \\ \widetilde{K}_{II} \end{array} \right\} = \left[\begin{array}{cc} +0.771 & \mp 0.834 \\ \pm 0.311 & +0.285 \end{array} \right] \left\{ \begin{array}{c} K_I L^{\lambda_I - 1} \\ K_{II} L^{\lambda_{II} - 1} \end{array} \right\}, \tag{5.11}$$

where λ_I, λ_{II} are the eigenvalues derived by Williams'. An approximate analytical solution to this problem was found by Khrapov [9], which agrees with these values. It is important to apply a rigorous sign convention so that we can obtain solutions for both the left and right edges of the contact. We adopt the convention that a positive stress on the bisector line, where the first two eigensolutions uncouple, gives rise to a positive stress intensity factor, and vice versa. This convention is applied to both the Williams' solution multipliers, and for the crack tip stress intensities. This has been built into equation (5.11) where we adopt the upper signs at the left hand contact corner and the lower signs at the right hand contact corner, Fig. 5.4.

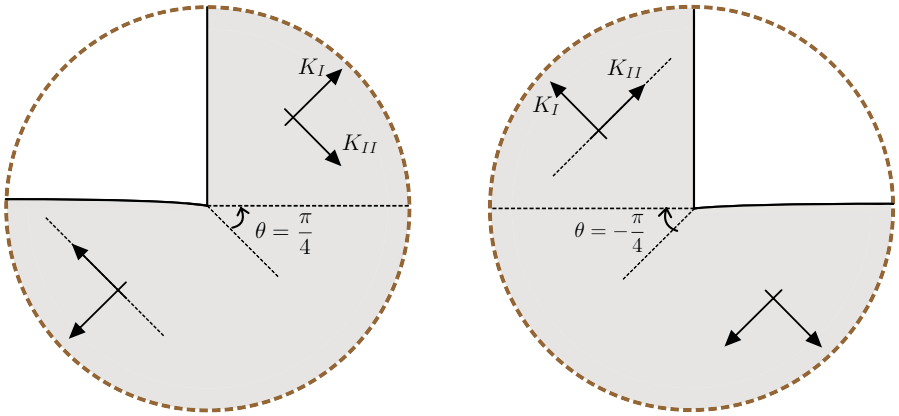


Figure 5.4: Sketch of both the left and right corners, where the interface at the left corner is described when $\theta = \pi/4$ and the interface at the right corner is described by $\theta = \pi/4$. K_I, K_{II} are the three-quarter plane stress intensity factors on Williams' solution.

5.4 Geometry specific calibration: External loads to Williams' Solution - *Phase (1)*

Phase (3) of the solution, described in Section 5.2 is universal in the sense that it can be applied to any conforming, slightly rounded contact, regardless of the overall geometry of the contacting bodies. The intermediate solution, described in Section 5.3, applies to any contact where the edge faces of the contact-defining body are orthogonal to the contacting interface. But, the first element of the solution, *phase*

(2), calibrating the Williams' stress intensity factors, is geometry-specific and here, we will consider the simple case of a square 'block', of side $2a$.

We have noted that there is a comprehensive calibration for the four effects of applied normal force, applied shear force, applied moment and underlying tension (P, Q, M, σ respectively), here we will concern ourselves with the first two quantities only. Fleury obtained calibrations for a square block pressed into a half-plane using a careful finite element analysis detailed in [4], giving the following

$$\left\{ \begin{array}{c} K_I a^{\lambda_I - 1} \\ K_{II} a^{\lambda_{II} - 1} \end{array} \right\} = \left[\begin{array}{cc} -0.4245 & \pm 0.5057 \\ \pm 0.2480 & +0.5032 \end{array} \right] \left\{ \begin{array}{c} P/2a \\ Q/2a \end{array} \right\}, \tag{5.12}$$

where, as earlier, the upper and lower signs correspond to the left and right corners respectively, Fig. 5.4.

As an aside, we note the condition for intimate contact at the left corner is that $\sigma_{\theta\theta}(\pi/4) < 0$ and at the right corner is that $\sigma_{\theta\theta}(-\pi/4) < 0$. Considering Williams' solution for general loading, Eq.(5.12) the conditions for intimate contact require $K_I < 0$ at both edges. This will put bounds on the acceptable combinations of $P, Q, M, \Delta\sigma$ where the solution to be developed applies. For simple P, Q loading, the limiting case for intimate contact is $\left|\frac{Q}{P}\right| < 0.93$.

5.5 Combining the phases: Contact law

Phase (1), for the overall contact, has the contacting body half-width, a, as its internal length dimension. *Phase (2)* which introduces the location of the contact flat-to-radius transition point from the normal free face, has L as its length scale. *Phase (3)* describing the edge-of-contact behaviour, has contact corner radius, R, as its length dimension. There is no necessity for the edge radius to subtend an angle of 90^o, but, to reduce the number of independent variables at this point we will set $L = R$. We may then combine *phases (1,2)* to arrive at

$$\frac{1}{\sqrt{R}} \left\{ \begin{array}{c} \widetilde{K}_I \\ \widetilde{K}_{II} \end{array} \right\} = \left(\frac{a}{R}\right)^{1-\lambda_1} \mathbf{A}\left(\tfrac{a}{R}\right) \left\{ \begin{array}{c} P/2a \\ Q/2a \end{array} \right\}, \tag{5.13}$$

$$\mathbf{A}\left(\tfrac{a}{R}\right) = \left[\begin{array}{cc} -\left(0.327 + 0.207\,(a/R)^{\lambda_1 - \lambda_2}\right) & \pm\left(0.390 - 0.420\,(a/R)^{\lambda_1 - \lambda_2}\right) \\ \mp\left(0.132 - 0.071\,(a/R)^{\lambda_1 - \lambda_2}\right) & +\left(0.157 + 0.143\,(a/R)^{\lambda_1 - \lambda_2}\right) \end{array} \right].$$

We might now easily develop a solution for the contact law, using the first of these equations, together with (5), to give

$$\left(\frac{d}{R}\right)^3 = \frac{9\pi^2}{4}\Bigg[-\left\{0.327\left(\frac{a}{R}\right)^{1-\lambda_1} + 0.207\left(\frac{a}{R}\right)^{1-\lambda_2}\right\}\frac{P}{2aE^*} \pm \left\{0.390\left(\frac{a}{R}\right)^{1-\lambda_1} - 0.420\left(\frac{a}{R}\right)^{1-\lambda_2}\right\}\frac{Q}{2aE^*}\Bigg]^2, \quad (5.14)$$

where the upper sign refers to the left-hand contact edge and the lower sign to the right-hand contact edge. This shows that the size of the contact is governed by the normal load, and it has a lateral shift caused by the shear load. Increasing the shear load increases the left contact size by the same magnitude that it decreases the right edge contact size. We contrast this solution with one derived by using Steuerman's half-plane solution for the whole contact, equation (5.2), where the contact size depends on the normal load alone, and its location is unaffected by applying a shear force.

This is shown in Fig. 5.5 which experiences a fixed normal load, $\frac{P}{2aE^*} = 10^{-3}$. This load was chosen because we could re-write the normalised normal load as $\left(\frac{P}{2a\sigma_y}\right)\left(\frac{\sigma_y}{E^*}\right)$ and, for common alloys the ratio σ_y/E^* is of order 10^{-3}, while the typical maximum average contact pressure for a stationary contact is often approximately equal to the yield stress in tension, σ_y. As the shear load is increased, the contact moves in the direction the shear load is applied, in accordance with Eq.(5.14).

When under normal loading only, i.e. $Q/P = 0$, the contact law using half-plane theory predicts a larger contact size for all geometries than the contact law based on rounded, three-quarter plane theory. When the flat-and-rounded body is pressed onto the surface, the upper contact-defining body tends to spread. The domain mismatch of the two bodies forms a frictional resistance inwards, against the outward spread of the contact, at both edges, under a normal load; geometric coupling therefore has the effect of reducing the predicted size of the contact under normal loading.

Increasing the shear load, i.e. moving up Q/P on the y-axis, causes the contact law based on the rounded, three-quarter plane theory to recede at the left edge, deviating from the contact law using half-plane theory. This is to be expected as the domain mismatch of the two bodies allows for the leading edge to grow and the trailing edge to lift in the presence of a shear load. The presence of geometric coupling has an increasing impact on the contact law at the trailing edge when under shear load.

The greater the ratio of a/R, the less both domains appear as two half-planes and the more valid the assumptions are in the three-quarter based model. For a large geometry ratio $a/R = 25$, at a reasonable external load ratio $Q/P = 0.55$, with

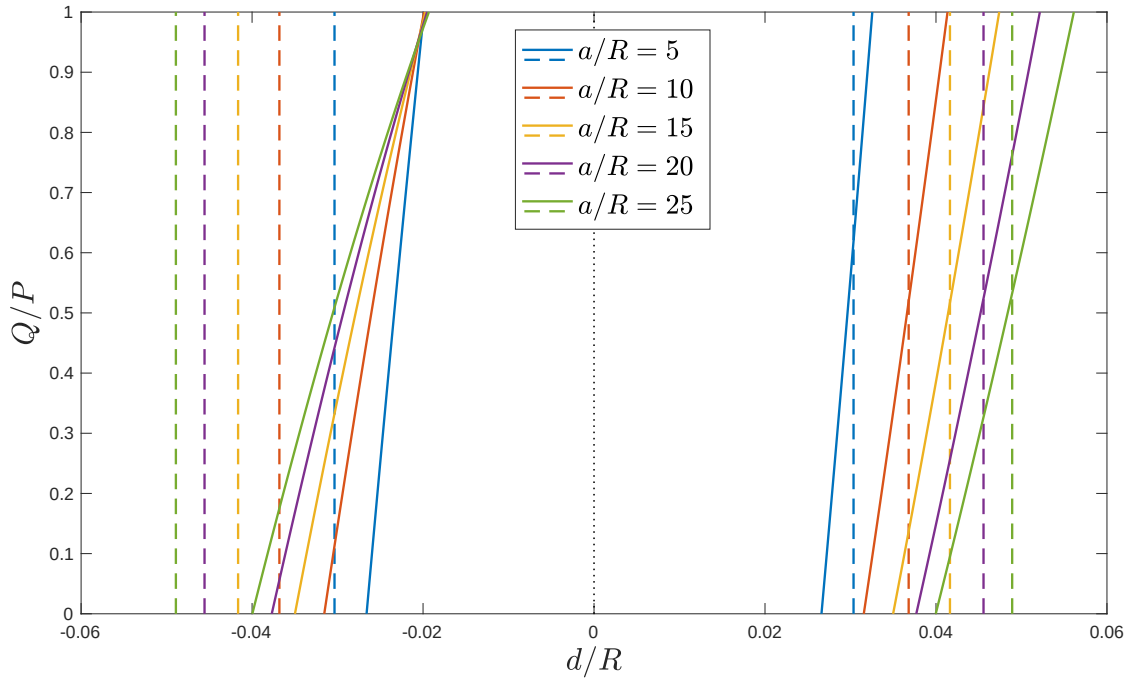


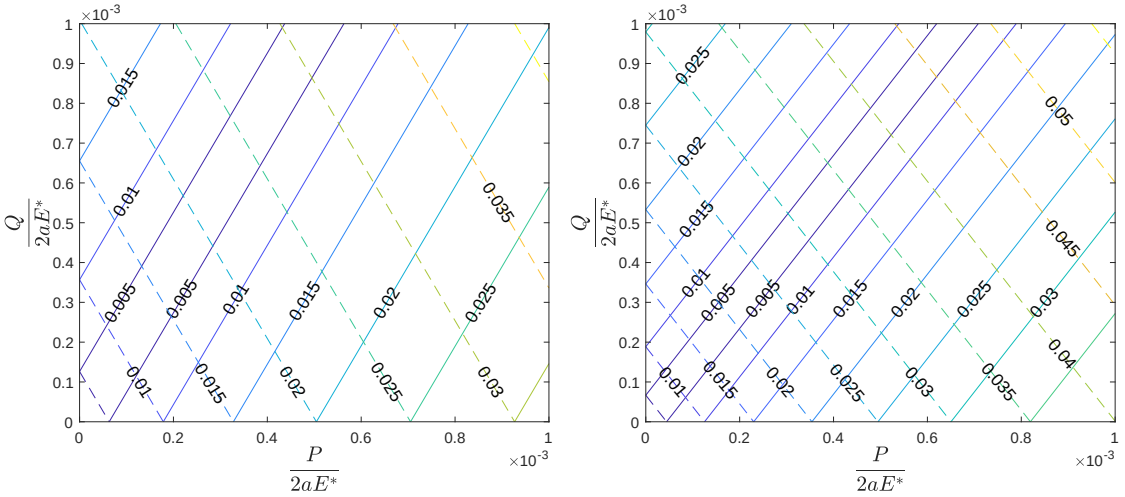
Figure 5.5: Contact law for the flat and rounded geometry under constant normal load, $\frac{P}{2aE^*} = 10^{-3}$, with increasing shear load on the y-axis for different contacting geometries using: rounded, three-quarter plane theory (solid lines) and half-plane theory (dashed lines).

normalised $P/2aE^* = 10^{-3}$, the contact law based on half-plane theory is over 60% larger at the left edge, highlighting the errors obtained when incorrectly applying half-plane theory to these domains.

Much of the analysis in this paper works on the assumption that the contact is stationary or advancing, by which we mean that the contact is remaining the same or increasing in size, whilst under loading. The condition required for stationary and advancing contact will differ between the two methods of analysis. When using the half-plane formulation for the whole contact, the necessary condition for both contact edges to advance is simply that $\Delta P > 0$. When using the approach being developed, the corresponding requirement is that $\Delta \widetilde{K}_I < 0$. By taking the complete differential in the first of equations (5.13) the restrictions in terms of the external load increments, $\Delta P, \Delta Q$, may be found.

Figure 5.6 displays the behaviour in a different way, by giving contours of the size of the contact, d/R, at both the left and right hand edges, as a function of the normalised normal and shear forces, $P/2aE^*, Q/2aE^*$. Changes in normal and shear load must always be such that we move in the sense of advancement, i.e. generally 'up and to the right' for the leading edge, and 'down and to the right' for the trailing

edge. Note that when a load change, $\Delta P, \Delta Q$, is infinitesimal at a particular edge, the change in shear traction resulting will become singular in character.



(a) $a/R = 10$ (b) $a/R = 25$

Figure 5.6: These graphs display contours of constant contact size, d/R, on an axis set of normalised external loads, $P/2aE^*$ and $Q/2aE^*$. The solid lines represent the left contact edge, and the dashed lines represent the right edge. Moving in the load space parallel to these contours results in a stationary contact at the respective edge. Moving through increasing/decreasing contour lines leads to an advancing/receding contact respectively.

We recognise that geometric coupling gives rise to a more stringent condition on the loading path required for both edges to advance compared to when using the half-plane formulation; the loading path in P, Q space must have a gradient with magnitude less than the contour line gradient as well as a positive horizontal component to advance the contact at both edges. The larger the geometry ratio, a/R, the stronger the effects of geometric coupling. This is seen in the plots because as we increase the geometry ratio from $a/R = 10$ in Fig. 5.6a to $a/R = 25$ in Fig. 5.6b, the contour lines become increasingly less vertical; the solution sensibly diverges from that expected by half-plane theory.

5.6 Combining the phases: Tractions under full stick

For a contact problem of given geometry, both the contact size and the contact pressure distribution are unique and independent of the loading path. The contact pressure distribution is given by equation (5.4), where $\widetilde{K}_I$ is given by the first of equations (5.13).

For a problem where there is a simultaneous change in both $\widetilde{K}_I, \widetilde{K}_{II}$ and $d\widetilde{K}_I > 0$ so that the contact is increasing in size, we may write the shear traction change by analogy with the work based on half-plane theory in [6, 10]. If a change of load occurs such that $d|\widetilde{K}_{II}|/d\widetilde{K}_I < \mu$, the coefficient of friction, the contact will be fully stuck and the change in shear traction at points near the edge, (where half-plane theory applies) will be proportional to change in contact pressure, i.e. $dq(x)/dp(x) = d\widetilde{K}_{II}/d\widetilde{K}_I$. If, now, we make this a finite proportional change in load, from state 1 to state 2 this gives

$$q_2(s) = q_1(s) + \frac{\widetilde{K}_{II_2} - \widetilde{K}_{II_1}}{\widetilde{K}_{I_2} - \widetilde{K}_{I_1}} \left(p(s; \widetilde{K}_{I_2}) - p(s; \widetilde{K}_{I_1}) \right). \tag{5.15}$$

5.7 Comparison of methods under full stick

We now wish to compare the solution of an example problem, tackled by three approaches. These are;

(a) the method developed in this chapter,

(b) the traditional half-plane formulation alone, and

(c) an 'exact' solution.

The last is a finite-element model, treated for the purpose of this comparison as the reference solution. Its setup and convergence are described in §5.7.1.

5.7.1 Finite-element reference solution

The analytical calibrations of §5.4 are validated against a finite-element (FE) solution which is treated, for the purpose of this comparison, as the reference ('exact') description of the contact tractions. The FE is intentionally a tool of validation only; it plays no further role in the development of the chapter.

The model represents the half-symmetry flat-and-rounded punch in contact with an elastic half-plane at the worked-example geometry $a/R = 25$, with the half-plane sized so that the bounding-box edges sit at least $20a$ from the contact patch and therefore do not perturb the corner stress field. Both bodies are elastically similar, linear-elastic, with $E = 114{,}800$ MPa and $\nu = 0.32$ (Ti–6Al–4V). The model and the loading are summarised in Fig. 5.7: the base of the half-plane is fully constrained, and the punch is loaded on its top surface by a uniform normal pressure which exerts a total normal load P, and a uniform shear traction with equal-and-opposite pair of

concentrated forces at the upper corners to provide the moment-balance correction associated with the shear traction, such that the shear load along the interface is Q. Loading is applied in two static steps under small-displacement assumptions, following the two step loading in Fig. 5.10. The contact interface is treated as fully adhered using the Abaqus `ROUGH` friction model (no relative slip permitted).

The discretisation uses four-node bilinear plane-strain quadrilaterals (`CPE4R`), with three-node plane-strain triangles (`CPE3`) introduced only as transition fillers where the mesh generator could not produce a clean quadrilateral cover. The mesh is strongly biased toward the contact corners, where the bounded-pressure asymptote $p(s) \sim L_{\mathrm{I}}\, s^{\lambda_{\mathrm{I}}-1}$ and the square-root-singular K_{II} shear field require high local resolution. The mesh near the receded contact corner is shown in Fig. 5.8.

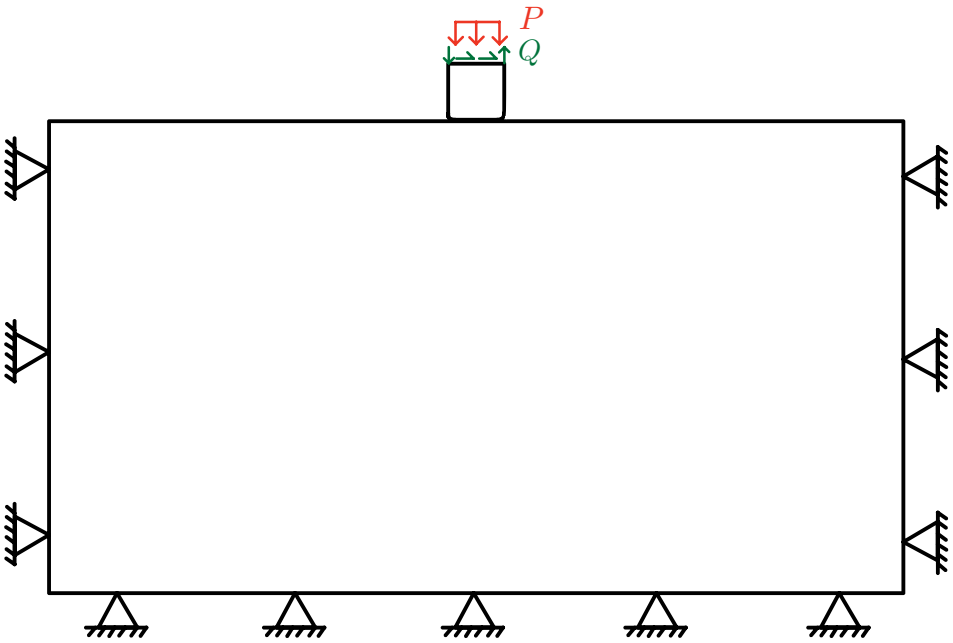


Figure 5.7: Finite-element model of the flat-and-rounded punch on an elastic half-plane at $a/R = 25$. The base of the half-plane is fully constrained (`ENCASTRE`); the top of the punch carries a uniform normal pressure, exerting a total normal load P, and a uniform shear traction with an equal-and-opposite pair of concentrated forces at the upper corners providing the moment-balance correction, exerting a shear load Q along the contact interface. The loading steps are defined in Fig. 5.10.

Mesh convergence. The mesh resolution was verified by a six-mesh refinement study spanning total node counts of 5×10^3 to 1.6×10^6. The contact pressure (`CPRESS`) and shear traction (`CSHEAR1`) from each mesh were interpolated onto a common 4000-point grid along the contact, and convergence was assessed through

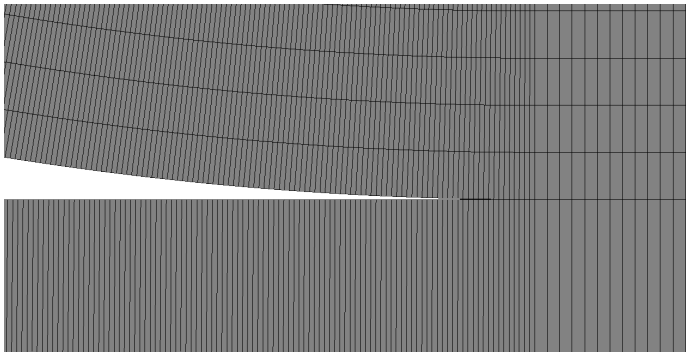


Figure 5.8: Production mesh used for the comparisons of §5.7.2 zoomed into the contact edge.

the RMS difference between successive meshes in the refinement sequence,

$$\mathrm{RMS}_T(\mathcal{M}_i) \;=\; \sqrt{\frac{1}{N_g}\sum_{j=1}^{N_g}\Big(T_{\mathcal{M}_i}(x_j) - T_{\mathcal{M}_{i-1}}(x_j)\Big)^2}, \qquad T \in \{p, q\}, \tag{5.16}$$

where $\mathcal{M}_{i-1}$ is the next-coarser mesh in the sequence. Each successive refinement should then produce a smaller change in the tractions than the previous one, which is the defining property of an asymptotically convergent sequence. Figure 5.9 reports the successive-mesh RMS difference for both tractions against the node count of the finer mesh of each pair. RMS_p decreases monotonically across the refinement sequence. RMS_q follows the same trend over most of the sequence, with a very slight rise at the finest step which is consistent with the shear field having reached the resolution limit of the discrete sampling of the steep K_{II} singularity at the corner. The production mesh used for the comparisons in §5.7.2 is therefore taken as converged. For this mesh, the smallest element edge along the curved portion of the contact surface is 1.5 μm, corresponding to approximately $R/670$.

Contact tractions are extracted from the converged final frame of loading step 2 at every node on the punch's contact surface, and compared directly to the method developed in this chapter, and traditional half-plane formulation.

5.7.2 Validation

The corresponding stress intensity factors arising at the contact edges can be found using the refined three-quarter plane calibrations, Eq.5.13, and are illustrated in the right plot of Fig. 5.10 for both contact edges.

The resulting normal and shear tractions are plotted for each method in Fig. 5.11. The most notable differences between the refined three-quarter-plane tractions and

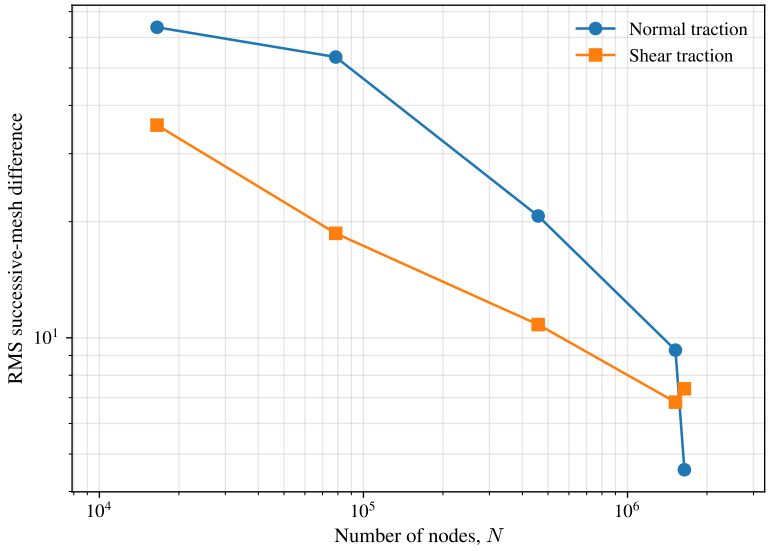


Figure 5.9: Root-mean-square difference of contact normal traction (circles) and shear traction (squares) between each mesh and the next-coarser mesh in the refinement sequence, plotted against the node count of the finer mesh of each pair on log-log axes.

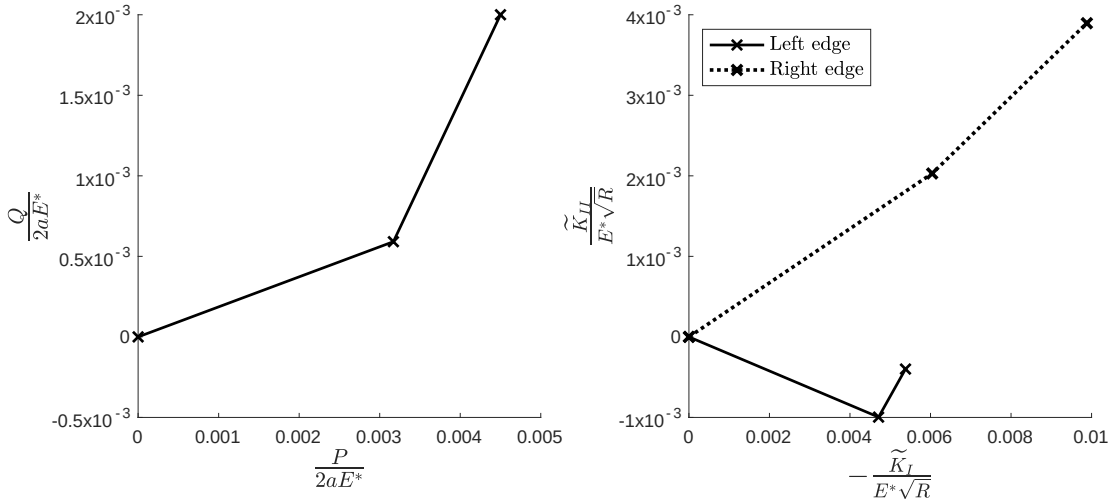
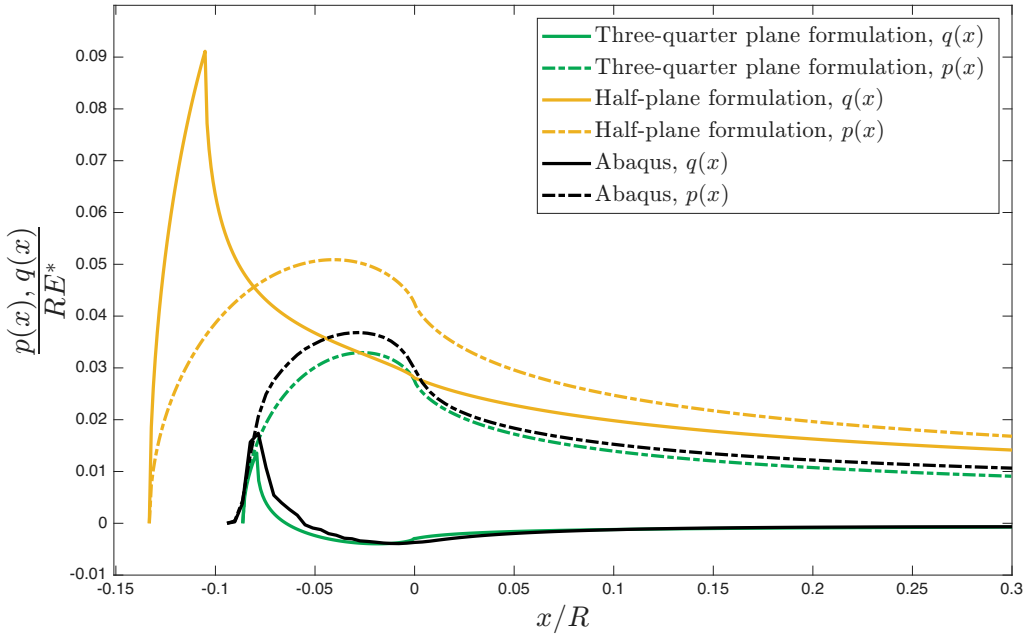


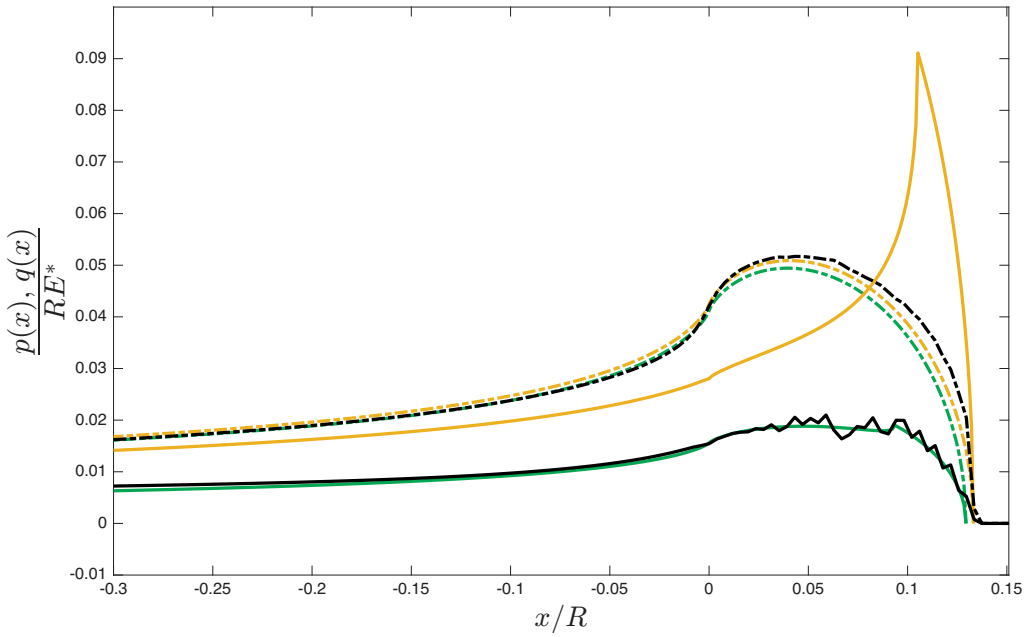
Figure 5.10: The left graph depicts an example loading history, (P, Q), for a flat and rounded contact pressed onto a half-plane. The right graph illustrates the corresponding contact edge stress intensity factors for the left and right contact edges, represented by solid and dashed lines, respectively.

the half-plane tractions for this example case are:

- The half-plane formulation provides an exceptionally poor prediction of shear traction at both contact edges; the shear traction obtained using the refined three-quarter-plane method is a much better prediction lying closely to the FE



(a) Left edge, x-axis centred at the left edge flat-to-round transition point.



(b) Right edge, x-axis centred at the right edge flat-to-round transition point.

Figure 5.11: Normal tractions (solid lines) and shear tractions (dashed lines) along the interface of a flat and rounded contact with a geometry ratio of $a/R = 25$, pressed onto a half-plane. The loading history is shown in Fig. 5.10. The results are compared using three methods: the refined three-quarter-plane formulation (green), the half-plane formulation (yellow), and FEA (black).

output.

- The half-plane formulation gives rise to symmetrical tractions which is of

particularly poor quality at the left edge, whereas the refined three-quarter-plane formulation more accurately predicts the different behaviour at the left and right contact edges.

A coincidental feature of Fig. 5.11 is that the contact half-length predicted on the right-hand edge by the half-plane and three-quarter-plane formulations is very similar. This is not a general result. As Fig. 5.5 shows, half-plane theory predicts a single contact size independent of the shear load, whereas the three-quarter-plane formulation predicts the leading (right) edge to grow and the trailing (left) edge to recede as Q is applied. The two right-edge predictions are therefore guaranteed to intersect at one particular value of Q/P, and the shear load used for Fig. 5.11 (approximately half the normal load) happens to lie close to that crossing. At any other shear load the two right-edge predictions would differ, and the left-edge predictions differ markedly at this load.

The refined three-quarter-plane method provides a significant improvement on the prediction of shear tractions compared to the half-plane formulation, which is crucial for understanding fretting fatigue. In this example, the contact is fully stuck, in other words the coefficient of friction is assumed infinite, however, as detailed in the following section, the condition for slip at the contact edges depends on the ratio of the change in shear to normal traction. As a consequence of the half-plane formulation's gross inaccuracy in predicting the shear traction for this geometry, the formulation would be unable to predict validly the onset of slip for a contact with realistic finite coefficient of friction ($\mu < 1$). The presence of slip plays a critical role in the prediction of wear, making accurate modelling essential. Since the refined three-quarter-plane method more accurately represents shear tractions at both contact edges, the method provides a much better understanding of the slip behaviour, and consequent state of stress at the contact edges. Furthermore, unlike the three-quarter plane formulation, the half-plane formulation cannot distinguish between the traction states at the left and right edges.

Compared with the finite element solution, an approach based on half-plane theory yields a reasonable prediction of the normal traction and contact law at the right edge but performs poorly at the left edge. The contact law refers to the size of the contact region within the radiused section of the geometry, where pressure remains non-zero in the outer-regions of the flat-to-round transition points. At the left edge, the half-plane solution produces an error of approximately 40% in this measure. In contrast, the formulation presented in this paper provides accurate predictions of both the normal traction distribution and the contact law at both edges, with negligible errors in the maximum tractions and contact law errors reduced

to around 10%.

All analysis up to this point has dealt with treating problems where there is no interfacial slip, and we now relax this assumption.

5.8 Condition for partial slip

A point within a contact will stay or become stuck when the ratio of the change in shear traction to the change in normal traction is less than the coefficient of friction, i.e. $d|q|/dp < \mu$.

There are two aspects to consider: sliding and partial slip. To prevent *sliding*, that is, rigid body motion, the criterion is simply described by the applied loads. The ratio of the applied loads must be less than the coefficient of friction, $Q/P < \mu$. Graphically, to ensure this, the loading path must remain within lines of gradient $\pm\mu$ from the origin in $P - Q$ space. The possibility of partial slip requires a much more detailed analysis.

In half plane theory, applied to a finite contact such as a Hertzian geometry, the condition to prevent *partial slip* is that the differential of the external loads is less than the coefficient of friction, i.e. full stick occurs when $d|Q|/dP < \mu$, if the contact is advancing. Graphically, for full stick, the instantaneous gradient must be less than the coefficient of friction.

However, for a flat and rounded geometry, the presence of coupling means that we can no longer state that $dq/dp = dQ/dP$. Instead, we must make use of the relationship outlined in Eq.(5.13) as we know the ratio of the changes in near-edge tractions are proportional to the changes in half-plane stress intensity factors, so that $dq/dp = d\widetilde{K}_{II}/d\widetilde{K}_I$, and the new condition for full stick is $d|\widetilde{K}_{II}|/d\widetilde{K}_I < \mu$.

To visualise the relationship between the external loads and the condition for partial slip, Fig. 5.12 plots the relationship between dQ/dP and $d|\widetilde{K}_{II}|/d\widetilde{K}_I$ for the left and right hand edge.

There are multiple ways to interpret this graph. One is to consider a coefficient of friction and a geometry e.g $\mu = 0.55$, and $a/R = 10$. For full stick, $d\widetilde{K}_{II}/d\widetilde{K}_I < \mu$. Therefore, tracing $d\widetilde{K}_{II}/d\widetilde{K}_I = 0.55$ we can determine the corresponding ratio of the external loads at the onset of slip. For the left edge, $dQ/dP \approx 1$ at the onset of slip, and for the right edge, $dQ/dP \approx 1.25$. So, while the condition for full-stick implied by half-plane theory is $dQ/dP < 0.55$, the tendency to slip is suppressed at both edges, but more-so at the right edge than the left edge.

Further analysing the results, we see that for pure normal loading, i.e. when $dQ/dP = 0$, the left and right hand edges will slip if $\mu < 0.25$ when $a/R = 5$, or

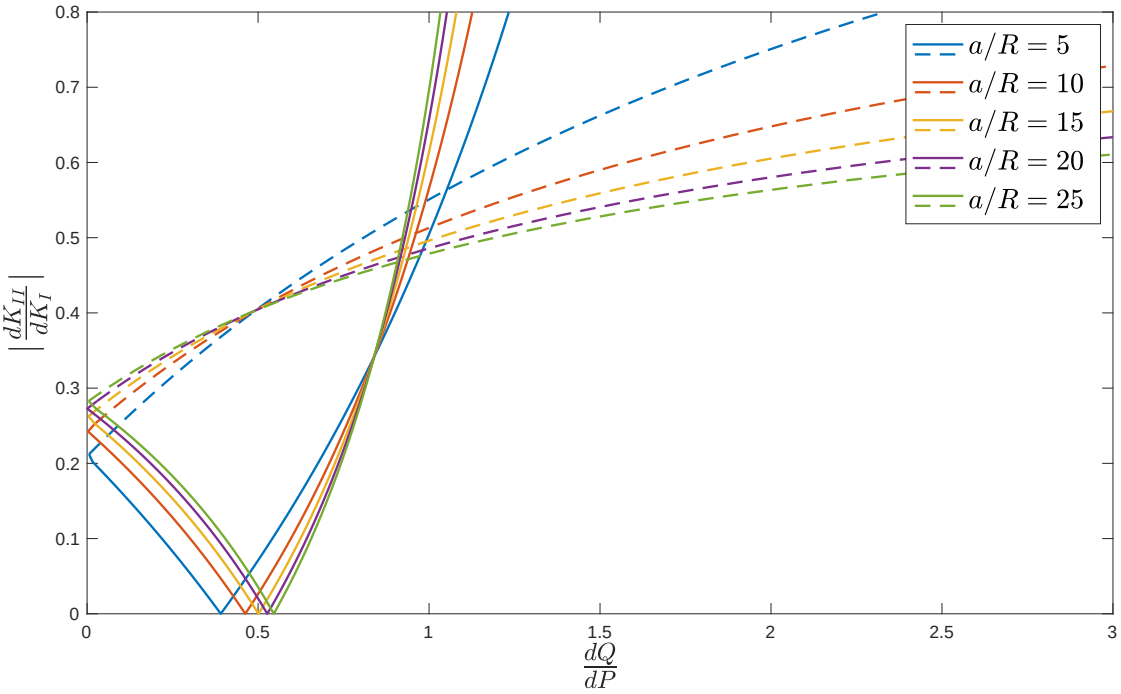


Figure 5.12: A graph to show the relationship between the infinitesimal change in the external loads to the near edge stress intensity factors, for different geometries. The left edge is represented by the solid line, the right edge is represented by the dashed.

$\mu < 0.3$ when $a/R = 25$ and so on. As we increase the ratio of dQ/dP, the condition for stick increases for the right hand side, but decreases for the left hand side until $dQ/dP \approx 0.5$, after which, the condition for stick increases in the opposite direction. Physically, this can be described by a pure normal load causing the spreading out of the contact due to coupling; the left edge creates a negative sense shear traction, whilst the right edge experiences a positive sense shear traction. When we increase the ratio of dQ/dP, we are increasing the positive sense shear traction at both edges until the left edge experiences a net zero shear traction at $dQ/dP \approx 0.5$. Increasing dQ/dP further leads to both edges experiencing increasingly positive shear tractions.

Fig. 5.13 plots multiple loading path trajectories to display the above findings. For all loading trajectories, the centre region of the contact remains stuck as they lie under a line with gradient μ from the origin in P, Q-space. According to half-plane theory, for a coefficient of friction $\mu = 0.55$, we would anticipate five out of the six paths to slip partially at both edges as $dQ/dP_2 \geqslant 0.55$, which is seen from the key in Fig. 5.13a where we denote Δ_2 as the gradient of the second step, i.e. $\Delta_2 = dQ/dP_2$. However, in Fig. 5.13b, the three-quarter plane solution implies the left edge will

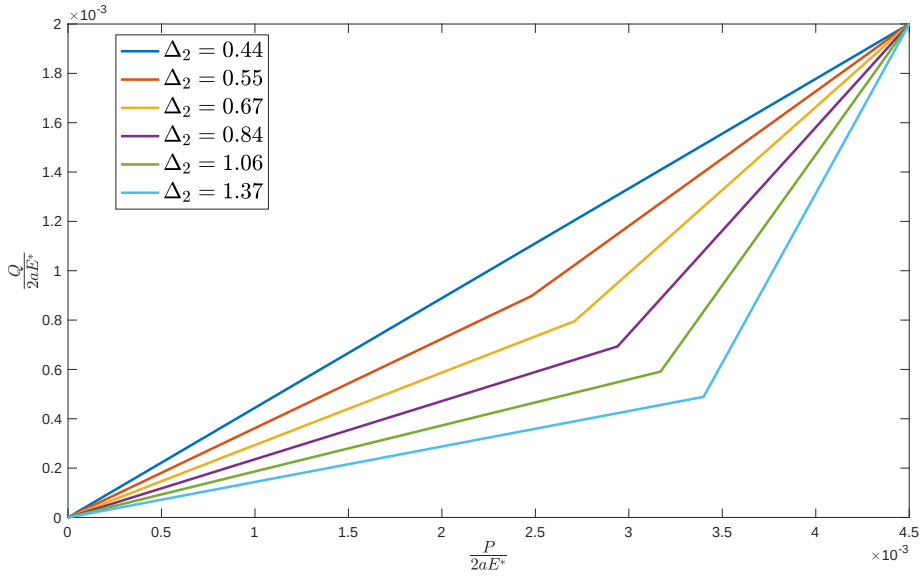
slip for two of the loading trajectories, and the right will slip for one out of the six loading paths. This supports the findings from Fig. 5.12 as the left edge slips when $dQ/dP > 1$ and the right edge when $dQ/dP > 1.25$; the condition for the gradient that induces slip is higher for the right edge compared to the left edge, which are both higher than that predicted by half plane theory. This is a crucial finding, and the first time we have been able to see, analytically, the influence of accurately modelling the vertical free surfaces of the contacting body on the condition for partial slip at each edge.

5.9 Shear tractions with partial slip

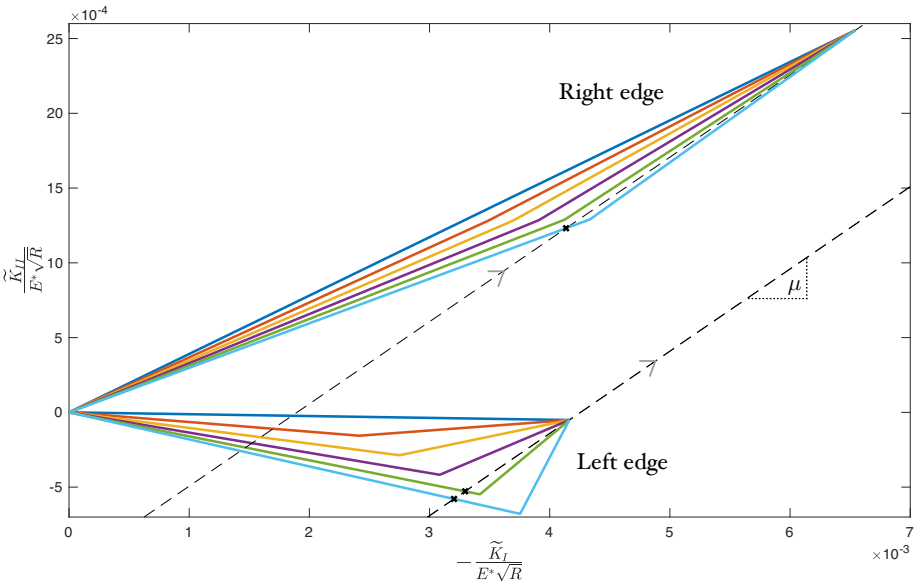
As detailed in the previous section, slip occurs at the contact edge when the ratio of the instantaneous change in stress intensity factors reaches the coefficient of friction, i.e. $d|\widetilde{K}_I|/\widetilde{K}_{II} = \mu$. The solution developed assumes that the majority of the contact is stuck; in the Williams' three-quarter plane analysis, any slip starting at the contact edge must not intrude far. It follows that, the value of $\widetilde{K}_I$ is unaffected by the presence of near-edge slip, and hence both the size of the contact and the pressure distribution remain as derived in Section 5.5 and Section 5.6.

Barber gives insight into analysing finite contact problems capable of the half-plane idealisation subject to complex loading trajectories [6], illustrated by Truelove [10]. Following this work, we may write analogous equations for this new formulation, where the half-plane representation of behaviour is valid, i.e. near the edges.

In Figure 5.13(a), a number of loading trajectories are plotted, with the second phase at a steeper gradient than the first. We now look at how those overall loading trajectories appear in $\widetilde{K}_I, \widetilde{K}_{II}$ space, and plotted out in 5.13(b). Assume that the coefficient of friction is sufficiently high for it to exceed the trajectory gradient (in 5.13(b)) during the first phase of loading, so that the contact will remain fully stuck up to the kink. If the gradient of the second phase of loading is also below the coefficient of friction, the contact will remain fully stuck, and the method described in Section 5.6 applies. But when the gradient of the second phase of loading (in 5.13(b)) is greater than the coefficient of friction, there will be some slip, and we will need to superpose a corrective term on the shear traction distribution in a similar manner to that defined by the Jaeger-Ciavarella theorem. We must find the corresponding transient stress intensity factor, $\widetilde{K}_{I_A}$, corresponding to the stick zone boundary, and lying on an earlier part of the loading path. To do this, we trace a construction line back from the final loading point, with gradient μ, until it intersects the loading path at an earlier point, marked by a black cross, which represents the



(a)



(b)

Figure 5.13: Two-stage loading paths for a flat-and-rounded contact with $a/R = 10$ pressed onto a half-plane. (a) Paths in the external-load plane (P, Q); Δ_2 denotes the gradient dQ/dP of the second step. (b) The same paths expressed in terms of the near-edge half-plane stress intensity factors for both edges (left edge in the lower group of curves, right edge in the upper group). Dashed construction lines have gradient μ and locate the transient stress intensity factor $\widetilde{K}_{I_A}$ for each slipping case, marked by a black cross.

transient stress-intensity factor, $\widetilde{K}_{I_A}$ we are looking for. The shear traction can then

be described by the following equation

$$q_2(x) = \frac{\widetilde{K}_{II_1}}{\widetilde{K}_{I_1}}\, p(x;\widetilde{K}_{I_A}) + \mu\left[p(x;\widetilde{K}_{I_2}) - p(x;\widetilde{K}_{I_A})\right] \tag{5.17}$$

where the first part of the equation provides the shear traction due to stick, and the second part represents the shear traction due to the slip region. The near-edge tractions developed are plotted in Fig. 5.14. As expected there is a significant difference between the two edges.

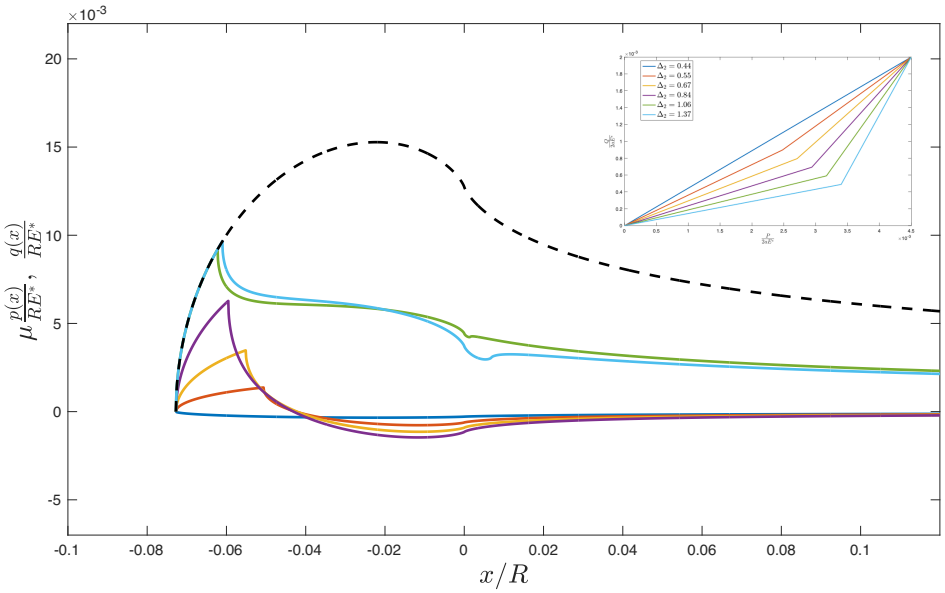
When a contact is subjected to cyclic loading with partial slip, the shear traction evolves toward a steady-state distribution, exhibiting partial shakedown. To illustrate this behaviour, we examine loading scenarios where all paths experience partial slip. A flat and a rounded contact is pressed onto a half-plane under a normal load P and a shear load Q. The contact is loaded along one of five uniquely coloured paths to their corresponding point (1), followed by cyclic loading and unloading along the black path between points (2) and (3). The corresponding P-Q loading trajectories, Fig. 5.15a, give rise to near-edge stress intensity factors, $\widetilde{K}_I$ and $\widetilde{K}_{II}$, Fig. 5.15b.

To find the final extent of slip, we must find the steady-state stress-intensity factor that corresponds to the permanent stick zone boundary locked into the contact, $\widetilde{K}_{I_B}$. To identify this, we trace along a line from point (3), with gradient $-\mu$ (downward sloping dashed line), until it intersects with the transient construction line (upward sloping dash line), indicated in Fig. 5.15b, analogous to [10]. All loading paths in Fig. 5.15 share the same steady-state $\widetilde{K}_{I_B}$ as they have the same cycling endpoints. If the steady-state stress-intensity factor is greater than the transient stress-intensity factor, i.e. $\widetilde{K}_{I_B} > \widetilde{K}_{I_A}$, there is a region of forward slip locked into the contact, such as for the red loading line. For the opposing case, where $\widetilde{K}_{I_B} < \widetilde{K}_{I_A}$, there is a region of reversing slip due to unloading that is locked into the contact.

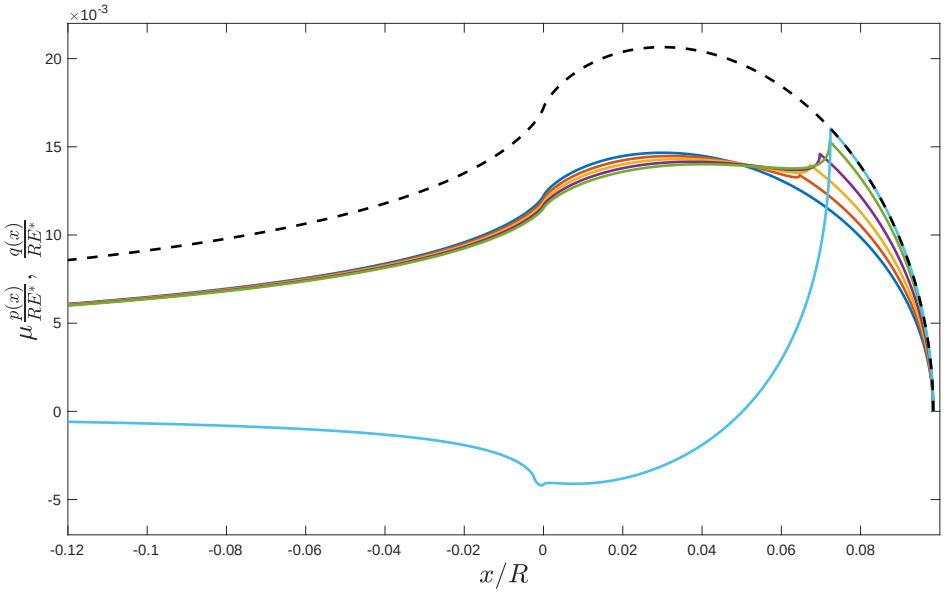
Firstly, we will consider the regime where the initial loading slip is locked into the contact. The shear traction, once loaded to (2) and unloaded to (3), can be described by the following equation

$$q_3(x) = \frac{\widetilde{K}_{II_1}}{\widetilde{K}_{I_1}}\, p(x;\widetilde{K}_{I_A}) + \mu\left[-p(x;\widetilde{K}_{I_2}) + 2p(x;\widetilde{K}_{I_B}) - p(x;\widetilde{K}_{I_A})\right]. \tag{5.18}$$

The first term represents the shear traction locked into the stick zone from the first loading step. The second term can be separated into two parts: $\mu[p(x;\widetilde{K}_{I_B}) - p(x;\widetilde{K}_{I_A})]$ is the remaining slip from the first step that is locked in by the following steps, and $-\mu[p(x;\widetilde{K}_{I_2}) - p(x;\widetilde{K}_{I_B})]$ is the shear traction from the reverse slip during



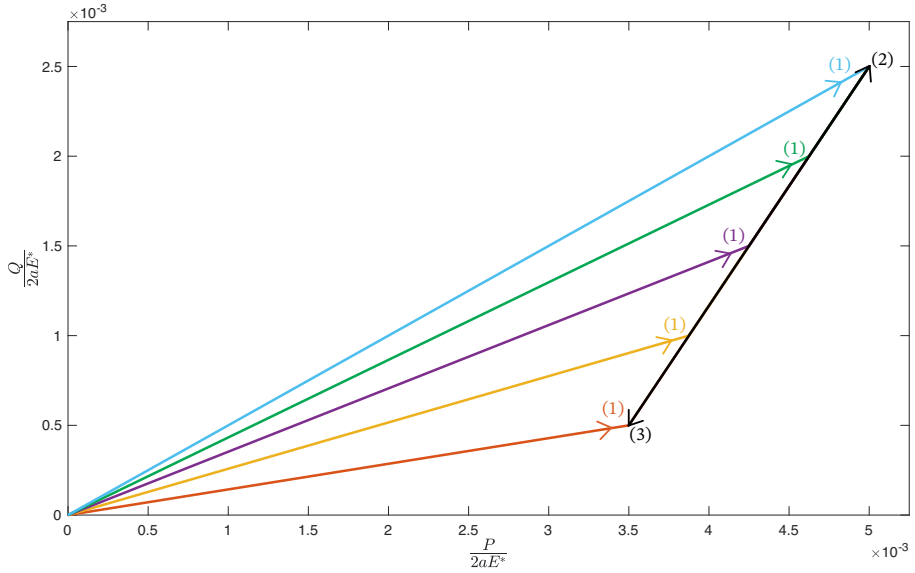
(a)



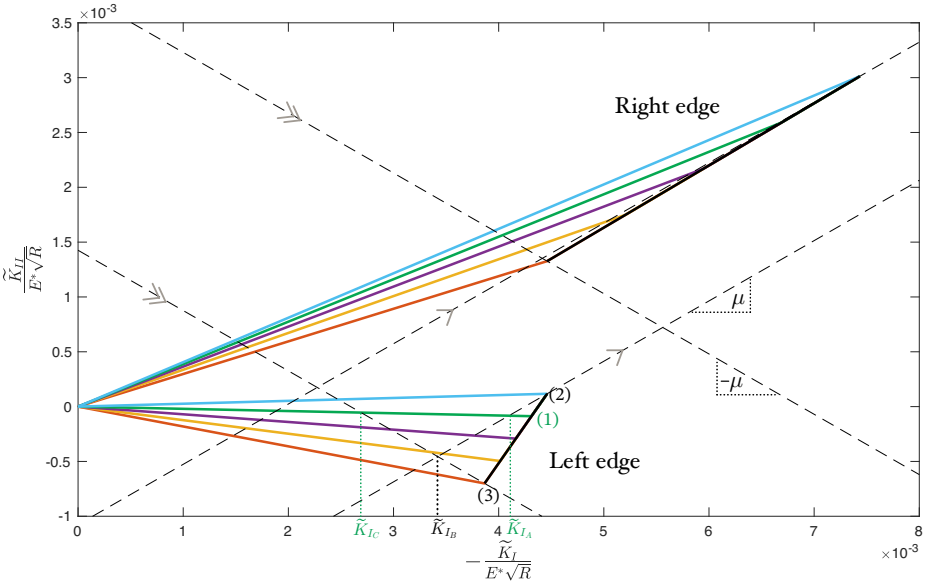
(b)

Figure 5.14: Shear (solid) and normal (dashed) tractions at the (a) left and (b) right contact edges of flat-and-rounded contacts loaded in two steps along the colour-coded paths of Fig. 5.13; the inset in panel (a) reproduces the colour key in (P, Q) space. All contacts have $a/R = 10$ and $\mu = 0.55$. On the left edge the blue and green paths are in partial slip; on the right edge the blue, green and purple paths are in partial slip.

unloading. When reloading the contact to (2), the shear traction restores to Eq. (5.17). The shear tractions have reached a steady-state and will oscillate between Eq. (5.18) and Eq. (5.17) as the contact is cycled between the two points. The



(a)

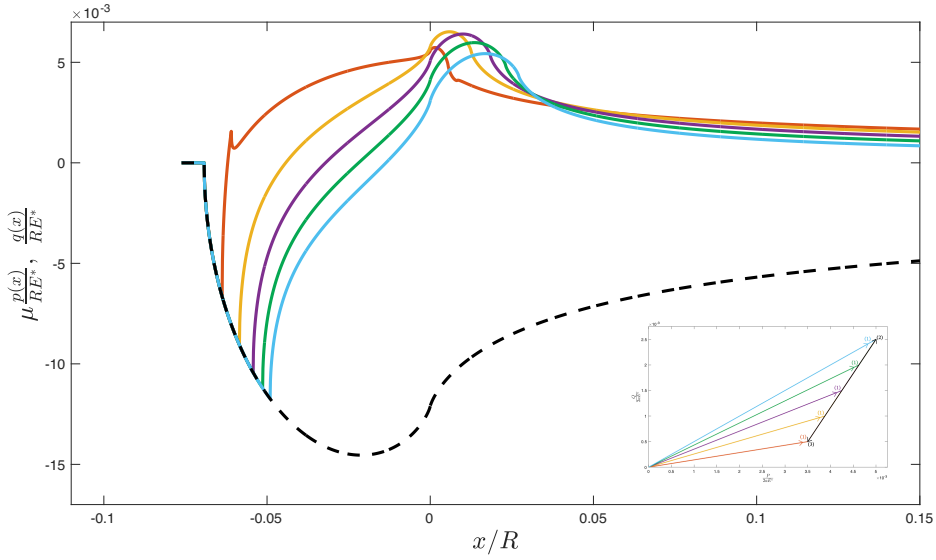


(b)

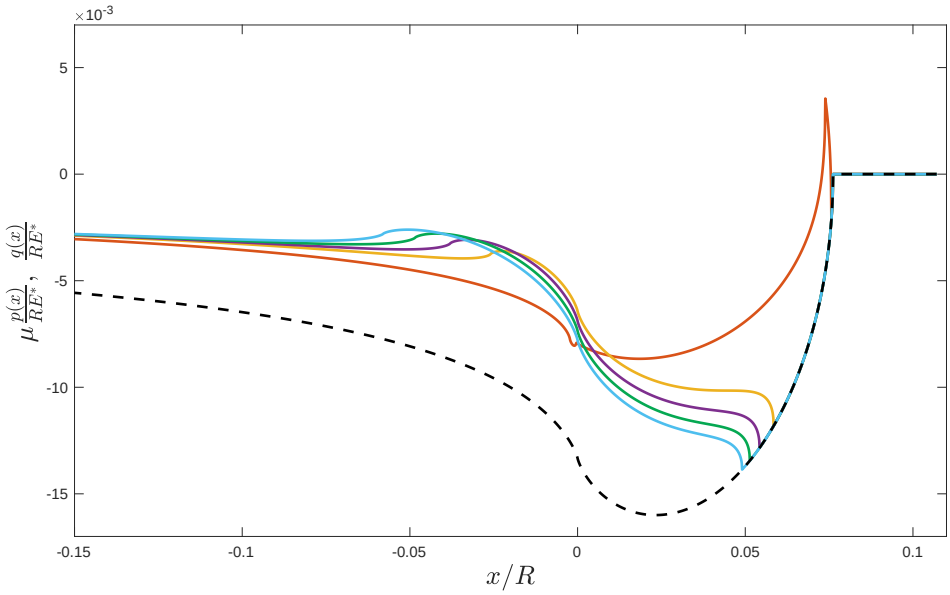
Figure 5.15: Five colour-coded loading paths, each driven to state (1) and then cycled between states (2) and (3) along the black segment, for a flat-and-rounded contact with $a/R = 10$. (a) Paths in the external-load plane (P, Q). (b) The same paths in near-edge stress-intensity-factor space, with the left edge in the lower group and the right edge in the upper group. Dashed construction lines of gradient $\pm\mu$ locate the transient stress intensity factors $\widetilde{K}_{I_A}$ and $\widetilde{K}_{I_C}$, shown for the green path as a representative example. The steady-state value $\widetilde{K}_{I_B}$ is identical for all paths because they share cycling endpoints.

unloaded and loaded tractions can be seen by the red line in Fig. 5.16 and Fig. 5.17 respectively. In the slip region, the shear tractions have a magnitude $q(x) = \pm\mu p(x)$

(dashed line).



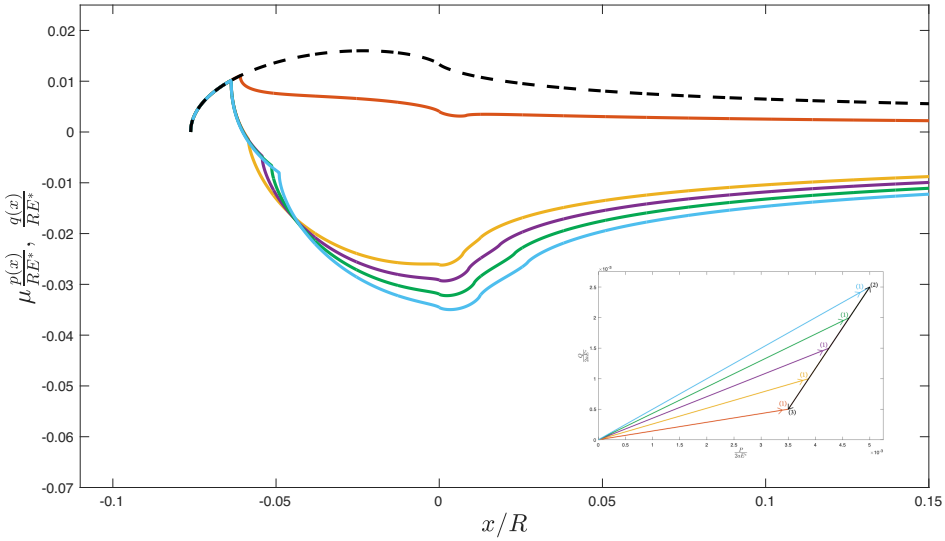
(a)



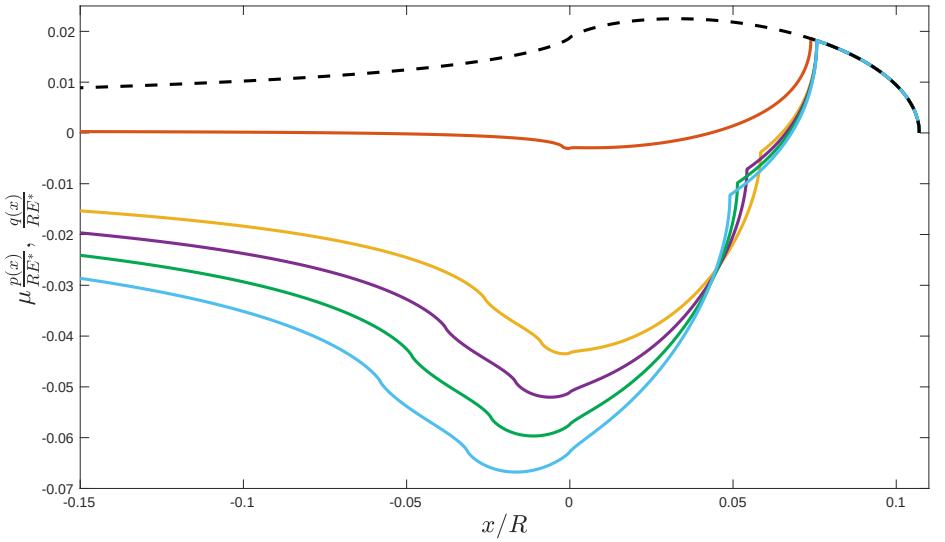
(b)

Figure 5.16: Steady-state shear tractions (solid) and friction limits $\pm\mu p(x)$ (dashed) at the (a) left and (b) right contact edges of flat-and-rounded contacts unloaded to state (3), following the colour-coded paths of Fig. 5.15; the inset panel (a) reproduces the colour key in (P, Q) space. All contacts have $a/R = 10$ and $\mu = 0.55$.

For the opposing regime, where $\widetilde{K}_{I_B} < \widetilde{K}_{I_A}$, we are interested in the size of the reverse slip zone during unloading, part of which will remain locked into the contact when cycled between (2) and (3). To determine this, we must calculate the stress-intensity factor that corresponds to the transient stick-zone during unloading,



(a)



(b)

Figure 5.17: Steady-state shear tractions (solid) and friction limits $\pm\mu p(x)$ (dashed) at the (a) left and (b) right contact edges of flat-and-rounded contacts reloaded to state (2), following the colour-coded paths of Fig. 5.15; the inset panel (a) reproduces the colour key in (P, Q) space. All contacts have $a/R = 10$ and $\mu = 0.55$.

$\widetilde{K}_{I_C}$. This is found by tracing the construction line with slope $-\mu$ through the unloaded state (3) and identifying its intersection with the initial loading path. For this case, the unloaded shear traction at point (3) can be described by

$$q_3(x) = \frac{\widetilde{K}_{II_1}}{\widetilde{K}_{I_1}}\, p(x; \widetilde{K}_{I_C}) - \mu\left[-p(x; \widetilde{K}_{I_3}) - p(x; \widetilde{K}_{I_C})\right]. \tag{5.19}$$

As before, the first term represents the shear traction locked into the stick zone from the initial loading. The second term corresponds to the reverse slip due to unloading. Note that, part of this region lies within the permanent slip zone, where the shear traction reaches limiting friction but does not slip further during subsequent loading cycles.

When the contact is subsequently loaded from (3) to (2), in this regime, the shear traction can be described by

$$q_2(x) = \frac{\widetilde{K}_{II_1}}{\widetilde{K}_{I_1}}\, p(x;\widetilde{K}_{I_C}) + \mu\left[p(x;\widetilde{K}_{I_2}) - p(x;\widetilde{K}_{I_C}) - 2p(x;\widetilde{K}_{I_B})\right]. \tag{5.20}$$

Example shear tractions for this regime (orange, purple, green and blue lines) are also plotted in Fig. 5.16 (unloaded) and Fig. 5.17 (loaded).

5.10 Conclusion

This paper has presented a refined formulation for analysing the behaviour of stationary, elastic, flat and rounded finite contacts with adjacent traction-free edges. The formulation exploits the properties of three domains; (a) a finite element model which is the union of the two contacting bodies, with the radius absent, and formed into a monolith, (b) a semi-infinite wedge (which becomes a three-quarter plane if the contact defining body has sides orthogonal to the front face) and incorporating a crack at the apex whose length is equal to the distance from the free edge to the flat-to-round transition point, and (c) a semi-infinite flat-and-rounded punch, derived from half-plane theory. These three domains, comprising the solution, are scaled by rigorously defined stress intensity factors. They are chosen to exploit the geometrical features that $a/R \ll 1$ (to connect domains (a,b)), and $d/R \ll 1$ (to connect domains (b,c)). The motivation for developing the technique is that it is feasible to obtain high-quality solutions for the near-edge tractions, including problems where some slip occurs. Further, through an example comparison with a problem solved also by assuming that the whole contact could be analysed by half-plane theory, we have demonstrated the significant influence of the traction-free surfaces on the solution, and have been able to solve the different stress states at each contact edge under normal and shear loading, for complex loading path, with much greater precision.

Through comparison with a full half-plane analysis we demonstrated the critical impact of accounting for traction-free surfaces. By validating the methods against a finite element model, we have shown that neglecting the traction-free edges leads

to significant inaccuracies in stress predictions and slip characterisation. For the example used, our refined three-quarter plane formulation minimised the maximum stress prediction errors by a factor of 5 at the left edge, whilst also reducing the error in the contact law to effectively negligible levels. The marked improvement provided by this refined solution has practical implications for safety-critical applications, such as turbine blade roots and subsea riser connections, where accurate modelling of stress states is essential for mitigating fretting fatigue and wear.

Notably, our proposed formulation also offers key advantages over traditional finite element methods. Most significantly, it achieves greater precision without numerical noise, enabling high confidence in the identification and extent of stick and slip zones — an essential consideration in fretting fatigue analysis. Furthermore, our approach can be readily applied to contacts involving bodies with differing length scales without additional modelling effort. This makes it a highly efficient and robust alternative to FEM in many practical settings.

Future work could involve simply extending the proposed model to allow for different types of loading, such as a moment and bulk tension, and with more complex loading histories, such as oscillatory loading with a phase shift between normal and shear forces. Additionally, revising this method for a contact with angled traction free surfaces would enhance its applicability to cases with similar geometry such as the dovetail root.

The formulation provides a powerful and versatile tool, advancing our understanding of contact mechanics for common geometries in engineering problems beyond the solutions provided by half-plane theory, and, when the solutions needed are derived, with very little analytical effort.

References

[1] B. Eames, D.A. Hills and M.R. Moore. “Elastic, flat and rounded finite contacts: When should we use half-plane theory?” in *European Journal of Mechanics - A/Solids* 106 (2024), 105306. ISSN: 0997-7538. DOI: https://doi.org/10.1016/j.euromechsol.2024.105306. URL: https://www.sciencedirect.com/science/article/pii/S099775382400086X.

[2] A. Mugadu, D.A. Hills, J.R. Barber and A. Sackfield. “The application of asymptotic solutions to characterising the process zone in almost complete frictional contacts”. in *International Journal of Solids and Structures* 41.2 (2004), 385–397. ISSN: 0020-7683. DOI: https://doi.org/10.1016/j.

ijsolstr.2003.09.038. URL: https://www.sciencedirect.com/science/article/pii/S002076830300550X.

[3] B. Eames, D.A. Hills and M.R. Moore. "Near edge tractions for a rounded quarter-plane pressed into an elastically similar half-plane". in *Tribology International* 186 (2023), 108582. ISSN: 0301-679X. DOI: https://doi.org/10.1016/j.triboint.2023.108582. URL: https://www.sciencedirect.com/science/article/pii/S0301679X23003699.

[4] Rodolfo Fleury, D. Hills and James Barber. "A corrective solution for finding the effects of edge-rounding on complete contact between elastically similar bodies. Part I: Contact law and normal contact considerations". in *International Journal of Solids and Structures* 85 (2016). DOI: 10.1016/j.ijsolstr.2015.11.031.

[5] Daniel J Riddoch, Nils Cwiekala and David A Hills. "Dislocations in an arbitrary angle wedge. Part II: Cracks in the wedge". in *The Journal of Strain Analysis for Engineering Design* 57.6 (2022), 433–444. DOI: 10.1177/03093247211047785. eprint: https://doi.org/10.1177/03093247211047785. URL: https://doi.org/10.1177/03093247211047785.

[6] J.R. Barber, M. Davies and D.A. Hills. "Frictional elastic contact with periodic loading". in *International Journal of Solids and Structures* 48.13 (2011), 2041–2047. ISSN: 0020-7683. DOI: https://doi.org/10.1016/j.ijsolstr.2011.03.008. URL: https://www.sciencedirect.com/science/article/pii/S0020768311001041.

[7] M Ciavarella, D A Hills and G Monno. "The influence of rounded edges on indentation by a flat punch". in *Proceedings of the Institution of Mechanical Engineers, Part C: Journal of Mechanical Engineering Science* 212.4 (1998), 319–327. DOI: 10.1243/0954406981521259. eprint: https://doi.org/10.1243/0954406981521259. URL: https://doi.org/10.1243/0954406981521259.

[8] A. Sackfield, A. Mugadu, J.R. Barber and D.A. Hills. "The application of asymptotic solutions to characterising the process zone in almost complete frictionless contacts". in *Journal of the Mechanics and Physics of Solids* 51.7 (2003), 1333–1346. ISSN: 0022-5096. DOI: https://doi.org/10.1016/S0022-5096(03)00020-6. URL: https://www.sciencedirect.com/science/article/pii/S0022509603000206.

[9] A A Khrapov. "Certain cases of the elastic equilibrium of an infinite wedge with a nonsymmetric notch at the vertex, subjected to concentrated forces". in *PMM* 35.4 (1971), 677–689.

[10] J.P.J. Truelove, L.E. Blades and D.A. Hills. “Half-plane contact problems in partial slip with varying normal and tangential loads”. in *European Journal of Mechanics - A/Solids* 94 (2022), 104590. ISSN: 0997-7538. DOI: https://doi.org/10.1016/j.euromechsol.2022.104590. URL: https://www.sciencedirect.com/science/article/pii/S0997753822000699.

Chapter 6

Matching the Slip Condition at Two Types of Contact

Contents

6.1 Introduction 121

6.2 Effects of small perturbations of loads 124

6.3 Calibrations for receded contact 125

6.3.1 Bounded pressure asymptote (L_I) 126

6.3.2 Singular traction changes (K_I, K_{II}) 127

6.3.3 Effect of remote tension 129

6.3.4 Summary of calibrations for the receded contact 129

6.4 Validation 132

6.5 Calibrations for Hertzian contact 134

6.6 Results of matching 135

6.6.1 Mean pressure term 136

6.6.2 Singular normal-traction term 136

6.6.3 Singular shear-traction term 136

6.6.4 Design form of the matching equations 137

6.6.5 Worked example 137

6.7 Limitations 138

6.8 Conclusion 141

In Chapters 3–5, a framework was developed for describing the near-edge tractions and stick–slip state in flat-and-rounded contacts where half-plane theory is not globally valid. The central idea was to express the contact-edge behaviour in terms of stress-intensity parameters which are correctly geared to the outer geometry. A natural question arising from this work is: how can these edge descriptions be used in practice?

One immediate application is in the design of fretting fatigue experiments. In many engineering assemblies, the contact geometry is not Hertzian; turbine blade roots, clamped joints and subsea connectors all involve contact configurations that are difficult to reproduce accurately in experiments. If the contact edge behaviour of a complicated geometry could be matched to that of a simpler, standard test configuration, then the fretting fatigue characteristics of the real contact could be investigated using conventional experiments. This problem is addressed in this chapter.

The key insight, following the recent work of Barber and Hills [1, 2], is that under small oscillatory perturbations about a mean loading state, the near-edge response of any non-conforming contact can be characterised by just three asymptotic parameters: a bounded-pressure multiplier L_I describing the mean loading state, and two stress-intensity factors K_I and K_{II} describing the changes induced by fluctuating normal and shear loading. These three parameters govern the cyclic motion of the contact edge, the maximum extent of the slip zone, and the local traction field. If they can be matched between two different contact geometries, the local edge conditions will be the same when conducting experiments, regardless of the global shape of the contacting bodies. The papers introducing this framework [1, 2] do not themselves include a worked example. The present chapter is the first such example.

This chapter demonstrates the matching procedure for a specific pair of geometries: a plane receded contact (an elastic strip pressed onto an elastically similar half-plane) and a Hertzian contact. The receded contact is chosen because it arises naturally in friction-grip bolted joints and similar clamped assemblies, yet it is difficult to test directly. The Hertzian contact is the standard laboratory configuration, requiring only a simple pad-on-dogbone arrangement.

Relative to the earlier draft included in submission, the version of the paper presented in this chapter contains four substantive revisions made during the journal review process. First, the notation conflict between the shear modulus and the friction coefficient (both previously labelled μ) has been resolved by writing the shear modulus as G_s throughout the derivations, with μ reserved for the Coulomb friction coefficient. Second, an improved numerical convergence study of the singular integral inversion

has updated the receded-contact calibrations and the corresponding matched-load coefficients (most visibly $b/h = 2.061$ at $\mu = 0.7$, and the leading bounded-pressure constant $L_I = 0.0665\,Ph^{-3/2}$). Third, an entirely new validation section (§6.4) checks the dislocation-method calibrations independently against a finite-element extraction of the near-edge asymptotes, finding agreement in sign for all seven coefficients and magnitudes within roughly ten per cent. Fourth, a worked example (§6.6.5) walks through the recipe for a representative receded contact and the equivalent Hertzian configuration, with side-by-side comparison plots of the matched edge fields. A standalone limitations section (§6.7) has also been added in response to a referee request to make explicit the local nature of the matching and the conditions under which the asymptotic description controls the edge field.

This chapter presents research currently in press as:

> **B. Eames**, L. Blades, S.A. MacLeod, D.A. Hills, Matching the slip condition at two types of contact, *Tribology International,* 2026.

This paper complements the preceding chapters by showing that the asymptotic edge descriptions developed for flat-and-rounded contacts are not merely of theoretical interest: the same class of edge parameters can be used to design equivalence between geometries, providing a practical route from analysis to experiment. It also extends the scope of the thesis from flat-and-rounded contacts to a different contact class (receding contacts), demonstrating the generality of the stress-intensity-factor-based approach to contact-edge characterisation.

Matching the slip condition at two types of contact

B. Eames, L. Blades, S.A. MacLeod, D.A. Hills.

Department of Engineering Science, University of Oxford, Parks Road, Oxford, OX1 3PJ, UK

Abstract

This paper develops a methodology to match the contact edge conditions between a plane-receded contact and a Hertzian contact, under oscillatory loading. This provides a route by which the edge conditions in a complicated contact configuration may be reproduced in a standard Hertzian experiment. A receded contact is formed by pressing an elastic layer against an elastically similar half-plane and then subjecting it to small fluctuations of load. From this analysis, we can describe the stress state at the contact edges in terms of stress intensity factors. By matching these descriptions to a Hertzian contact, we reproduce the leading near-edge stress and slip descriptors of the receded contact. The method provides an edge-equivalent configuration for subsequent fretting fatigue experiments. The advantage of using the equivalent Hertzian geometry is that the same local edge quantities can be generated in a simpler, well-defined contact configuration, using at most a two-actuator test machine.

6.1 Introduction

Fretting fatigue and wear are governed by the local conditions near the edge of contact in partial-slip problems. For many engineering joints, the contact geometry is not Hertzian, which makes controlled testing and interpretation difficult. This paper shows how to map the edge-of-contact behaviour of a plane-receded contact onto an equivalent Hertzian contact, so that the same local edge conditions can be generated using standard pad-specimen experiments.

Our goal is to determine load relations for a Hertzian pad-specimen test, Fig. 6.2b, that reproduce the same near-edge partial-slip and stress characteristics as the receded contact. Once these are matched between geometries, the local slip extent, stick zone, and near-edge stress field follow. The practical advantage is that the 'edge-equivalent' Hertzian test requires only the standard pad contact and loading control without sacrificing generality of the edge loading history; one actuator suffices when normal load is constant, or two actuators if P oscillates.

The procedure we will implement has been recently developed in two papers [1, 2]. Detailed derivations are given in those two articles, while the salient points are summarised here. The analysis is designed to treat contact problems which are

non-conforming (so that the contact pressure falls smoothly to zero at the edges), and where first large load is applied to define the mean conditions, and some small oscillatory load is also present. The first important property that we note is that, even though each body may not be capable of being represented using half-plane ideas, the edges of the contacts will be; that is, we can always find a region near the contact edge where the tractions and displacements are correctly described by the Flamant solution. So, when we think about *changes* in the applied loads - those representing the fluctuating (usually some form of vibrational) effects the behaviour of the contact edges, viz. the movement of the contact edge and the presence of reversing slip zones, may also be treated using our familiar half-plane analysis, suitably scaled. Secondly, we can see that, sufficiently close to the contact edges, the state of stress may be thought of as selective terms from a conventional eigenfunction expansion of a crack tip field: the mean contact pressure corresponds to the symmetric $r^{1/2}$ term, the T-stress (r^0) term corresponds to the stress lying at the surface and parallel with it, and the singular ($r^{-1/2}$) terms correspond to the changes in state of stress, assuming that the contact interface is bonded at the mean extent. The description of a contact edge through stress intensity factors of this type originates with the crack analogue model [3] and the contemporaneous use of Williams' eigenfunction expansion to characterise complete-contact edges [4], in which the singularity is an inherent property of the static field at a stationary complete-contact corner. The incomplete contact considered here differs: the mean pressure is square-root bounded, and the singular descriptors arise only in the changes of traction under load perturbation. The matching is performed using three edge parameters that govern the asymptotic contact behaviour under small load perturbations [2]:

1. L_I, the amplitude of the square-root bounded mean pressure field near the contact edge;

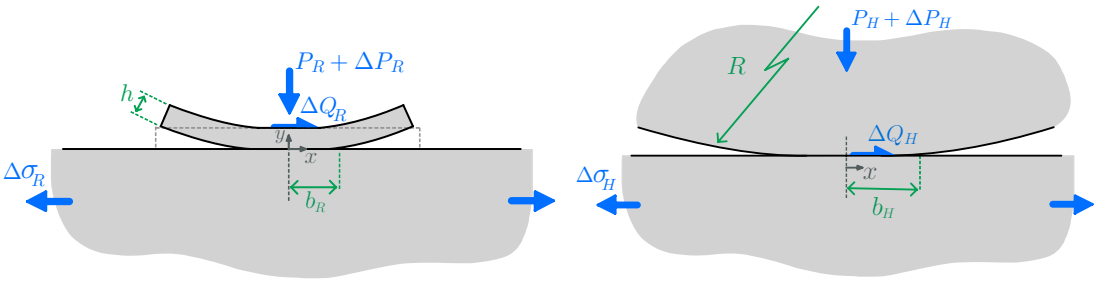
2. K_I, the stress intensity factor associated with small changes in normal traction;

3. K_{II}, the corresponding amplitude associated with oscillatory shear tractions.

We will expand our description of this procedure in Section 6.2 but, fundamentally, the K_{II} term is relaxed out by permitting the interface to slip, and the K_I term is relaxed out by permitting the contact surfaces to roll into and out of contact.

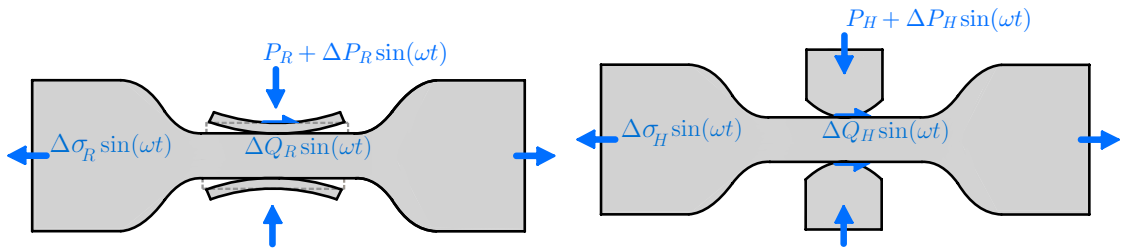
The original papers [1, 2] provide no examples of the procedure, and this is the first practical example, chosen because it is substantially, in this case, in closed form for the calibrations, and also because it illustrates how contacts from two different classes may, with appropriately scaled loads, be made to look the same in terms of the varying state of stress at the edges, which is precisely where cracks nucleate.

We study the configuration shown in Fig. 6.1a, where a strip of thickness h is pressed onto an elastically similar, frictional half-plane by a normal load P, increased monotonically to its mean value and then held. The system is then subjected to small, periodic perturbations of amplitude ΔP, ΔQ, and $\Delta\sigma$, representing fluctuations in normal load, tangential load, and remote tension in the half-plane. All perturbations are taken to be in phase and at the same frequency. This loading set captures key features of friction-grip bolted-joint fretting problems, and it corresponds closely to the experimental arrangement in Fig. 6.2a (a dogbone specimen with thin clamped strips).



(a) (b)

Figure 6.1: The two contact configurations whose near-edge conditions are matched in this chapter: (a) a receded contact formed by pressing an elastic strip of thickness h onto an elastically similar half-plane, with contact half-length b controlled by the coefficient of friction; (b) a Hertzian contact formed by pressing an elastic Hertzian body of radius R onto an elastically similar half-plane, with contact half-length b set by the normal load.



(a) (b)

Figure 6.2: Equivalent pad-on-dogbone experimental configurations: (a) an elastic strip clamped against the dogbone, producing a receded contact; (b) Hertzian pads pressed against the dogbone, producing a Hertzian contact. When the loads are matched using the relations derived in Section 6.6, the near-edge stress fields in the two configurations are equivalent, so the more complicated receded geometry can be tested using the simpler Hertzian arrangement.

To match the contact edge stress descriptions, we first summarise the asymptotic framework for non-conforming contacts under fluctuating loads in Section 6.2, arriving

at the three governing edge parameters. Section 6.3 calibrates these parameters for the plane-receded contact, summarising the calibrations for an example problem with coefficient of friction $\mu = 0.7$ in Section 6.3.4. Section 6.4 provides an independent finite-element check on those calibrations. Section 6.5 then recalls the corresponding Hertzian calibrations. Section 6.6 compares the calibrations for the two problems and derives the matching relations used to design equivalent experiments; Section 6.6.5 walks through a worked example, and Section 6.7 discusses the limitations of the method.

6.2 Effects of small perturbations of loads

First, we consider the mean contact pressure, associated with the mean load P. Points close to the mean contact edge position can be described by the first-order asymptotic representation

$$p(x) = L_I\sqrt{b-x} + O(b-x)^{3/2}\,. \tag{6.1}$$

The value of L_I must be established for the geometry under consideration, and its calibrations for the receded and Hertzian contacts are given in §6.3.1 and §6.5, respectively.

Secondly, we have the influence of small changes in load. In a cyclically loaded problem whose properties are (locally) governed by half-plane relationships the normal and shear tractions are uncoupled, and hence, under cyclically varying loads, the problem will follow Melan's criterion and tend towards a shaken-down state [5]. This means that the majority of the interface (here the interval $-b \leqslant x \leqslant b$) will be permanently stuck. As a consequence, a contribution to *changes* in the local state of stress — in particular, the change in local shear traction at the contact edge — will be governed by the mode II crack-tip stress intensity factor[1]

$$q(x) = \frac{K_{II}}{\sqrt{b-x}} + O(b-x)^{1/2}\,. \tag{6.2}$$

The effects of a small change in normal load are harder to understand, but stem from the attendant change in the position of the contact edge resulting from a change

[1]Note that we define both stress intensity factors in this paper without the usual $\sqrt{2\pi}$ factor historically included in fracture mechanics analysis.

in the (local) normal load, so that

$$\Delta p(x) = \frac{\partial}{\partial b}\left(L_I\sqrt{b-x}\right)\Delta b = \left[\frac{L_I}{2\sqrt{b-x}} + \sqrt{b-x}\,\frac{\partial L_I}{\partial b}\right]\Delta b. \tag{6.3}$$

If the change in normal load is small, the second term is negligible in the immediate edge asymptote, so the *change* in contact pressure is given by

$$\Delta p(x) = \frac{K_I}{\sqrt{b-x}} + O(b-x)^{1/2} \tag{6.4}$$

where $K_I = L_I\Delta b/2$. Equations (6.1), (6.2) and (6.4) define the mean pressure and the implied traction changes when the coefficient of friction inhibits all slip at the contact edge. When we permit slip, but the coefficient of friction μ is sufficiently large to restrict the maximum extent of the cyclic slip zone d to lie within the region where these equations apply (and in practice realistic coefficients of friction achieve this), the maximum extent of cyclic slip is given by [1]

$$d = \frac{2K_{II}}{\mu L_I}. \tag{6.5}$$

For details of the origin of the following results the reader is referred to [2]. During a loading cycle the contact extends and contracts from its mean position by $\pm\Delta b$, where

$$\Delta b = \frac{2K_I}{L_I}. \tag{6.6}$$

As a result, three key parameters describe the contact edge behaviour under small perturbations of load: *(1)* L_I, describing the mean contact pressure; *(2)* K_I, due to fluctuations of normal traction; and *(3)* K_{II}, due to fluctuations of shear tractions.

6.3 Calibrations for receded contact

The main task within this paper is to develop calibrations for the quantity $L_I(P)$, representing the effect of the mean pressure, and the six quantities $K_I(\Delta P, \Delta Q, \Delta\sigma)$ and $K_{II}(\Delta P, \Delta Q, \Delta\sigma)$, representing the effect of the oscillatory loading. Once these have been determined, equations (6.5,6.6) define the contact edge geometry and equations (6.1)–(6.4) define the tractions.

We consider a contact such that, in the deformed state under mean loads, the contact edge is distant from all salient geometric features, such as an abrupt corner or hole. Although the contact shown in Fig. 6.1a has the free surface $y = h$ relatively close to the interface $y = 0$, points can always be found sufficiently close

to the contact edge that $|x - b| \ll h$ and therefore, locally, tractions and their resulting displacements are related by Flamant's half-plane solution [6]. This is a very important observation, because it means that small changes in the state of stress and accompanying displacements in this neighbourhood are related by half-plane theory, and hence that there are three quantities only which define the resulting cyclic slip behaviour [1].

For a non-conforming contact, we are interested in the response of the contact edge when first loaded to a mean contact pressure, then subject to small perturbations of load. This work is introduced in [1], and a much fuller description is given in [2]. Those papers should be consulted for background; here we give a brief description of the results.

6.3.1 Bounded pressure asymptote (L_I)

The receding contact itself is solved in [7], and we use that solution here. In this section we restrict ourselves to the case where the normal load P alone has been applied. The coefficient of friction alone defines the mean extent of the contact. The contact is therefore symmetrically positioned beneath the line force and both ends display the same pressure distribution. The solution for the effect of the normal load has been found [8], and therefore the densities of the climb dislocations B_y over $-\infty < x < -b$ and $b < x < \infty$ are known [7]. The edge of contact between two bodies displaying (here locally) half-plane behaviour is characterised by the series expansion for a wedge of total included angle 2π — i.e. a crack tip — and the eigensolution corresponding to a square-root bounded state of stress applies. We particularise the solution to the wedge bisector, here the line $y = 0$, and the relationship between the contact pressure and the multiplier L_I is given by equation (6.1). If we assemble the complete Williams eigensolution for this problem we can find the corresponding displacement field, including the opening displacements $u_y(0^+)$ and $u_y(0^-)$ along the free surfaces of the contacting bodies just external to the contact region. The difference between these is the gap between the contact surfaces, $g(x)$, which at the right-hand edge is given by

$$g(x) = u_y(0^+) - u_y(0^-) = 2\,\frac{\kappa + 1}{G_s}\,\frac{L_I}{3}\,(x - b)^{3/2} \tag{6.7}$$

where κ is Kolosov's constant and G_s is the elastic shear modulus. This may be differentiated to find the angle between the contact surfaces, which is also given by

the dislocation density $B_y(x-b)$ as $x \to b^+$. Therefore, just external to the contact,

$$L_I = \lim_{x \to b^+} \frac{2G_s}{\kappa+1} \frac{1}{\sqrt{x-b}} \frac{dg}{dx} = \frac{2G_s}{\kappa+1} \frac{1}{\sqrt{x-b}} B_y(b^+). \tag{6.8}$$

We require the value of the dislocation density as the observation point approaches the contact edge, so that the coordinate of the collocation points $t \to -1$, and so can calibrate L_I in terms of the unknown function as

$$L_I = \frac{2G_s}{\kappa+1} \frac{1}{\sqrt{\eta b}} \phi_y(-1^+), \tag{6.9}$$

where the quantity $\phi(t)$ is known only at the collocation points but the standard interpolation formula devised by Krenk [9] enables it to be determined very accurately as the end point is approached, and η is a quadrature parameter that controls the spread of interpolation nodes.

6.3.2 Singular traction changes (K_I, K_{II})

In the formulation for the effects of the mean load [7], distributions of climb dislocations $B_y(x)$ were applied over the intervals (with $y = 0$) $-\infty < x < -b$ and $b < x < \infty$ as mentioned in §6.3.1. They were chosen to be bounded in form as the contact edges were approached, as is appropriate when solving for the locations of the end points of a non-conformal contact. Now, to find the effect of changes in (P, Q), we must fix the contact width at its mean value (corresponding to the mean value of P) and determine the singular change in tractions at the edges, as quantified by the crack-tip stress intensity factors (defined, as stated earlier, without the customary factor of $\sqrt{2\pi}$). To do this, we must first find distributions of climb dislocations $B_y(x)$ and glide dislocations $B_x(x)$ that ensure the same intervals, external to the contact, are traction-free. In this case the dislocation densities should be square-root singular in form as the contact edges are approached from outside the contact.

For the case of normal tractions this is the same integral equation as that enforced to define the contact, but now with the 'singular at contact edges' fundamental function, and this is given by

$$\begin{aligned} \int_{-\infty}^{-b_0} \left(\left[\frac{1}{x-\xi} + G_{yyy}(x,\xi) \right] B_y^L(\xi) + G_{xyy}(x,\xi)\, B_x^L(\xi) \right) d\xi \\ + \int_{b_0}^{\infty} \left(\left[\frac{1}{x-\xi} + G_{yyy}(x,\xi) \right] B_y^R(\xi) + G_{xyy}(x,\xi)\, B_x^R(\xi) \right) d\xi \\ = -\frac{\pi(\kappa+1)}{2G_s}\, p(x), \end{aligned}$$

$$\text{for } -\infty < x \leqslant -b_0 \text{ and } b_0 \leqslant x < \infty. \quad (6.10)$$

Here G_s is the elastic shear modulus, and G_{yyy}, G_{xyy}, G_{xxy}, G_{yxy} are the associated dislocation kernels. For the shear tractions, the equation takes a similar form, but it is now the kernels for the glide dislocations which include the Cauchy term,

$$\int_{-\infty}^{-b_0} \left(\left[\frac{1}{x-\xi} + G_{xxy}(x,\xi) \right] B_x^L(\xi) + G_{yxy}(x,\xi)\, B_y^L(\xi) \right) d\xi + \int_{b_0}^{\infty} \left(\left[\frac{1}{x-\xi} + G_{xxy}(x,\xi) \right] B_x^R(\xi) + G_{yxy}(x,\xi)\, B_y^R(\xi) \right) d\xi = -\frac{\pi(\kappa+1)}{2G_s}\, q(x), \quad \text{for } -\infty < x \leqslant -b_0 \text{ and } b_0 \leqslant x < \infty. \quad (6.11)$$

Equations (6.10, 6.11) are two coupled Cauchy singular integral equations in terms of the two dislocation densities. Solutions are sought which are bounded at very remote points but square-root singular in character at the edges of the 'contact', which is now a region of bonding between the strip and the layer of length $2b$.

Once the two dislocation densities are found, effectively represented by functions $\phi_x(x)$, $\phi_y(x)$ as the required end behaviour is incorporated into multiplicative fundamental functions, the stress intensity factors may be found. As in §6.3.1 we appeal to the Williams eigensolution for a wedge of included angle 2π, but now make use of the first term in the expansion, which gives square-root singular stress behaviour. On the line of the interface, equations (6.10, 6.11) apply, and the corresponding part of the eigensolutions providing the displacement field, particularised to the free surfaces just external to the contact, are

$$u_y^+(x) = -u_y^-(x) = \frac{\kappa+1}{2G_s}\, K_I \sqrt{x-b}, \quad (6.12)$$

$$u_x^+(x) = -u_x^-(x) = \frac{\kappa+1}{2G_s}\, K_{II} \sqrt{x-b}. \quad (6.13)$$

As before for the bounded asymptote, these expressions may be differentiated to provide a relation between the incremental stress intensity factors and the relative-displacement gradients, which are in turn given by the dislocation densities. Taking the limit $x \to b^+$, equivalent to $t \to -1$ in the quadrature, the stress intensity factors are calibrated by

$$K_I = -\frac{2G_s}{\kappa+1} \sqrt{\eta b}\, \phi_y(-1) \quad (6.14)$$

and

$$K_{II} = -\frac{2G_s}{\kappa + 1}\sqrt{\eta b}\,\phi_x(-1). \tag{6.15}$$

6.3.3 Effect of remote tension

The problem we wish to solve is displayed in Fig. 6.1a, but it is much easier to think of the solution as the superposition of two problems.

Although the bulk tension is applied to the half-plane, this can be written as the sum of a uniform tension (in both the strip and the half-plane), which does not produce any stress intensity factors, and a uniform tension or compression applied to the strip alone. This means the required stress intensity factors can be found by solving the problem where the tension is applied to the strip alone.

The strip and half-plane are first treated as separate bodies, with no bond, and the remote tension is applied to the strip. This causes a uniform strain in the strip (Fig. 6.3a. To restore the bonded condition over the interval $-b < x < b$, a uniform distribution of glide dislocations causing an equal and opposite strain is applied over the region $|x| < b$ (Fig. 6.3b. This ensures the relative slip displacement is zero over the bonded region. The uniform distribution induces σ_{xx} and σ_{xy} stresses outside the bond, so additional unknown glide and climb distributions must be found that satisfy the traction-free boundary conditions over the regions $|x| > b$ (Fig. 6.3c). These unknown distributions will be square-root singular at $|x| = b$ and square-root bounded at infinity. Once the additional dislocation distributions are solved for, the stress intensity factors can be calibrated in the same way as the shear-force case.

6.3.4 Summary of calibrations for the receded contact

Figure 6.4 displays the results for the stress intensity factors induced by small oscillatory changes in the normal load applied to the upper surface; Fig. 6.5 gives the corresponding results for remote tension; and Fig. 6.6 gives the corresponding results for a shear load applied to the upper surface. The results are displayed as a function of the coefficient of friction μ, which defines the contact-size ratio b/h [8].

Figure 6.7 displays both the strip lift-off point and the initial extent of the slip zone under the normal load alone. As stated earlier, most of the slip zone is shaken down by the oscillatory loads. As the coefficient of friction increases, both the contact size and the stick zone grow.

For an explicit calibration we now fix the coefficient of friction at $\mu = 0.7$. An improved convergence study of the singular integral inversion gives the contact half-width as $b/h = 2.061$. For this particular case, the contact pressure at the contact

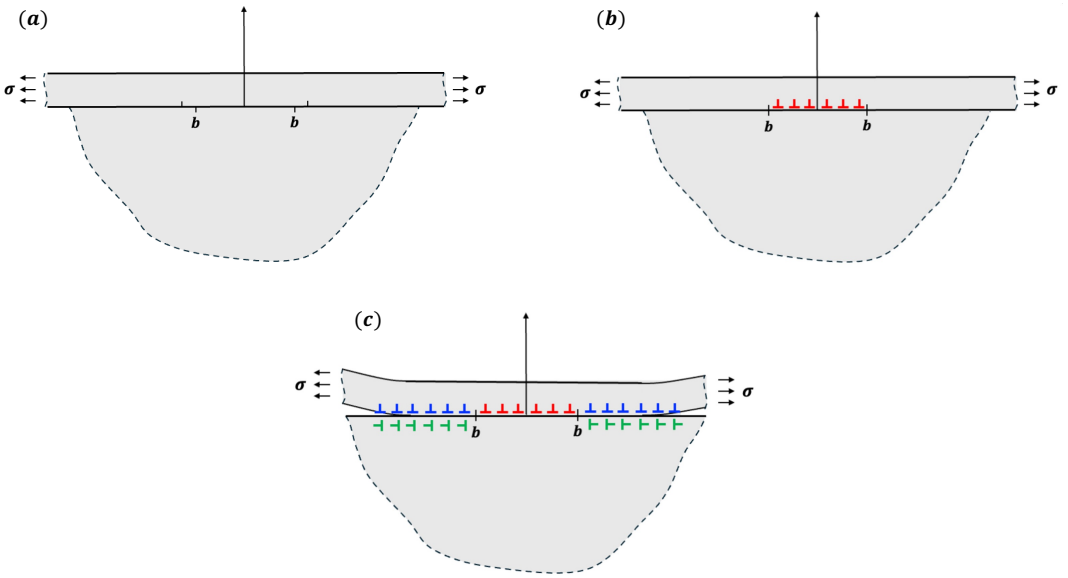


Figure 6.3: Dislocation decomposition for remote tension applied to the receded contact. (a) Uniform tension on the strip alone produces a uniform strain; (b) a uniform glide-dislocation distribution over $|x| < b$ restores the bonded condition by cancelling the relative slip; (c) additional square-root singular glide and climb distributions over $|x| > b$ then satisfy the traction-free boundary conditions external to the contact, and the resulting end fields give the stress intensity factors.

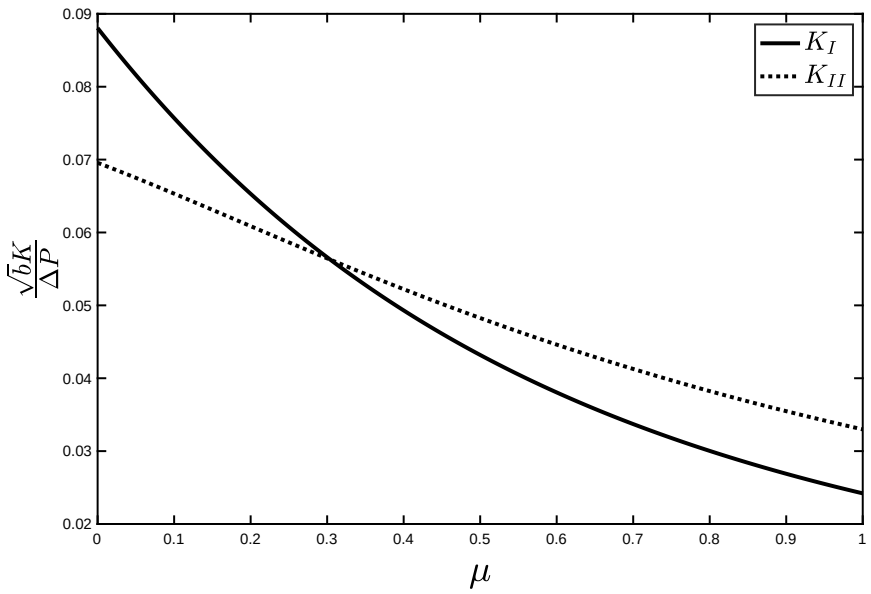


Figure 6.4: Normalised stress intensity factors at the receded-contact edges as a function of friction coefficient μ, induced by an oscillatory normal load ΔP applied to the upper surface of the strip.

edges is given by

$$L_I = 0.0665\, P\, h^{-3/2} = 0.197\, P\, b^{-3/2}, \tag{6.16}$$

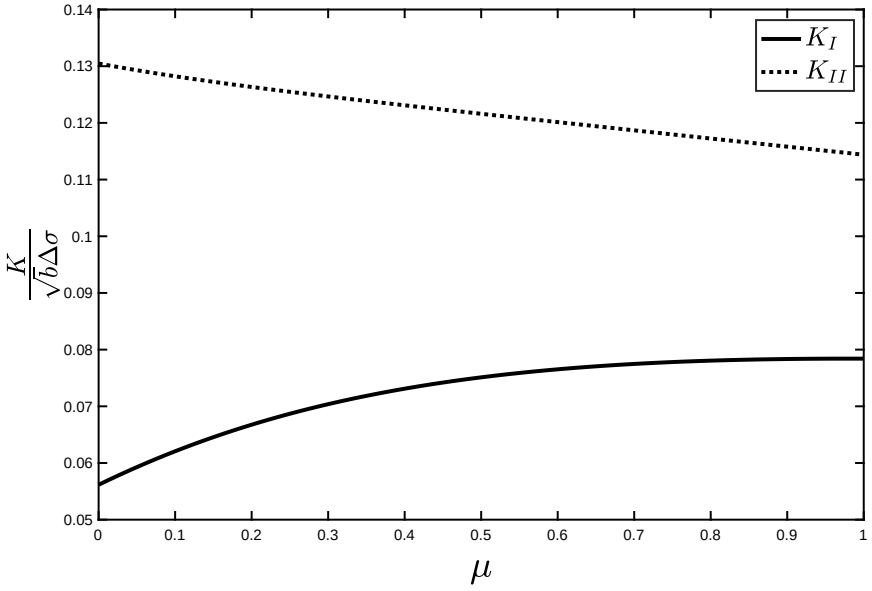


Figure 6.5: Normalised stress intensity factors at the receded-contact edges as a function of friction coefficient μ, induced by an oscillatory remote tension $\Delta\sigma$ in the half-plane.

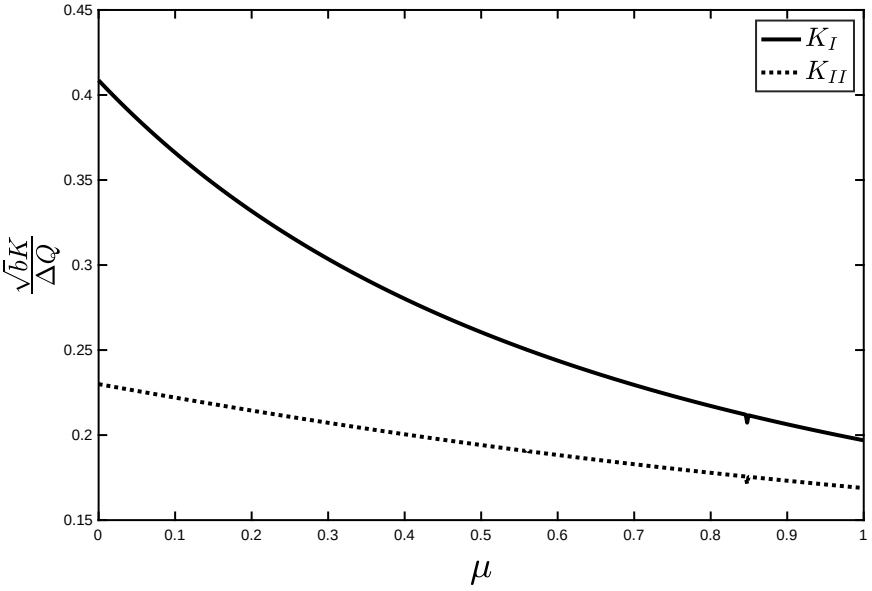


Figure 6.6: Normalised stress intensity factors at the receded-contact edges as a function of friction coefficient μ, induced by an oscillatory shear load ΔQ applied to the upper surface of the strip with no applied resultant moment.

while the effects of the fluctuating loads are given by

$$\begin{Bmatrix} K_I \\ K_{II} \end{Bmatrix} = \begin{bmatrix} +0.0345 & -0.0785 & \mp 0.223 \\ \mp 0.0428 & \pm 0.1178 & +0.184 \end{bmatrix} \begin{Bmatrix} \Delta P/\sqrt{b} \\ \Delta\sigma\sqrt{b} \\ \Delta Q/\sqrt{b} \end{Bmatrix}. \tag{6.17}$$

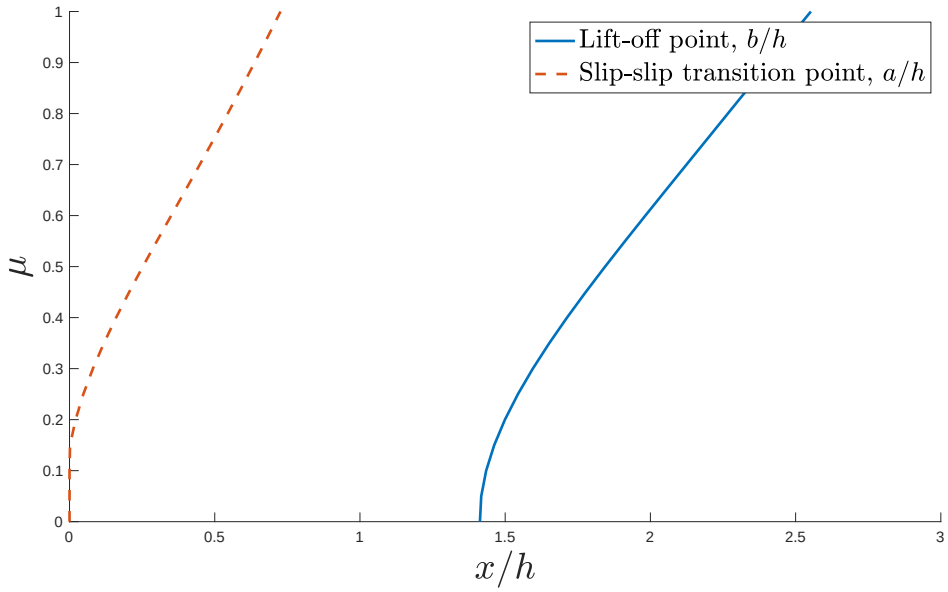


Figure 6.7: Normalised contact half-width b/h (solid line) and stick–slip transition a/h (dashed line), as a function of the coefficient of friction μ, for the receded contact under the mean normal load alone.

Here, and throughout the remainder of this chapter, the upper sign corresponds to the left edge and the lower sign to the right edge, using the positive sign convention in Fig. 6.8. The signs of the first two entries in the K_I row are those obtained when the dislocation-method convention is checked against the finite-element extraction described in the next section.

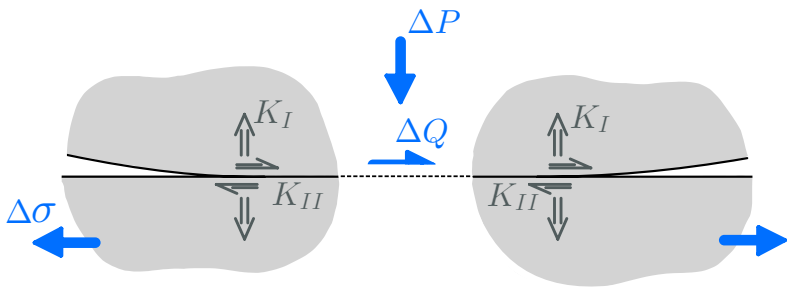


Figure 6.8: Sign convention for positive stress intensity factors at the right and left edges of a contact, used consistently in equations (6.17) and (6.23).

6.4 Validation

The work presented in the previous section uses a numerical inversion of the singular integral equations. The quadrature is accurate, but it is still useful to check the resulting edge amplitudes by a route which is independent of the dislocation

calculation. We therefore re-worked the receded contact using a finite-element model of the whole problem and extracted the same asymptotic constants directly from the near-edge tractions.

The finite-element calculation, built in Abaqus/Standard with plane-strain `CPE4` elements, was used as an independent check on the local asymptotic calibration. The model represents an elastic strip ($h = 2$ mm, half-width 500 mm) on a 1000×500 mm half-plane block, both with $E = 200$ GPa and $\nu = 0.3$, with the half-plane base fully constrained. The interface uses surface-to-surface, `HARD` pressure-overclosure contact with penalty friction at $\mu = 0.7$ (elastic-slip tolerance 10^{-8} mm); the contact mesh is power-law graded from 0.2 μm elements held over a narrow band straddling the mean contact edges at $|x| = b$, growing smoothly to 20 μm in the interior and out to the far field. A mean receded-contact state was first generated by ramping the normal line load to $P = 1000\ \mathrm{N\,mm^{-1}}$ and running a short frictional shakedown cycle. The active contact patch of this mean solution was then locked by replacing the contact pair with bilateral node-to-node ties inside $|x| < b$; outside the lock the surfaces are free to interpenetrate. This 'welded' interface reproduces the bonded-edge condition assumed in the asymptotic derivation, so that subsequent small perturbations excite the singular K_I, K_{II} tractions directly. Each fluctuating load was applied separately, with all other fluctuations set to zero. The amplitudes were $25\ \mathrm{N\,mm^{-1}}$ for ΔP and ΔQ, and $25\ \mathrm{N\,mm^{-2}}$ for $\Delta\sigma$. The contact pressure and shear traction from the mean solution were subtracted from the corresponding perturbed solution to give Δp and Δq. If ξ is measured into the contact from the left edge, the quantities extracted from the finite-element solution were

$$\frac{p(\xi)}{\sqrt{\xi}} \to L_I, \qquad \Delta p(\xi)\sqrt{\xi} \to K_I, \qquad \Delta q(\xi)\sqrt{\xi} \to K_{II}. \tag{6.18}$$

In each case we fitted only the leading-order edge asymptote. The purpose of the fit was therefore not to reproduce the complete contact pressure or shear traction distribution, but to extract the local coefficient multiplying the one-term edge field. The first finite-element contact node was omitted, since this point is most sensitive to the contact enforcement and local convergence at the edge. For each calibration, a single constant edge offset was applied before fitting due to issues with the convergence of the FE at the contact edge. The near-edge coordinate ξ was then measured from this shifted, effective contact edge. The coefficient was then obtained by a least-squares fit to the next ten contact nodes. The comparison with the dislocation calibration is given in Fig. 6.9. The dislocation values in the figure correspond to equation (6.17).

The agreement is not exact, and we do not expect it to be exact. The finite-

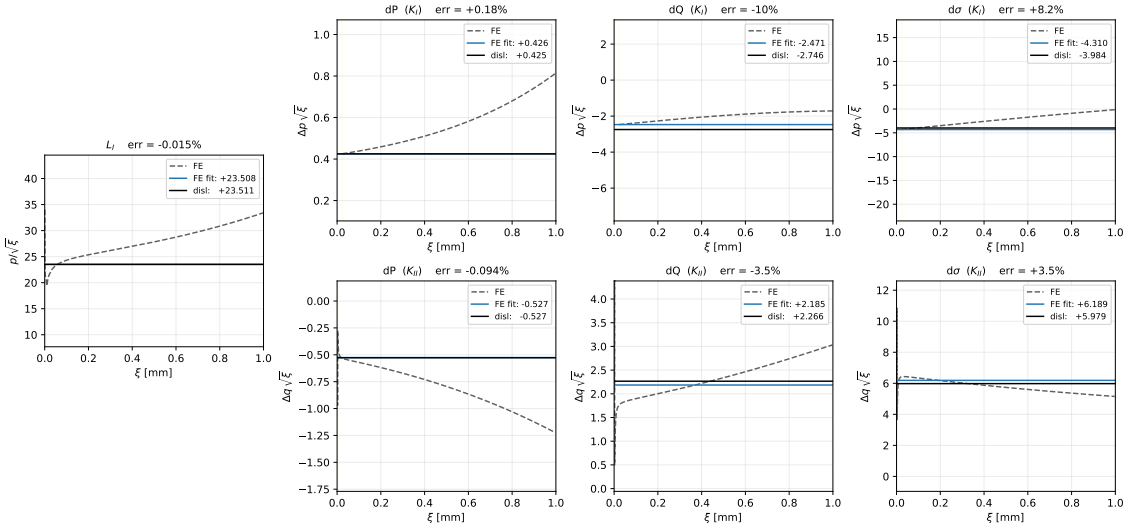


Figure 6.9: Finite-element extraction of the receded-contact edge asymptotes compared with the updated dislocation-method calibration of equation (6.17). The loading conditions used are $h = 2$ mm, $P = 1000\ \mathrm{N\,mm^{-1}}$ and an amplitude of 25 on each fluctuating load type.

element calculation contains a penalty contact representation, a finite block in place of the half-plane, and a finite fitting window at the contact edge. Nevertheless, all seven extracted amplitudes have the same sign as the dislocation calculation, and all magnitudes agree to within about ten per cent. This is a useful check because it validates the local asymptote calibrations, in particular the signs in terms of the convention of Fig. 6.8.

6.5 Calibrations for Hertzian contact

The Hertzian contact arises when $h \to \infty$, so that the problem becomes amenable to half-plane theory. In this limit, the problem becomes uncoupled, so that fluctuations in normal load excite changes in K_I, while fluctuations in shear Q or tension σ excite changes in K_{II} only.

In a Hertzian contact where the relative radius of curvature of the bodies is R (Fig. 6.1b), the overall plane-strain modulus of both bodies is $E^* = E/[2(1-\nu^2)]$, and the load P is per unit depth, the mean pressure effect is given by

$$L_I = \frac{2\sqrt{2}}{\pi}\, P\, b^{-3/2} = \frac{2\sqrt{2}}{\pi}\left(\frac{\pi E^*}{4R}\right)^{3/4} \sqrt[4]{P}, \tag{6.19}$$

where

$$b^2 = \frac{4PR}{\pi E^*}. \tag{6.20}$$

The effect of a change in normal load for this configuration is

$$K_I = \frac{\Delta P}{\pi\sqrt{2b}} = \Delta P \sqrt[4]{\frac{E^*}{16\pi^3 PR}}. \tag{6.21}$$

For shear load and tension, the calibration for K_{II} is independent of the form of the bodies defining the contact [10]:

$$K_{II} = \frac{\Delta Q}{\pi\sqrt{2b}} \pm \frac{\Delta\sigma}{4}\sqrt{\frac{b}{2}} = \Delta Q \sqrt[4]{\frac{E^*}{16\pi^3 PR}} \pm \frac{\Delta\sigma}{4}\sqrt[4]{\frac{PR}{\pi E^*}}. \tag{6.22}$$

We may write the stress intensity factors in matrix form as

$$\begin{Bmatrix} K_I \\ K_{II} \end{Bmatrix} = \begin{bmatrix} +0.225 & 0 & 0 \\ 0 & \pm 0.177 & +0.225 \end{bmatrix} \begin{Bmatrix} \Delta P/\sqrt{b} \\ \Delta\sigma\sqrt{b} \\ \Delta Q/\sqrt{b} \end{Bmatrix}, \tag{6.23}$$

where, as before, the upper and lower signs correspond to the left and right edges, respectively, using the sign convention in Fig. 6.8.

6.6 Results of matching

To use these calibrations to relate the receded and Hertzian dogbone experiments of Fig. 6.2, we match the three local edge quantities L_I, K_I, and K_{II}. There is no requirement for the two contact widths to be the same; the quantities to be matched are the asymptotic coefficients themselves. We therefore write the final conditions in terms of the dimensions which are set in the experiment, namely h for the height of the receded strip and R for the Hertzian radius.

Where there is ambiguity in the notation, the subscript R is added for the receding contact and H for the Hertzian contact. The following conditions are for a coefficient of friction $\mu = 0.7$, so that $b_R/h = 2.061$. The upper sign corresponds to the left edge and the lower sign to the right edge throughout. Once an edge is chosen the same sign must be used in both singular matching conditions.

6.6.1 Mean pressure term

The bounded pressure term fixes the mean Hertzian load. Equating equations (6.16) and (6.19) gives

$$[L_I] \qquad 0.0665\, h^{-3/2}\, P_R = 0.751 \left(\frac{E^*}{R}\right)^{3/4} \sqrt[4]{P_H}. \tag{6.24}$$

This is the only condition on the mean load. Once it is satisfied, the two contacts have the same value of L_I at the chosen edge, even though the corresponding contact half-widths will in general be different.

6.6.2 Singular normal-traction term

With the mean Hertzian load fixed by equation (6.24), the next condition matches the coefficient of the singular change in normal traction. Equating equations (6.17) and (6.21) gives

$$\begin{aligned}[K_I] \quad & 0.0240\, \frac{\Delta P_R}{\sqrt{h}} - 0.1127\, \Delta\sigma_R \sqrt{h} \mp 0.155\, \frac{\Delta Q_R}{\sqrt{h}} \\ & = 0.212\, \Delta P_H \sqrt[4]{\frac{E^*}{P_H R}}.\end{aligned} \tag{6.25}$$

This equation determines the required oscillatory normal load in the Hertzian test. It is independent of the way in which the shear-mode term, K_{II}, is produced.

6.6.3 Singular shear-traction term

The remaining edge condition is the match in K_{II}. It gives

$$\begin{aligned}[K_{II}] \quad & \mp 0.0298\, \frac{\Delta P_R}{\sqrt{h}} \pm 0.169\, \Delta\sigma_R \sqrt{h} + 0.128\, \frac{\Delta Q_R}{\sqrt{h}} \\ & = \pm 0.188\, \Delta\sigma_H \sqrt[4]{\frac{P_H R}{E^*}} + 0.212\, \Delta Q_H \sqrt[4]{\frac{E^*}{P_H R}}.\end{aligned} \tag{6.26}$$

Only the combination of $\Delta\sigma_H$ and ΔQ_H is fixed by this scalar condition. If both are available experimentally there is therefore a family of equivalent Hertzian loadings. For example, if the Hertzian shear actuator is not used, set $\Delta Q_H = 0$ and the condition gives the required bulk tension directly.

6.6.4 Design form of the matching equations

For setting up a test it is useful to solve the matching statements, equations (6.24)–(6.26), once. This gives the following recipe for the Hertzian dogbone, given the receded geometry and loading.

Step 1. Set the mean normal load by

$$P_H = 6.14 \times 10^{-5} \left(\frac{R}{h^2 E^*} \right)^3 P_R^4. \tag{6.27}$$

Step 2. Set the oscillatory normal load from

$$\Delta P_H = \left[0.113 \, \frac{\Delta P_R}{\sqrt{h}} - 0.532 \, \Delta\sigma_R \sqrt{h} \mp 0.733 \, \frac{\Delta Q_R}{\sqrt{h}} \right] \left(\frac{P_H R}{E^*} \right)^{1/4}. \tag{6.28}$$

Step 3. Choose how the Hertzian test is to supply the shear-mode term. With no applied Hertzian shear load, $\Delta Q_H = 0$, and equation (6.26) reduces to

$$\Delta\sigma_H = \left[-0.159 \, \frac{\Delta P_R}{\sqrt{h}} + 0.901 \, \Delta\sigma_R \sqrt{h} \pm 0.683 \, \frac{\Delta Q_R}{\sqrt{h}} \right] \left(\frac{E^*}{P_H R} \right)^{1/4}. \tag{6.29}$$

If a Hertzian shear load is also applied, equation (6.26) should be used directly with the chosen split between $\Delta\sigma_H$ and ΔQ_H. The important point is that the same edge sign is used throughout the three steps.

These equations are edge-matching conditions, not full-field matching conditions. Two Hertzian tests which use different mixtures of shear load and bulk tension may be equivalent at the contact edge while still having different shear-traction distributions away from the edge.

6.6.5 Worked example

We now use the method outlined above to give one numerical example of a receded contact and a Hertzian contact with matched contact-edge stress states. All components are elastically similar, with $E = 200$ GPa, $\nu = 0.3$ and $\mu = 0.7$. For the receded contact, the strip width and applied loads are

$$h = 2 \text{ mm}, \qquad P_R = 1000 \text{ N mm}^{-1}, \qquad \Delta P_R = 25 \text{ N mm}^{-1}.$$

Using the matching equations (6.27)–(6.29) and equation (6.26) with $\Delta\sigma_H = 0$, we obtain the matched edge Hertzian case,

$$R = 10{,}000 \text{ mm}, \qquad P_H = 723.4 \text{ N mm}^{-1},$$
$$\Delta P_H = 5.71 \text{ N mm}^{-1}, \qquad \Delta Q_H = -7.09 \text{ N mm}^{-1}.$$

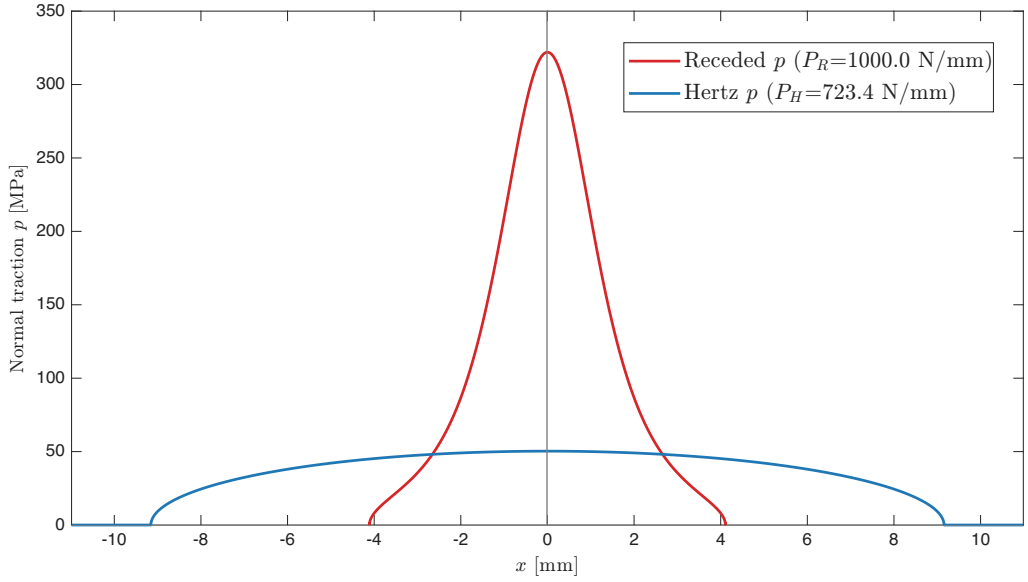
For illustrative purposes, a finite-element analysis was used for the receded contact. The model has the same numerical limitations as those described in Section 6.4 — in particular the representation of the half-plane and strip by finite bodies, and the use of a finite fitting region close to the edge. The contact was first loaded to the mean normal load P_R and then cycled five times between $P_R + \Delta P_R$ and $P_R - \Delta P_R$; in this calculation, five cycles was sufficient to reach a steady cyclic state. For the Hertzian contact, the steady-state tractions were found analytically using the method of [11], starting from $(P_H, 0)$ and then cycling between $(P_H + \Delta P_H, \Delta Q_H)$ and $(P_H - \Delta P_H, -\Delta Q_H)$.

Figure 6.10 compares the mean normal tractions. The first point to notice is that the full pressure distributions are not the same, and are not intended to be the same. The receded contact has a different contact size and a different pressure distribution away from the edge. The matching condition is a condition on the leading term in the edge expansion. When the two pressure distributions are plotted with their origins placed at the left contact edge, Fig. 6.10(b), both contacts follow the same $L_I\sqrt{\xi}$ asymptote over the near-edge region. This is the part of the pressure field that is used in the matching.

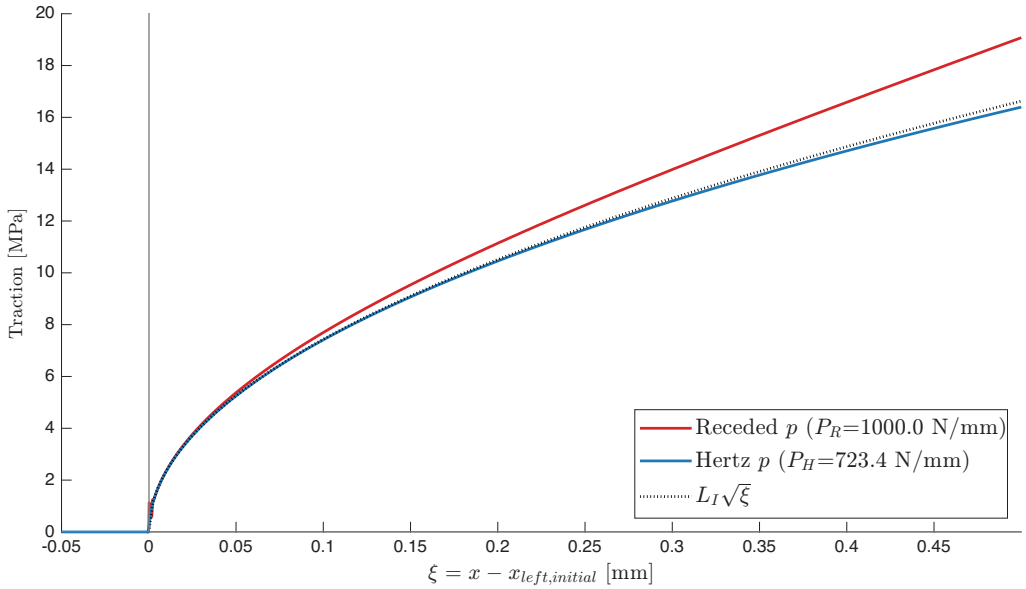
Figure 6.11 shows the corresponding cyclic shear tractions and friction envelopes at the left edge. Again, the comparison should be interpreted locally. The two contacts do not have identical shear tractions over the whole contact, but the active slip region sits in the same small neighbourhood of the edge and is controlled by the same values of L_I, K_I, and K_{II}. Within the numerical limitations of the finite-element calculation, the receded contact and the matched Hertzian contact give the same kind of edge response. This is the sense in which the two contacts are equivalent.

6.7 Limitations

The matching developed in this chapter is deliberately local. It is not a statement that the two contacts have the same pressure distribution, the same shear-traction distribution, or the same contact size. It is a statement that, sufficiently close to the



(a)



(b)

Figure 6.10: Comparison of mean normal tractions between the matched Hertzian and receded contacts. (a) Full contact tractions for each contact; the contact size is not a matching requirement. (b) Left contact edge for both contacts, plotted with the matched bounded-pressure asymptote $L_I\sqrt{\xi}$ on a common origin at the contact edge.

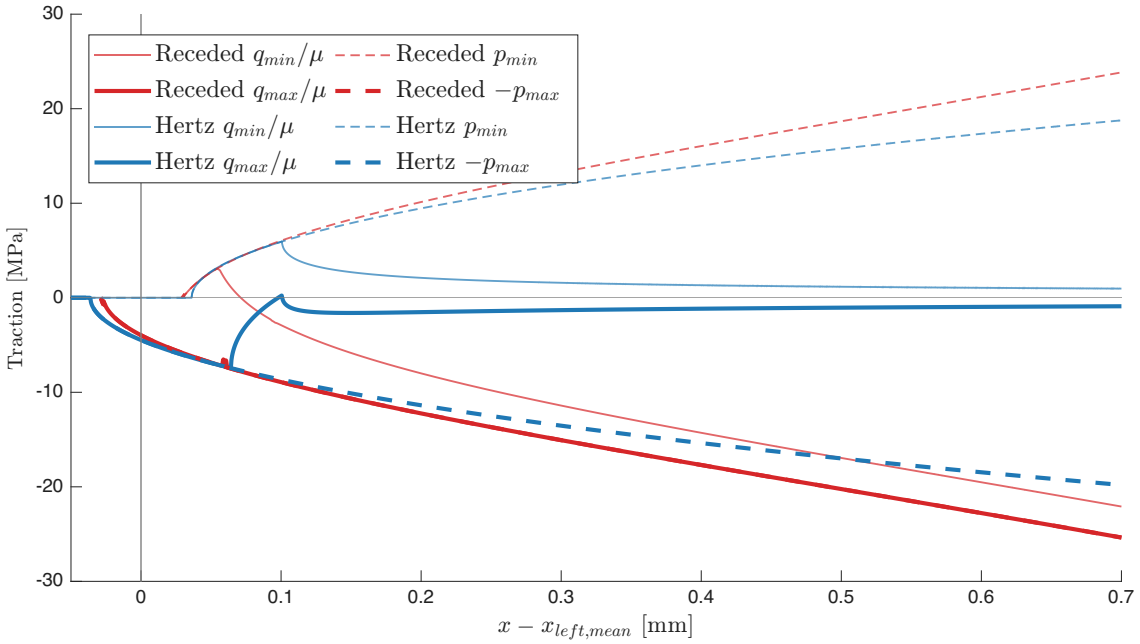


Figure 6.11: Normalised cyclic shear tractions for the matched receded and Hertzian contacts at the left edge, plotted at the maximum and minimum perturbed loading conditions alongside the corresponding normal-traction friction envelopes $\pm\mu p(x)$. The active slip region lies within the asymptotic region and is controlled by the matched L_I, K_I, and K_{II}.

chosen contact edge, the leading terms in the asymptotic descriptions are the same. The method should therefore be used only when those leading terms dominate the part of the contact which is physically important.

The restriction is closely analogous to the usual restriction in fracture mechanics. There, a crack-tip stress intensity factor is useful only when the singular field describes the stress state over a region larger than the plastic zone. Here the corresponding requirement is that the contact-edge asymptote describes the pressure and shear tractions over a region larger than the cyclic slip zone. In particular, the square-root bounded pressure term must reach far enough into the contact that the stick–slip transition lies within the region where this one-term description is still adequate. Any feature that strongly shapes the pressure distribution — a nearby corner, hole, free surface, or discontinuity in slope — must therefore be sufficiently far from the edge being matched.

There is also a restriction on the perturbation size. The oscillatory loads must be small compared with the mean load in the sense required for the contact-edge motion and the cyclic slip zone to remain local. If the perturbation is large enough that the contact edge moves through a distance comparable with the scale over which higher-order terms in the pressure expansion become important, then K_I is no longer

a satisfactory one-parameter description of the normal response. Similarly, if the shear perturbation is large enough that the slip zone is no longer small, then the estimate $d = 2K_{II}/(\mu L_I)$ is no longer a local edge result.

The coefficient of friction must be the same in the two contacts, and it must be large enough, for the loading considered, to keep the cyclic slip zone within the asymptotic region.

For a prescribed receded-contact value of L_I, equation (6.27) may require a large Hertzian radius so that the corresponding Hertzian pressure remains below the elastic limit. This is a practical experimental limitation rather than a change in the asymptotic argument, but it may be important when designing a real test.

Finally, matching L_I, K_I, and K_{II} does not imply equality of the full-field tractions. The present method is an edge-equivalence condition for crack-nucleation-scale fields. Whether that edge equivalence is sufficient to reproduce measured fretting fatigue lives or wear rates is a question to be validated experimentally.

6.8 Conclusion

This chapter has applied the contact-edge asymptotic framework of [1, 2] to the practical problem of matching a plane-receded contact with a Hertzian contact. The matching is made through three local quantities: the bounded mean-pressure multiplier L_I, the normal-perturbation stress intensity factor K_I, and the shear-perturbation stress intensity factor K_{II}. Once these three quantities are matched at a chosen edge, the two contacts have the same leading local description of mean pressure, contact-edge movement, and cyclic slip.

For the receded contact, the required calibrations were obtained from the singular integral formulation and then checked independently using a finite-element extraction of the near-edge tractions. The finite-element calculation is not exact, since it contains the usual approximations associated with finite bodies and a finite fitting window, but it gives comparable magnitudes for all the edge coefficients. It also confirms an important point for the present application: after the receded contact has been formed, its edge is not fixed under a cyclic normal-load perturbation. The receded and Hertzian contacts can therefore be compared through their local edge motion as well as through their slip behaviour.

The resulting design equations give the mean Hertzian load, the oscillatory Hertzian normal load, and the required shear-mode contribution for an equivalent Hertzian dogbone experiment. The worked example shows the nature of the equivalence: the full pressure distributions of the receded and Hertzian contacts are

different, but their near-edge pressure fields collapse onto the same asymptote, and the cyclic shear response is comparable in the edge region, which is the region being matched.

The purpose of the method is therefore not to reproduce the whole contact problem in another geometry. Rather, it is to reproduce the leading local edge fields in a simpler and more controllable Hertzian experiment, which is the part of the field expected to be most relevant to fretting crack nucleation. The subsequent step, which remains to be done experimentally, is to determine whether matching these edge quantities is sufficient to reproduce measured fretting fatigue lives, and to what extent wear evolution is also controlled by the same local parameters.

References

[1] J. R. Barber and D. A. Hills. "Fretting Fatigue starting from the edges of incomplete contacts under general periodic loading - an asymptotic approach". in *Theoretical and Applied Fracture Mechanics* (2025). DOI: https://doi.org/10.1016/j.tafmec.2025.105054.

[2] J. R. Barber and D. A. Hills. "Periodic Loading of a frictional contact". Journal of Mechanics and Physics of Solids. In press. 2026.

[3] A.E. Giannakopoulos, T.C. Lindley and S. Suresh. "Aspects of equivalence between contact mechanics and fracture mechanics: theoretical connections and a life-prediction methodology for fretting-fatigue". in *Acta Materialia* 46.9 (1998), 2955–2968.

[4] A. Mugadu, D.A. Hills and L. Limmer. "An asymptotic approach to crack tip stress intensity factors in fretting fatigue of complete contacts". in *Journal of the Mechanics and Physics of Solids* 50.3 (2002), 531–547.

[5] J.R. Barber. *Contact Mechanics*. Solid Mechanics and Its Applications. Springer International Publishing, 2018, 29–39. ISBN: 9783319709390. URL: https://books.google.co.uk/books?id=4GNLDwAAQBAJ.

[6] J. R. Barber. *Elasticity*. 4th. Switzerland: Springer Nature, 2022.

[7] S.A. MacLeod and D.A. Hills. "Receding contact of a layer on an elastically similar half-plane". in *European Journal of Mechanics - A/Solids* 116 (2026), 105853. ISSN: 0997-7538. DOI: https://doi.org/10.1016/j.euromechsol.2025.105853. URL: https://www.sciencedirect.com/science/article/pii/S0997753825002876.

[8] T. Chaise, R.J.H. Paynter and D.A. Hills. "Contact analysis of a semi-infinite strip pressed onto a half plane by a line force". in *International Journal of Mechanical Sciences* 81 (2014), 60–64. ISSN: 0020-7403. DOI: https://doi.org/10.1016/j.ijmecsci.2014.02.001. URL: https://www.sciencedirect.com/science/article/pii/S0020740314000411.

[9] S. Krenk. "On the use of the interpolation polynomial for solutions of singular integral equations". in *Quarterly of Applied Mathematics* 32 (1975), 479–484.

[10] D.A. Hills, R.M.N. Fleury and D. Dini. "Partial slip incomplete contacts under constant normal load and subject to periodic loading". in *International Journal of Mechanical Sciences* 108-109 (2016), 115–121. ISSN: 0020-7403. DOI: https://doi.org/10.1016/j.ijmecsci.2016.01.034. URL: https://www.sciencedirect.com/science/article/pii/S0020740316000485.

[11] J.P.J. Truelove, L.E. Blades and D.A. Hills. "Half-plane contact problems in partial slip with varying normal and tangential loads". in *European Journal of Mechanics - A/Solids* 94 (2022), 104590. ISSN: 0997-7538. DOI: https://doi.org/10.1016/j.euromechsol.2022.104590. URL: https://www.sciencedirect.com/science/article/pii/S0997753822000699.

Chapter 7

Conclusions and Future Work

Contents

7.1 Summary of Contributions 146

7.1.1 Key Findings from Chapter 3 147

7.1.2 Key Findings from Chapter 4 148

7.1.3 Key Findings from Chapter 5 149

7.1.4 Key Findings from Chapter 6 150

7.2 Overall Significance 150

7.3 Limitations 151

7.4 Future Work 152

7.5 Closing Remarks 162

To conclude this dissertation in contact mechanics, it is helpful to discuss how the engineering world compares plain fatigue and fretting fatigue, and the implications of using the concept of an S-N curve for fretting problems.

Plain fatigue is a stochastic process where freely initiated cracks start at a free surface in components with no more than mild stress gradients. The alternating stress probes the strength of the material over a significant area, and finds its weakest spot (a machine mark, the triple point between grains, a region of unexpected tensile residual stress, for example). We know, qualitatively, that surface finish and residual states of stress have important effects, and all practising engineers are very familiar with the concept of an S-N curve, which goes back some 160 years. The total life of a component is related mainly to the reversing (principal) component of surface stress. Some materials show a fatigue limit (endurance limit) below which the material may be expected to live forever, i.e. no crack will be initiated. Because early tests were all done under fully reversing stress conditions (rotating-bending tests) a means of judging the influence of a mean stress was needed and this has, historically, been considered by many people whose names have gone into the subject index (Gerber, Soderberg, Haigh, Goodman, and there are others), although these approaches lack underlying physical reasoning, and are essentially correlations. But they are widely used. The usually accepted wisdom is that these corrections may be applied to both the fatigue limit (where it exists) and the finite life part of the S-N curve.

For many practising engineers, this is the starting point for analysis of fretting fatigue problems, and they think in terms of a knockdown factor for the detrimental effect of surface damage. We have started from a different point. Unlike plain fatigue, fretting cracks start from a very well specified location: the edge of a contact. Although the contact concerned may, nominally, be stationary and stuck, it is quite common for contacts in assemblies to be subject to vibration, and hence local slip. It follows that the environment in which the crack starts should be capable of a description, to some degree of fidelity, by asymptotic forms.

It has to be recognised that there are essentially two kinds of contact edge which can arise: (a) those where we have conforming contacts whose edges are defined by some discontinuity in profile of one body, and (b) those which are non-conforming and the location of the contact edge is self-determined by the local normal load. Certainly, there are other possibilities, but this will cover the vast majority of cases, and we have, so far, restricted studies to problems where gradients along the nominal contact edge are modest, i.e. no three-dimensional effects are permitted. Here, we have thought primarily about non-conformal (incomplete) contacts with a rounded edge, because these are ubiquitous in engineering practice and because the near-edge

fields are central to fretting fatigue initiation.

Plain fatigue and fretting fatigue, in terms of initiation and in the very early stages of propagation, are therefore very different. Not only does the latter impose surface damage, but the whole stress environment in the neighbourhood is quite different. For the reasons stated there is another aspect which is different: when the crack is forming, in the case of plain fatigue there is one component of normal stress, parallel with the surface, which is principal and responsible for early crack development. Any perpendicular principal stress will probably have little effect. If the crack forms in the freely initiated sense away from any stress raising feature, it follows that stress gradients with depth are likely to be mild. It is likely, therefore, that as soon as the concept of a crack tip stress intensity factor becomes viable it will have the same calibration (for example $K_I \sim \sigma\sqrt{\pi a}$), so that the transition from the processes of nucleation are smooth and probably quite similar in all cases.

By contrast, in the case of nucleation at a contact edge, the transition will take place in a very complicated environment with steep stress gradients. So, in the case of plain fatigue it makes complete sense to think of the S in S-N (which is the σ in the crack tip stress intensity) as controlling early crack development. An equivalent statement cannot be made for fretting. These observations make us increasingly uneasy about using the S-N curve concept in fretting; and, by implication, related methods such as the Takahashi idea look less than rigorous. For similar reasons, all those adjustments which may be made to S-N data (Haigh/Soderberg/Gerber etc.) seem even less rigorous than they do in plain fatigue.

The biggest remaining problem is to extend the idea of the contact edge asymptotic solution into the finite life regime, because of the transition from contact edge stress field to crack evolution. But those concerns disappear when we are investigating the conditions for threshold, or 'infinite life'. The work in this thesis has therefore been directed primarily towards obtaining robust, physically interpretable descriptions of near-edge tractions (and the stick–slip state) which can underpin threshold-type assessments, and which can ultimately serve as boundary conditions for more complete finite-life frameworks.

7.1 Summary of Contributions

In terms of the research questions posed in Chapter 1, the contributions of this thesis may be summarised as follows:

1. A closed-form representation of the state of stress at a contact edge in the presence of geometric coupling has been developed by matching the local, half-

plane-controlled behaviour to an outer field which respects the true domain shape (i.e. the influence of traction-free sides).

2. Guidance has been established on when half-plane theory is appropriate for representing the whole of flat-and-rounded contacts, and when it is not. In particular, as the ratio of flat length to edge radius grows, the adjacent traction-free surfaces can no longer be neglected without significant loss of fidelity.

3. A practical link has been constructed between contact-edge fields and a crack description, by using stress-intensity factors as the scaling parameters for the near-edge traction field. This provides a disciplined route for importing well-developed partial slip methodology into a coupled (geometrically realistic) setting.

4. A framework has been developed for matching near-edge conditions between a plane-receded contact under oscillatory loading and an equivalent Hertzian contact using asymptotic edge parameters. This provides a practical route for designing one laboratory test which can reproduce the local stick–slip and stress state of more complicated contacts.

7.1.1 Key Findings from Chapter 3

Chapter 3 addressed a fundamental deficiency of the standard half-plane description for flat-and-rounded contacts. Although the very near-edge behaviour can be described using half-plane theory, the traditional half-plane model does not represent the adjacent traction-free boundary of a flat-and-rounded contacting body. Consequently, the half-plane solution has an incorrect far-field structure for the rounded three-quarter-plane geometry.

The chapter demonstrated that:

- A truncated, purely local asymptotic expansion is generally not adequate for flat-and-rounded contacts whenever the region of interest extends a significant distance from the edge (as it typically does for slip zones). This motivates the use of a representation that is correct both locally and in the far field.

- A closed-form near-edge traction description can be obtained by collocating the convenient half-plane solution into a far-field governed by Williams' solution for the three-quarter plane. This provides, for the first time, a tractable analytical description of edge tractions which respects the presence of the traction-free side.

- The principal physical effect captured by this procedure is geometric coupling: the realistic domain shape permits normal loading to excite shear tractions, as it modifies the relation between contact tractions and imposed loads. This coupling is absent from the uncoupled half-plane idealisation.

Taken together, these points establish a method for obtaining near-edge tractions of good quality, while retaining the transparency and ease of a closed-form solution.

7.1.2 Key Findings from Chapter 4

Chapter 4 applied the Chapter 3 methodology to finite, flat-and-rounded contacts and addressed the practical question: 'When should we use half-plane theory?'

The key findings were:

- The accuracy of the half-plane solution deteriorates as the relative size of the flat segment of the contacting body increases. In this regime, the traction-free sides are 'felt' by the contact, and the uncoupled half-plane assumptions become increasingly misleading.

- The rounded, three-quarter-plane formulation becomes increasingly accurate as the relative flat length increases. Comparisons with finite element output showed that, for moderate-to-large geometry ratios (in particular $a/R \gtrsim 6$), the rounded three-quarter-plane approach gives a marked improvement over the traditional half-plane model in both the normal and shear tractions, while retaining a compact analytical form.

- The presence of coupling was demonstrated; even under pure normal loading, realistic geometries exhibit non-zero shear traction distributions. This is of immediate relevance to fretting because the onset and extent of slip, and hence the local stress state, depend sensitively on the shear traction field.

- For contacts where the traction-free boundary is 'felt', the contact law is not just a function of normal load, but a function of tangential load too. The traditional half-plane model, by construction, cannot capture this behaviour.

A significant outcome of Chapter 4 is a clear, geometry-based statement of when the rounded three-quarter plane method is required. This is particularly valuable in industrial settings, where half-plane theory is often applied by default.

7.1.3 Key Findings from Chapter 5

Chapter 5 extended the method to the case of partial slip under multi-stage and cyclic loading. This is the regime of greatest practical interest for fretting fatigue and wear, because the stick–slip state governs both the local stress field and the damage mechanisms.

The principal contributions were:

- A refined hybrid procedure was developed which exploits three domains: (a) a finite-element calibration for the sharp-cornered (monolithic) geometry, (b) a wedge/three-quarter-plane intermediate problem incorporating an edge-crack analogue, and (c) a half-plane, semi-infinite flat-and-rounded contact providing an explicit near-edge traction form. These domains are rigorously connected by stress intensity factors, connecting the global geometry to the contact edge behaviour.

- By introducing the crack phase into the wedge formulation, the near-edge tractions are parameterised by square-root singular decaying asymptote. Since the near-edge behaviour is now controlled by the remote-from-edge asymptote, it allows us to apply the pre-existing half-plane partial slip methodology to contacting geometries better described by wedge theory.

- A physically meaningful condition for the onset of slip was obtained for the coupled geometry. Rather than relying on the classical half-plane criterion based on increments of $|Q|/P$, the relevant measure is the ratio of the incremental stress-intensity-factors at the contact edge, $\Delta K_{II}/\Delta K_I$. As implied by this, Chapter 5 demonstrates that the two edges of a flat and rounded contact can exhibit different behaviour for slip under the same external loading history.

- Comparisons with finite element output showed that the refined formulation can deliver higher-quality near-edge tractions with less numerical noise, and it corrects the gross errors that arise when the entire problem is treated as an uncoupled half-plane contact. In the example considered, the improvements are sufficient to change materially the predicted stick–slip state and the peak near-edge stresses, and therefore the interpretation of fretting risk.

Overall, Chapter 5 shows that the principal ideas developed in Chapters 3 and 4 are not restricted to proportional loading under full stick. Rather, the hybrid formulation provides a workable framework for contacts subjected to complicated loading histories, and it exposes the fundamentally asymmetric nature of geometrically coupled contacts in partial slip.

7.1.4 Key Findings from Chapter 6

Chapter 6 addressed the practical problem of running experiments for different contacting geometries by characterising fretting behaviour in a complicated contact using a simpler, standard test. A plane receded contact (an elastic strip pressed onto an elastically similar half-plane) was analysed under oscillations of normal load, shear load and bulk tension. The near-edge response was expressed using a small set of asymptotic parameters, from which the cyclic motion of the contact edge and the extent of the permanent stick zone could be obtained.

The chapter showed that:

- Under small perturbations about a mean state, the contact-edge behaviour can be characterised by three quantities: a bounded-pressure parameter L_I describing the mean state, and two stress-intensity-type quantities ΔK_I and ΔK_{II} describing the changes induced by fluctuating normal load and by fluctuating shear/bulk tension, respectively.

- These parameters provide direct measures of key fretting-relevant features: the cyclic movement of the contact edge and the maximum extent of cyclic slip can be written in terms of L_I, ΔK_I, ΔK_{II} and the coefficient of friction.

- By calibrating $(L_I, \Delta K_I, \Delta K_{II})$ for both the receded contact and a Hertzian contact, and then equating them, an explicit set of load relationships can be obtained which defines an 'equivalent' Hertzian experiment. The resulting Hertzian configuration can reproduce the local near-edge stress and slip conditions of the receded contact while using a simpler experimental arrangement.

7.2 Overall Significance

The work presented in this thesis demonstrates that the standard half-plane approach to flat-and-rounded contacts can be inadequate when the contact-defining body has a moderate flat-to-rounded geometry ratio. Using the traditional half-plane approach in these cases can lead to significant inaccuracies such as incorrect predictions for (i) whether shear tractions exist under normal load, (ii) how contact size evolves with tangential loading, and (iii) the onset and distribution of slip.

From a contact mechanics perspective, the thesis provides two broad advances.

First, it provides a systematic way to construct closed-form near-edge traction descriptions which are correctly geared to the outer field. This means that the

contact tractions are valid relatively far in from the contact edge, in the regions of interest where we expect to see partial slip and fretting.

Secondly, it provides a practical framework for geometrically coupled contacts that mirrors the logic of fracture mechanics. By expressing near-edge behaviour in terms of stress-intensity-factors, it becomes possible to (a) analyse the near-edge tractions under multi-stage loading, (b) import well-established partial slip solution strategies into geometries where half-plane theory is not globally valid, and (c) move towards an improved description of threshold behaviour at a fretting contact edge.

From a practical standpoint, the significance is that a large class of contacts in safety-critical applications (for example turbine blade roots and subsea connector segments) can be analysed with a level of edge fidelity that would otherwise require careful and computationally expensive finite element work, and which is often difficult to obtain numerically because of near-edge gradients and mesh sensitivity. The methods developed here, therefore, offer a robust framework for assessing contact-edge stresses and stick–slip states in geometries where half-plane methods are routinely used but not necessarily justified.

A second practical significance, developed in Chapter 6, aids our ability to test contacts experimentally. The use of stress-intensity-type edge parameters makes it possible not only to compare geometries analytically, but also to design equivalence between a complicated contact and a standard laboratory test. In particular, a plane receded contact subjected to combined oscillatory loading can be represented by a Hertzian pad contact by matching the governing edge parameters. This opens the possibility of characterising fretting behaviour of realistic assemblies using well-controlled Hertzian experiments.

7.3 Limitations

It is important to recognise the limitations of the present work, both in terms of the physics represented and the scope of the geometries treated.

- **Two-dimensional idealisation.** Throughout, the analysis has been restricted to two-dimensional formulations. This excludes three-dimensional effects such as gradients, corner effects, finite depth, and misalignment, in the third dimension. In many practical problems these effects can be important.

- **Elasticity and friction idealisation.** The contacting bodies are treated as linearly elastic and the interface is governed by Coulomb friction with a constant coefficient. Plasticity, roughness, wear evolution, debris/oxidation effects, and

frictional variations with slip amplitude or pressure are not represented, however are likely to contribute to finite-life fretting behaviour.

- **Scope of contact class.** The work has primarily focussed on incomplete flat-and-rounded contacts with sides at 90° to the interface and receding contacts. For this case, the coefficient of friction must satisfy the condition for the wedge description, $\mu \geqslant 0.54$ due to Williams' solution. Flat and rounded contacts with acute or obtuse contacting bodies have not been developed in the same detail in the present framework, despite having practical relevance.

- **Calibration dependence.** The hybrid method relies on calibrated relationships between external loads and stress-intensity-factors for the relevant sharp-cornered geometry. While this is a strength in practice as it reduces the numerical task to a one-time calibration, it does mean that each new geometry (wedge angle) requires an initial calibration step, and the quality of the results depends on the quality of that calibration.

- **Small-perturbation and synchronous loading assumption.** The matching procedure in Chapter 6 is built on the asymptotic response to small load perturbations about a mean state, and the illustrative development assumes the fluctuating load components act at the same frequency and without phase shift. Extending the matching to larger excursions, non-synchronous histories or general phase relationships remains to be established.

- **Finite-life transition.** One of the most difficult outstanding issues is the transition from a contact-edge stress field to the finite-life regime. The present work provides a framework for describing the near-edge tractions, but it does not yet deliver a complete predictive framework for propagation life under fretting.

These limitations are not shortcomings of the approach, but they define the boundary of what has been tackled here. They also indicate what areas might be tackled next to improve our finite-life fretting fatigue procedures.

7.4 Future Work

Based on the findings of this thesis, several natural extensions present themselves. Some are broad (e.g. additional loading components and three-dimensionality), but the most immediate and mechanically interesting next step is to generalise the

'traction-free boundary' framework beyond orthogonal side faces. I have started this endeavour, and outline it first below.

(1) Angled traction-free faces: sharp flat contact with an angled wedge body

A direct extension of Chapters 3–5 is to consider a contact-defining body whose side surfaces are not orthogonal to the interface, i.e. an angled wedge pressed into an elastically similar half-plane. To simply apply the framework outlined in Chapter 5, we must ensure the limiting coefficient of friction is maintained, and then run the relevant calibrations for that particular wedge angle in a finite element model. However, if the coefficient of friction is below this critical value, the edges may slip and we must use a different method to describe the contact behaviour. The coefficient of friction required to maintain Williams' adhesion limit can be very high for acute wedge angles meaning these contacts can be prone to significant partial slip and in some cases separation. Once slip occurs, the local corner field is governed by a sliding-wedge eigensolution, rather than Williams' solution, whose dominant eigenvalue can be real or complex, with correspondingly different contact-edge behaviour: bounded, singular or separation.

The work divides naturally into four tasks.

1. **Adhesion limit and fully-adhered asymptotics.** For each wedge angle 2α, compute the dominant Williams' eigenvalue for the monolithic wedge and hence the critical friction coefficient for adhesion. When the coefficient of friction exceeds this limit, the contact remains fully adhered and the asymptotic corner fields can be obtained directly from Williams' solution. This provides the 'upper envelope' against which partial slip solutions must be judged.

2. **Classification of edge behaviour below the adhesion limit.** For coefficients of friction below the adhesion limit, we can apply the sliding-wedge-on-a-half-plane formulation locally at each contact edge. The dominant eigenvalue then determines whether the edge behaviour is (a) separating (complex eigenvalue), (b) bounded (real eigenvalue > 1), or (c) singular (real eigenvalue < 1). By solving this for each contact angle, we can map the different contact behaviour for a given contact wedge angle and coefficient of friction.

3. **Finite element validation and the role of secondary eigenvalues.** The regime map and the local eigensolutions must be tested against finite element

output. A sensible validation path is: (i) symmetric normal loading (both edges effectively 'leading' in the local sense), followed by (ii) combined normal and shear loading, in which the local edge roles are distinct. Particular attention should be paid to the neighbourhood of eigenvalue-boundary transitions; preliminary results suggest that the onset of separation and the extent of a receding contact can differ from what is predicted by the most-dominant eigenvalue. Quantifying where and why this happens, such as through the increasing influence of secondary eigenvalues, is necessary before the local asymptotics can be used as a reliable tool.

4. **Embedding in the thesis 'three-domain' philosophy.** Once the local edge fields are validated, the aim is to embed them into an extension of the Chapter 5 hybrid framework: an outer calibration mapping $(P, Q, \ldots)$ to appropriate stress-intensity factors at the corner of the sharp wedge geometry; an intermediate description of the stress-intensity factors oriented along the contacting interface, now angle-dependent and potentially separating; and an inner description of a rounded-edge dictated by half-plane theory for practical applications with a finite radius.

I have made a start on this work which will commence here:

Tasks 1 & 2: Edge-behaviour classifications

To obtain the critical coefficient for adhesion, we must turn to Williams' solution. The critical friction coefficient is a function of the monolithic wedge angle, 2α and the dominant eigenvalue λ_I [1]. The dominant eigenvalue can be calculated for a given wedge-angle by solving the characteristic equation [2]

$$\lambda_I \sin(2\alpha) + \sin(2\lambda\alpha) = 0. \tag{7.1}$$

By considering the stress components along the interface, the critical coefficient of friction can be described by [1]

$$\mu(\alpha;\lambda) = \frac{(1-\lambda_I)\sin[(1-\lambda_I)(\pi-\alpha)] + \Gamma_I(1-\lambda_I)\sin[(1+\lambda_I)(\pi-\alpha)]}{(\lambda_I+1)\cos[(1-\lambda_I)(\pi-\alpha)] + \Gamma_I(1-\lambda_I)\cos[(1+\lambda_I)(\pi-\alpha)]}, \tag{7.2}$$

where

$$\Gamma_I = -\frac{\sin[(1-\lambda_I)\alpha]}{\sin[(1+\lambda_I)\alpha]}. \tag{7.3}$$

Figure 7.1 plots this solution with a dashed line for the trailing edge (positive friction coefficient).

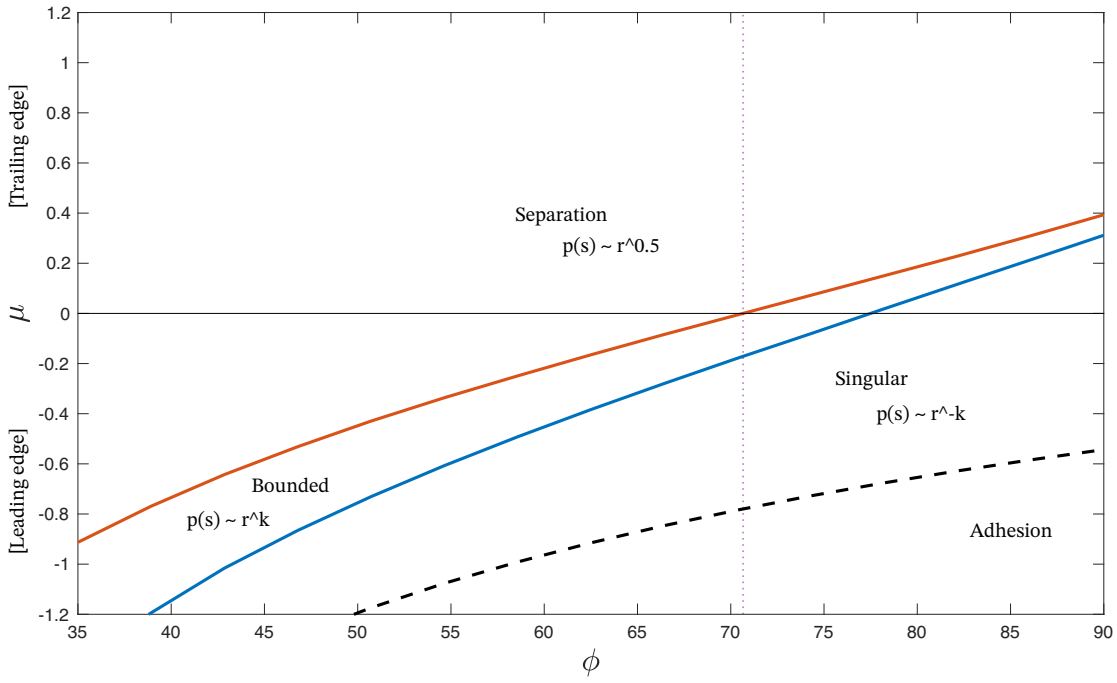


Figure 7.1: Positive coefficient of friction, μ, refers to the trailing edge, whilst a negative coefficient of friction refers to the leading edge. ϕ is the wedge angle of the contacting body.

When the practical coefficient of friction is less than the adhesion limit, we must consider the type of contact edge behaviour. To do this, we turn to the sliding-wedge-on-a-half-plane formulation. Karuppanan investigated the contact problem for a sliding semi-infinite wedge on a half-plane using the characteristic equation [3]

$$\cos\lambda\pi(\sin^2\lambda\phi-\lambda^2\sin^2\phi)+0.5\sin\lambda\pi(\sin 2\lambda\phi+\lambda\sin 2\phi)+\mu\sin\lambda\pi(\lambda(1+\lambda)\sin^2\phi)=0. \tag{7.4}$$

The contact edge behaviour is governed by the dominant eigenvalue, which is represented by the smallest value of λ that satisfies the equation 7.4.

The local contact pressure distribution can be described by

$$\sigma_{ij} \sim r^{\lambda-1} f_{ij}(\theta). \tag{7.5}$$

When the dominant eigenvalue is greater than unity, the local contact pressure distribution will be bounded. When it is less than unity, the pressure distribution will be singular. And finally, when it is complex, the contact edge will separate. The key coefficients of friction that correspond to these distinct boundaries are plotted by the solid lines in Fig. 7.1 for each wedge angle.

Example: 45-degree wedge

For a more detailed understanding, we will isolate the case of a 45-degree wedge pressed onto a half-plane.

The adhesion-limiting friction coefficient for a 45-degree wedge pressed onto a half-plane is $\mu_A = 1.3$. Practical coefficients of friction are likely to be less than this, so we can expect that the contact edges to be in partial slip. Applying the sliding characteristic equation at the contact edges we obtain the eigenvalues plotted in Fig. 7.2 for the leading ($\mu < 0$) and trailing ($\mu > 0$) edges. For a contact under normal loading only, both edges can be considered as leading.

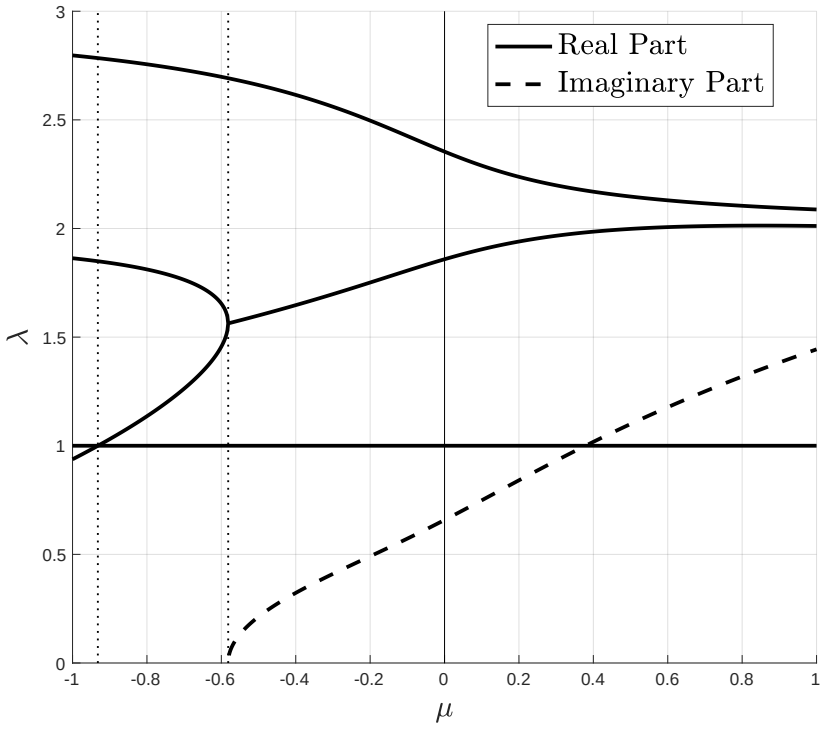


Figure 7.2: Dominant eigenvalues for a 45-degree wedge sliding on a half-plane. The left half of the graph ($\mu < 0$) corresponds to the leading edge, and the right half ($\mu > 0$) corresponds to the trailing edge. The vertical dotted lines represent the boundaries between the different types of dominant eigenvalues that give rise to the different contact pressure behaviours: singular $\lambda < 1$, bounded $\lambda > 1$ and separation λ is complex

.

From Fig. 7.2 we can see that, provided the coefficient of friction is less than the adhesion-limit, the trailing edge will separate for all coefficients of friction. However, when considering the leading edge, the edge will recede if the coefficient of friction $\mu <\sim 0.6$, have a bounded contact pressure if $0.6 < \mu < 0.95$ or experience singular

contact pressure if $0.95 < \mu < \mu_A$.

By applying our understanding of the sliding wedge to the partial slip problem, we are assuming that the dominant eigenvalue governs the behaviour a significant way into the contact, whilst the centre of the contact remains stuck. To validate this assumption we will turn to Finite Element Analysis, using Abaqus.

Task 3: Finite Element Analysis with normal load

For the simple problem of a 45-degree wedge pressed with a normal load only onto a half-plane, both edges are considered 'leading' and symmetrical. The edge position and slip-stick transition points are plotted against the coefficient of friction in Fig. 7.3 for the left half of the contact.

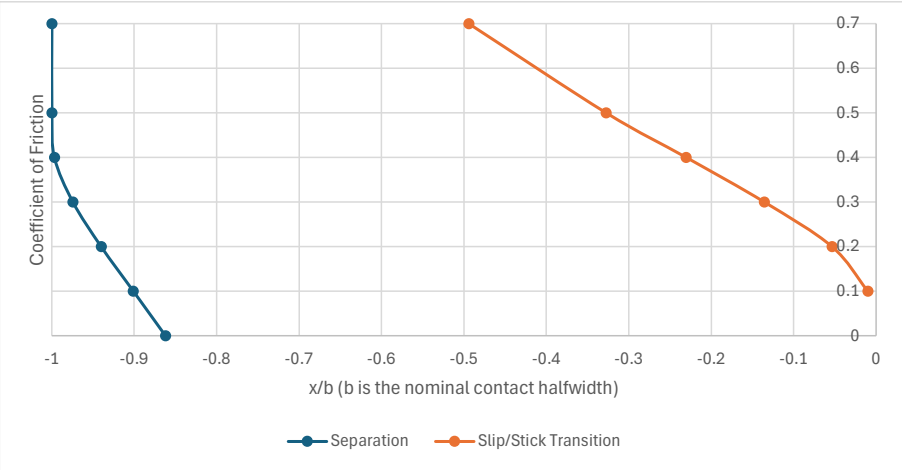


Figure 7.3: Results from finite element analysis of a 45 degree wedge loaded normally onto a half-plane with varying coefficients of friction. The contact edge position (blue) and stick-slip transition point (orange) are plotted against the coefficient of friction.

From Fig. 7.3 we can see that as the coefficient of friction decreases, the extent of separation at the contact edges increases. For low coefficients of friction, $\mu < 0.3$, the extent of separation relates approximately linearly to the coefficient of friction. However, as the coefficient of friction approaches the limiting value for separation the rate of change of separation decreases. From Fig. 7.2 we would expect separation to occur when the coefficient of friction is as high as $\mu = 0.59$, however, we can see from Fig. 7.3, that separation only occurs when $\mu <\sim 0.4$. This discrepancy may be due to the fact that as we approach the eigenvalue boundaries, the influence of the secondary eigenvalues may increase.

In Fig. 7.3, the slip region of the contact at each coefficient of friction is between the contact edge (blue marker) and stick/slip transition point (orange marker). The

centre of the contact is stuck. Under normal loading only, the contact edges will slip in opposing directions. For low coefficients of friction, the majority of the contact is in slip. When the coefficient of friction is 0.7, the slip region is approximately half of the contact.

For realistic coefficients of friction, we can see that the contact has slip regions that constitute $\sim 65\%$ of the contact region and do not separate.

Tasks 3 & 4: Next steps

One possible continuation of this work would involve applying a shear load to the finite element model and see how the asymmetric slip zones grown through the contact.

However, to build on our framework for flat and rounded contacts with wedge angles, the next step would be to obtain calibrations for the small changes in contact edge stress intensity factors, $\Delta K_I, \Delta K_{II}$, due to small changes in normal and shear loads. By obtaining these parameters, along with the contact edge multiplier L_I for the mean loading state, analogous work to that seen in Chapter 5 can be obtained.

(2) Calibration for receding and separating edges: $\mathrm{d}P, \mathrm{d}Q \leftrightarrow \mathrm{d}K$

Throughout this thesis we have relied on a calibration step that maps external loads (P, Q, σ, M) to the stress-intensity factors that control the near-edge behaviour. For the flat-and-rounded contacts of Chapters 3–5, this means mapping the applied loads to the multipliers on Williams' solution for a three-quarter-plane corner; for the receded contact of Chapter 6, the calibration connects the applied loads to L_I, K_I and K_{II} using known analytical results for the strip geometry. An important next step is to extend this calibration to a broader class of edge types.

1. **Receding contacts with general geometry.** The receded contact in Chapter 6 is a relatively simple configuration (a uniform strip on a half-plane) for which the mean-loaded state and perturbation solutions can be obtained in closed form. Many practical receding contacts, however, involve non-uniform cross-sections, finite substrates, or multiple contact patches. For these geometries the calibration $(\mathrm{d}P, \mathrm{d}Q, \mathrm{d}\sigma) \leftrightarrow (\mathrm{d}K_I, \mathrm{d}K_{II})$ would need to be obtained numerically, for example by perturbing a finite element solution about the mean contact state and extracting the edge parameters. By establishing a robust extraction procedure, the matching methodology of Chapter 6 could be applicable to a much wider range of engineering contacts.

2. **Separating edges.** When the coefficient of friction is below the adhesion limit for a given wedge angle, and the loading is such that the contact edge tends to lift according to the sliding wedge criteria described in Future Work **(1)**, the edge behaviour transitions from stuck or slipping to separation. The local field near a separating edge is governed by different eigensolutions (with complex eigenvalues in some regimes), and we would need to map the applied loads to the corresponding separation-mode intensity factors. This is particularly interesting for geometries where one edge separates while the other remains in contact, and it would complement the work outlined in Future Work **(1)**.

3. **Unified calibration tables.** A practical goal would be to compile calibration data, whether in closed form or as tabulated numerical results, for a library of common contact configurations: flat-and-rounded contacts at various wedge angles, receded contacts with different strip aspect ratios, and Hertzian contacts under combined loading. Such a library would allow the matching procedure of Chapter 6 to be applied routinely without requiring bespoke finite element work for each new geometry.

(3) A fretting fatigue threshold criterion and experimental validation

The opening discussion of this chapter argued that the S–N approach to fretting fatigue is fundamentally limited, because the stress state at a contact edge shares little resemblance with the uniform stress field assumed in plain fatigue. We now have, for a useful class of geometries, a description of the near-edge stress state in terms of three stress descriptors. The pressing question is whether these parameters can be used to formulate a practical fretting fatigue threshold criterion, and ultimately to build a finite-life framework.

1. **Formulating a threshold criterion.** In plain fatigue, the endurance limit is expressed as a critical alternating stress below which cracks are not expected to initiate. For fretting, the analogous statement should be in terms of the contact-edge parameters. The simplest candidate is a critical combination of L_I, ΔK_I and ΔK_{II}, below which the local stress conditions are insufficient to nucleate a crack. To establish such a criterion we would need to: (i) identify the appropriate combination of parameters (for example, is a mixed-mode threshold of the form $\Delta K_{\text{eff}} = f(\Delta K_I, \Delta K_{II})$ adequate, or does the mean-state parameter L_I play an independent role analogous to the mean stress in plain fatigue?), and (ii) calibrate the threshold against experimental data for at

least one well-controlled geometry, most naturally the Hertzian pad-on-dogbone arrangement. If the threshold can be expressed in terms of the same edge parameters used in the matching procedure of Chapter 6, then data obtained from a Hertzian experiment could be applied directly to predict threshold behaviour in more complex geometries.

2. **Experimental validation of the matching procedure.** The matching methodology of Chapter 6 predicts specific load relationships for a Hertzian experiment that should reproduce the near-edge conditions of a receded contact. This prediction has not yet been tested experimentally. A natural programme of work would be: (i) manufacture a receded-contact specimen (elastic strip on a dogbone) and a Hertzian pad pair; (ii) run the receded-contact test under combined oscillatory loading recording the damage pattern (slip marks, crack location, surface profiles); (iii) run the predicted equivalent Hertzian test and compare the damage directly. If the damage patterns agree, this would validate not only the matching procedure but also the underlying assumption that the asymptotic edge parameters are the quantities that govern fretting damage. If they do not, there are likely to be additional features such as finite-slip effects, surface roughness or debris effects that need to be incorporated.

3. **From threshold to finite life.** Once a threshold criterion has been obtained, the next step is to extend this into the finite-life regime. As discussed at the opening of this chapter, the biggest difficulty is that the transition from a contact-edge stress field to a propagating crack takes place in a steep, mixed-mode stress gradient, very different from the mild gradients of plain fatigue. One option may be to embed a short crack at the contact edge and use the contact-edge traction field (parameterised by the stress-intensity-factors developed in this thesis) as the boundary condition for a weight-function or distributed-dislocation crack model. The crack-tip stress intensity factor for the embedded crack would then depend on both the crack length and the contact-edge parameters, assuming a smooth transition from the initiation-dominated regime (controlled by contact-edge ΔK_I, ΔK_{II}) to the propagation-dominated regime (controlled by the crack-tip ΔK). Coupling this with a Paris-type growth law, or a short-crack growth model, would provide a finite-life prediction that is rooted in the edge mechanics rather than in an empirical knockdown of bulk S–N data.

(4) Third-dimension effects, material mismatch, surface roughness and damage-mechanism coupling

We have, so far, restricted the analysis to two-dimensional, elastically similar contacts with Coulomb friction. These assumptions were adopted deliberately to isolate the effects of geometric coupling and to build a clean framework, but several extensions would be needed before the method can be applied to the full range of engineering fretting problems.

1. **Three-dimensional effects.** Real contacts are three-dimensional with a finite depth. Even when the nominal contact is two-dimensional, end effects and gradients along the contact line can significantly alter the local slip state and stress field. Extending the asymptotic edge descriptions to three dimensions is challenging due to additional gradients as the calibration becomes a function of position along the contact line. One approach would be to treat slowly varying three-dimensional contacts by applying the two-dimensional framework locally at different cross-sections, solving for the stress parameters that vary along the contact edge. This would give an approximate description for how the stress parameters vary through contacts with modest along-edge gradients.

2. **Material mismatch.** When the contacting bodies are not elastically similar, the normal and tangential problems are coupled even in the half-plane limit. This Dundurs driven coupling would interact with the geometric coupling studied in this thesis, and the combined effect has not been investigated. For dissimilar materials we would no longer be able to treat the contact as a monolith and use Williams' eigensolutions for the wedge corner. It is important to investigate whether the stress parameterisation remains a useful indicator of fatigue, as this will be of great practical significance.

3. **Surface roughness and competing stress concentrations.** Throughout this thesis the contacting surfaces have been treated as nominally smooth, with the near-edge stress field arising from loading the macroscopic contact geometry. Real engineering surfaces, however, carry roughness which itself introduces stress concentrations at the asperity scale. Whether these asperity-scale stresses are significant relative to the macroscopic near-edge concentrations is fundamentally a question of competing length scales; the relevant comparison is between the absolute size of the contact (or its near-edge stressed region) and a characteristic roughness length, such as the mean asperity wavelength or RMS height. For large contacts, the macroscopic near-edge field may

be large enough that the roughness is insignificant, such that the smooth-surface solutions developed in this thesis should give a faithful description of the average near-edge state. For sufficiently small contacts, however, the stressed region may approach the characteristic roughness length, and asperity-scale stress concentrations can become comparable to those arising from the contact geometry itself. The smooth-surface idealisation therefore has a regime of validity that diminishes as the contact shrinks. A useful programme of work would be to (i) define a non-dimensional ratio of contact length scale to roughness length scale that delimits these regimes; (ii) compare directly, for representative geometries, the peak stresses arising from asperity-scale concentrations against those from the smooth-surface near-edge field; and (iii) investigate how the stress-intensity-type edge parameters of Chapter 5 are modified when the underlying surfaces are rough, for example by superposing a statistical roughness contribution onto the smooth near-edge field. This would clarify the range of applicability of the present smooth-contact framework and indicate the small-contact regime in which an explicit rough-contact treatment is required.

4. **Damage-mechanism coupling.** The framework, as it stands, gives us the stress and slip fields needed to assess fretting risk, but it does not model the evolution of damage. In practice, fretting involves wear such as material removal changing the surface profile; oxidation; plasticity under steep stress gradients altering the stress distributions near the contact edges; and crack nucleation and growth altering the local compliance. Coupling even one of these to the present elastic framework, for example, by allowing the contact profile to evolve incrementally with wear, or by embedding the near-edge stress field into a short-crack growth law, would be a significant step towards a finite-life predictive capability.

7.5 Closing Remarks

We set out with the observation that the stress environment at a contact edge is fundamentally different from the uniform field assumed in plain fatigue, and that treating fretting as a knockdown of S–N data is therefore unsatisfying. The work in this thesis provides an alternative starting point, rooted in the local mechanics of the contact edge. We now have closed-form descriptions of near-edge tractions that respect the true geometry, a stress-intensity factor framework that makes those descriptions portable between loading histories and partial slip behaviour, and a

matching procedure that connects complicated contacts to standard laboratory tests. There is, of course, much still to do, but I hope that this thesis has laid a foundation on which a more physically grounded approach to fretting fatigue can be built.

References

[1] D. A. Hills and D. Dini. "What level of friction guarantees adhesion in a complete contact?" in *The Journal of Strain Analysis for Engineering Design* 39.5 (2004), 549–551. DOI: 10.1243/0309324041896425.

[2] J. R. Barber. *Elasticity*. Solid Mechanics and Its Applications. Springer Dordrecht, 2009. **chapter** 12.5.3. ISBN: 978-90-481-3809-8. DOI: https://doi.org/10.1007/978-90-481-3809-8.

[3] Saravanan Karuppanan. "Analysis of incomplete and complete contacts in sliding and partial slip". Doctor of Philosophy (DPhil) thesis. Green College, Oxford: University of Oxford, Department of Engineering Science, 2007. URL: https://ora.ox.ac.uk/objects/uuid:f56f9ed2-3f52-4bc0-8d49-43450b9353db.

Appendix

Statement of Authorship

Chapter 2 is based on the following publication:

> **B. Eames**, D.A. Hills, *"A review of partial slip solutions for elastic contacts,"* European Journal of Mechanics – A/Solids, Vol. 113, 2025, 105698. DOI: 10.1016/j.euromechsol.2025.105698.

Candidate	Beth Eames
Publication Status	Published
Supervisor	Prof. David A. Hills
Chapter	2. Literature Review

Candidate's Contribution

B. Eames carried out a comprehensive literature review, classified contacts into their fundamental types, compiled and synthesised prior results for both complete and incomplete contacts, and prepared all figures. The candidate wrote and edited the manuscript drafts, and revised it in response to peer review.

Certification

By signing below, the candidate and supervisor certify that the candidate made a substantial contribution to the above publication and that the description of contributions is accurate.

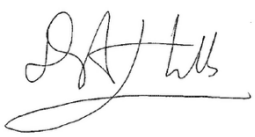
Candidate:



Beth Eames

Date: 23/03/2026

Supervisor:



Prof. David A. Hills

Date: 23/03/2026

Statement of Authorship

Chapter 3 is based on the following publication:

> **B. Eames**, D.A. Hills, M.R. Moore, *"Near edge tractions for a rounded quarter-plane pressed into an elastically similar half-plane,"* Tribology International, Vol. 186, 2023, 108582. DOI: 10.1016/j.triboint.2023.108582.

Candidate	Beth Eames
Publication Status	Published
Supervisor	Prof. David A. Hills
Chapter	3. Near Edge Tractions for a Rounded Quarter-plane Pressed into an Elastically Similar Half-plane

Candidate's Contribution

B. Eames developed the analytical framework for collocating the half-plane closed-form solution into the three-quarter plane far-field solution; conducted formal analysis; derived comparisons with other methods; prepared all figures and plots; wrote and edited the manuscript drafts, and revised it in response to peer review.

Certification

By signing below, the candidate and supervisor certify that the candidate made a substantial contribution to the above publication and that the description of contributions is accurate.

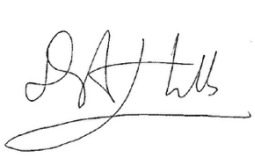
Candidate:



Beth Eames

Date: 23/03/2026

Supervisor:



Prof. David A. Hills

Date: 23/03/2026

Statement of Authorship

Chapter 4 is based on the following publication:

> **B. Eames**, D.A. Hills, M.R. Moore, *"Elastic, flat and rounded finite contacts: When should we use half-plane theory?,"* European Journal of Mechanics – A/Solids, Vol. 106, 2024, 105306. DOI: 10.1016/j.euromechsol.2024.105306.

Candidate	Beth Eames
Publication Status	Published
Supervisor	Prof. David A. Hills
Chapter	4. Elastic, Flat and Rounded Finite Contacts: When Should We Use Half-Plane Theory?

Candidate's Contribution

B. Eames extended the three-quarter plane formulation to finite contacts, developed the methodology for determining when half-plane theory is applicable versus when the novel method should be used, performed the finite element analyses and analytical computations, visualised and prepared all figures and plots, wrote and edited the manuscript drafts and revised it in response to peer review.

Certification

By signing below, the candidate and supervisor certify that the candidate made a substantial contribution to the above publication and that the description of contributions is accurate.

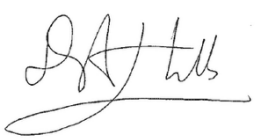
Candidate:



Beth Eames

Date: 23/03/2026

Supervisor:



Prof. David A. Hills

Date: 23/03/2026

Statement of Authorship

Chapter 5 is based on the following publication:

> **B. Eames**, D.A. Hills, J.R. Barber, *"Elastic, flat and rounded finite contacts in partial slip: A novel solution based on wedge and half-plane formulations,"* International Journal of Solids and Structures, Vol. 321, 2025, 113543. DOI: 10.1016/j.ijsolstr.2025.113543.

Candidate	Beth Eames
Publication Status	Published
Supervisor	Prof. David A. Hills
Chapter	5. Elastic, Flat and Rounded Finite Contacts in Partial Slip

Candidate's Contribution

B. Eames developed the refined formulation for partial slip, extended the method to multi-stage loading histories, performed all finite element analyses and coding, characterised the slip conditions at each contact edge, visualised and prepared all figures, wrote and edited the manuscript drafts and revised it in response to peer review.

Certification

By signing below, the candidate and supervisor certify that the candidate made a substantial contribution to the above publication and that the description of contributions is accurate.

Candidate:



Beth Eames

Date: 23/03/2026

Supervisor:



Prof. David A. Hills

Date: 23/03/2026

Statement of Authorship

Chapter 6 is based on the following publication:

> **B. Eames**, S.A. MacLeod, D.A. Hills, *"Matching the slip condition at two types of contact,"* Tribology International *(under review).*

Candidate	Beth Eames
Publication Status	Submitted for Publication, Under Review
Supervisor	Prof. David A. Hills
Chapter	6. Matching the Slip Condition at Two Types of Contact

Candidate's Contribution

B. Eames conducted the formal analysis of matching the contact edge conditions between a plane-receded contact and a Hertzian contact under oscillatory loading, derived the stress intensity factors for the Hertzian contact, prepared figures and plots, wrote and edited the manuscript drafts.

Certification

By signing below, the candidate and supervisor certify that the candidate made a substantial contribution to the above publication and that the description of contributions is accurate.

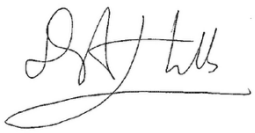
Candidate:



Beth Eames

Date: 23/03/2026

Supervisor:



Prof. David A. Hills

Date: 23/03/2026